Imaging Super-Deep Gas Plays across the Gulf of Mexico Shelf with Multicomponent Seismic Technology

Final Report

DOE Contract: DE-FC26-04NT42239

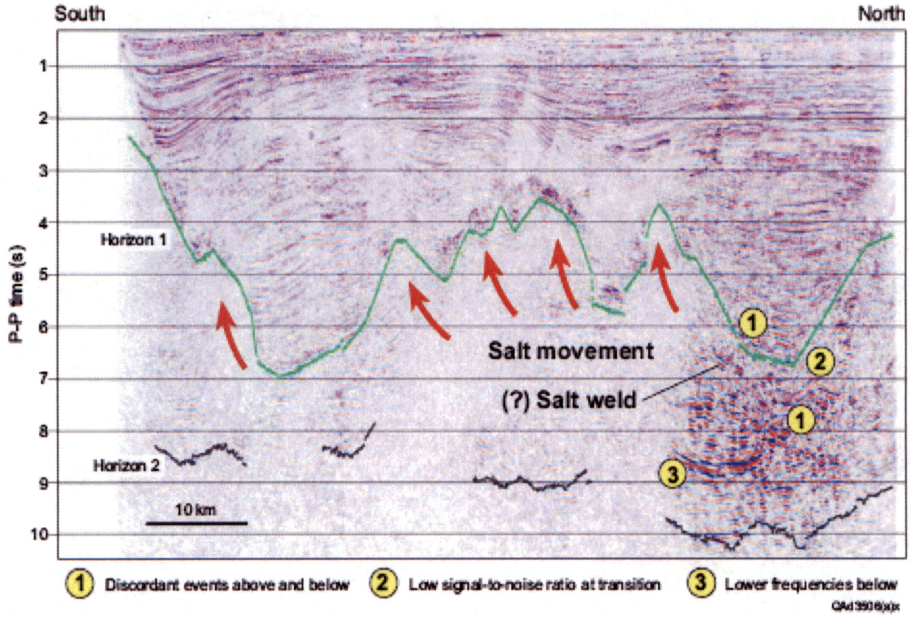

Submitted by:

Bureau of Economic Geology
The University of Texas at Austin
Austin, TX 78713-8924

September 2007

Research team: Bob A. Hardage (Principal Investigator), Michael V. DeAngelo, Sergey Fomel, Khaled Fouad, Paul E. Murray, Randy Remington, and Diana Sava

QAe7185

Disclaimer

Abstract

This continuation report is the final reporting requirement for Year 2 of the project, ***Imaging Super-Deep Gas Plays across the Gulf of Mexico Shelf with Multicomponent Seismic Technology***. The objective of our research is to investigate the value of long-offset multicomponent seismic data for studying deep-gas geology across the northern shelf of the Gulf of Mexico (GOM). WesternGeco has allowed our research team to analyze their long-offset, multi-client, 4-component ocean-bottom-cable (4-C OBC) seismic data across a large area spanning ~24,500 km^2 (~9,600 mi^2) of the northern shelf so that this research could be done. This study area is the largest ever interpreted with multicomponent seismic data. These OBC data were processed by WesternGeco using source-to-receiver offsets extending to 10 km, which is the offset range required for optimal imaging of geology at depths of 10 km. Our research demonstrates that the popular P-P seismic mode used by most of the gas exploration industry images geology beneath the northern GOM shelf to depths of 12 to 13 km, which is a depth range that exceeds industry's current objective of drilling targets to depths of 9 to 10 km (30,000 to 33,000 ft). A more important research finding in our opinion is that the converted-S (P-SV) mode images geology beneath our study area to depths of 9 to 10 km, which allows super-deep gas plays to be analyzed with multicomponent seismic data and with elastic wavefield stratigraphy (combined P-P and P-SV images) rather than limiting prospect evaluation to single-component seismic data and to conventional P-P seismic stratigraphy.

An important aspect of our research has been the application of elastic wavefield stratigraphy through the comparison of P-P and P-SV seismic sequences and seismic facies across deep target intervals. Our investigation shows that although P-P seismic sequences and seismic facies often differ from P-SV sequences and facies across these intervals, both the P-P and the P-SV sequence interpretations and facies models are correct when proper rock physics theory is used to describe the seismic propagation medium. We use several rock physics concepts to calculate P-P and P-SV reflectivity behaviors that explain why P-P seismic sequences and facies differ from P-SV sequences and facies and then demonstrate these reflectivity behaviors with real P-P and P-SV images.

Contents

Figures

Abbreviations, Acronyms, and Glossary

4C: 4-component

basement: In the Gulf of Mexico, seismic basement is defined as rock beneath an unconformity at the base of the marine Mesozoic section that is overlain by Middle Jurassic salt (and equivalents) and younger rocks and underlain by Lower Jurassic and older rocks.

depositional sequence: a stratigraphic unit composed of a relatively conformable succession of genetically related strata and bounded at its top and base by unconformities or their correlative conformities. See **seismic sequence**.

elastic wavefield stratigraphy: a method of seismic interpretation based on the concept that any mode of a seismic wavefield may provide unique seismic sequence information and/or unique seismic facies information across some stratigraphic intervals that cannot be observed with other modes of the wavefield. See **seismic stratigraphy**.

facies: a unique aspect or recognizable property of an object. See **seismic facies**.

GOM: Gulf of Mexico

Horizon 1: a surface interpreted across the study area that defines the depths of the deepest continuous seismic reflections for either the P-P or the P-SV wave mode.

Horizon 2: a surface interpreted across the study area that defines the depths of the deepest discontinuous seismic reflections for either the P-P or the P-SV wave mode.

interval velocity: the average seismic velocity measured from normal-moveout calculations across an interval of the subsurface positioned between two seismic reflection events

Moho: In the Gulf of Mexico, the Moho is defined as a deep Earth layer in which P-wave velocity exceeds 7.6 km/s

OBC: ocean-bottom cable

OBS: ocean-bottom-sensor

P: P-wave

P-P: a seismic wave mode involving a downgoing P wave and an upgoing P wave

P-SV: a seismic wave mode involving a downgoing P wave and an upgoing SV wave

P-wave wipeout zone: any portion of P-P image space where gas-charged sediment attenuates P-wave reflection signal to such an extent that P-P data can create no image.

S: S-wave

salt weld: a physical union of younger post-salt rocks with older pre-salt rocks that occurs when the sediment load is sufficient to cause complete salt evacuation through lateral salt movement with the result that post-salt strata then contact pre-salt strata.

seismic facies: any seismic attribute that distinguishes one succession of seismic reflections from another succession of seismic reflections

seismic sequence: a succession of relatively conformable seismic reflections bounded by unconformable reflections or their correlative conformable reflections. See **depositional sequence**.

seismic stratigraphy: a method of seismic interpretation based on recognizing seismic sequences and seismic facies and using the spatial geometries, arrangements, and distributions of these sequences and facies to infer depositional environments and lithofacies patterns. See **elastic wavefield stratigraphy**.

stacking fold: the number of seismic reflection events that can be summed at a common subsurface image point to make a final reflection response at that subsurface coordinate

super deep: the first strata that infilled the Gulf of Mexico basin as continental plate movements provided the initial accommodation space for sediment deposition

time warping: adjustment of the image-time coordinates of one elastic mode of a seismic wavefield to be depth equivalent to the image-time coordinates of another elastic mode of the same wavefield

$\mathbf{V_P}$: P-wave velocity

$\mathbf{V_S}$: S-wave velocity

Summary

Long-offset four-component ocean-bottom-cable (**4-C OBC**) seismic data have been analyzed to determine if increased source-to-receiver offsets improve the ability of **P-P** and **P-SV** modes to image deeper geology across gas-producing areas of the northern shelf of the Gulf of Mexico (**GOM**). In this study, the term ***long offset*** means that the 4-C OBC data we interpreted were processed using uniformly sampled source-to-receiver offsets that ranged from 0 to 10 km, which is an optimal offset range for imaging geology at depths of 10 km. Approximately five years ago (~2001), seismic contractors developed technology that allows ships to tow hydrophone cables extending to 10 km. However, towing cables 10 km long is an open-water technology that needs to be used where there are no (or few) obstructions to limit boat and cable movement. Thus, seismic data with 10-km offsets are rare across shallow-water areas where congested production facilities have developed over decades of exploration and development. The long-offset 4-C OBC data used in this study were acquired across an extensive area of approximately 24,500 km^2 (~9,600 mi^2) on the Louisiana shelf noted for prolific gas production specifically because no other long-offset data existed there. The P-P and P-SV images produced from these long-offset reflection data were interpreted by our research team to determine the relative depth-imaging capabilities of these two seismic modes. In this study area, both P-P and P-SV data provided good-quality images of geology to depths of 9 km (30,000 ft), the present deepest drilling depth being considered by operators along the GOM shelf. In areas of thickest sediment deposition, P-P reflections were observed from depths of 18 km (60,000 ft), and P-SV reflections returned from depths of 12 km (40,000 ft). We claim that no study has ever interpreted multicomponent seismic data over an area as large as what has been done in this project.

Introduction

This research project provides an opportunity to answer some important questions related to the recent objective of gas-producing companies to drill super-deep (9 km [30,000 ft]) targets across the northern shelf of the GOM. Some of the questions that are answered or partially answered by our research are:

1. Do long-offset seismic data improve the image quality of super-deep targets?
2. How can long-offset seismic data be acquired in congested areas?
3. What is the maximum imaging depths of the P-SV seismic mode relative to the more popular P-P mode?
4. Can P-P and P-SV images acquired with long-offset technology be properly depth registered?
5. Can a new migration concept based on constant-angle gathers improve the quality of deep P-P and P-SV images?
6. What advantage is 4C seismic data over 1C data for evaluating super-deep targets?

Answers, partial answers, and comments about these questions will be emphasized throughout this report.

Advantage 1 of Long-Offset 4C OBC Technology: Imaging Deep Geology

Operators across the GOM are targeting deeper and deeper drilling objectives. For deep targets to be evaluated, seismic data must be acquired with long source-receiver offsets. In order to create an optimal image of geology at a depth Z, a fundamental requirement is that data must be acquired that have source-to-receiver offsets equal to or exceeding Z. This principle is illustrated in Figure 1. Although seismic data acquired with short offsets illuminate deep geologic targets, these targets cannot be optimally imaged because short-offset data do not allow interval velocities that are needed for imaging purposes to be accurately determined across deep layers. Long-offset data are needed to define accurate **interval velocities** across deep layers so that both short-offset and long-offset data can be properly focused.

In addition to improving the accuracy of imaging velocities, long-offset seismic data also have a greater **stacking fold** than do limited-offset data. This

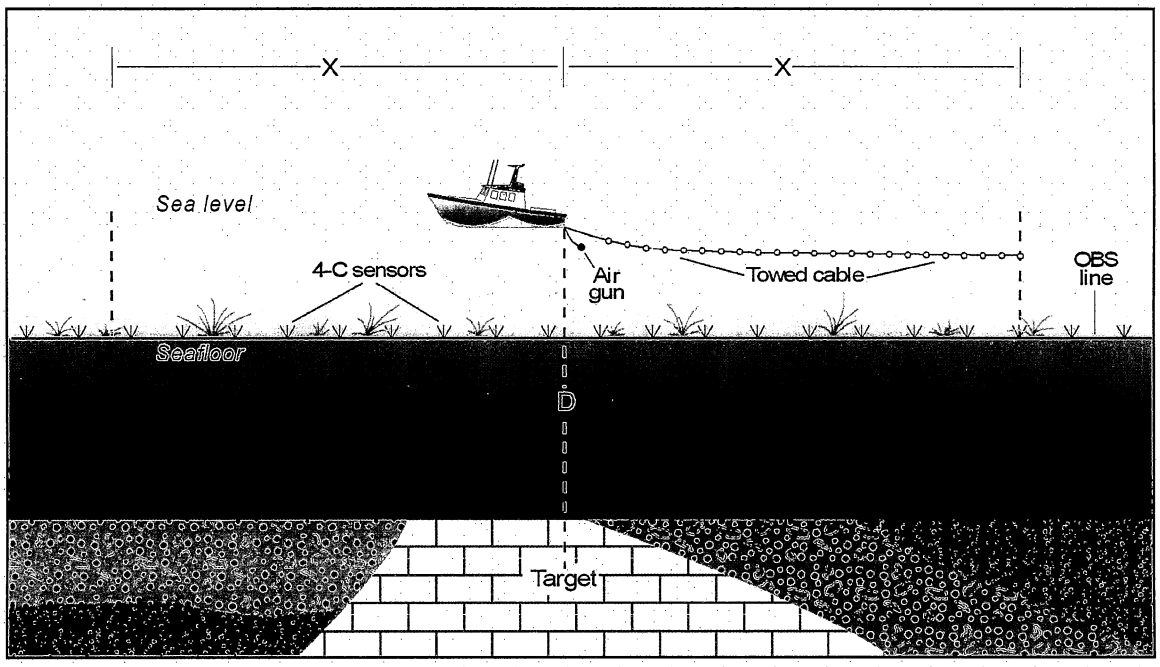

Figure 1. To create an optimal-quality seismic image of a target at a depth Z, data must be acquired with source-to-receiver offsets extending to a distance X, such that X ≥ Z. In a marine environment, the receiver can be deployed either as a towed-cable array or as seafloor-based sensors.

increased stacking fold causes deep data to have a higher signal-to-noise ratio, with the result being a significant improvement in the quality of the properly focused deep-target images that result by using more accurate, long-offset-based, interval velocities. Most shallow-water operators in the GOM consider 30,000 ft (9

km) to be the deepest target depth that will be drilled across the northern shelf for the next several years. For geology at these new target depths of 9 to 10 km to be imaged in an optimal manner, seismic reflection data must be acquired with source-to-receiver offsets of 10 km or more. The 4C OBC data used in our research had source-to-receiver offsets that extended from 0 to 10 km in uniform increments of 25 m and are to our knowledge the longest offset seismic data across the northern shelf of the GOM.

Advantage 2 of Long-Offset 4C OBC Technology: Operation in Congested Areas

Long-offset seismic data are difficult to acquire with conventional towed-cable seismic technology in areas that are congested with production facilities, which is the situation across many shallow-water lease blocks on the northern GOM shelf. However, ocean-bottom-cable (OBC) and ocean-bottom-sensor (**OBS**) seismic technologies are ideal options for acquiring long-offset data in congested production areas because seafloor-based sensors remain stationary once they are deployed and can be positioned quite close to platforms and other obstructions that interfere with towed-cable operations. One example of a deployment of ocean-floor sensors through a typical production area inside the 4C OBC seismic surveys that we studied is illustrated in Figure 2. North-south OBC lines AA and BB and east-west OBC line CC are actual profiles that were analyzed in our study. Once 4C seafloor receivers were deployed along these profiles, a source boat towing only a short array of air guns then maneuvered close to platforms and wellheads and proceeded along each receiver line to generate P-P and P-SV data from long offset distances. As a result, each of these OBC lines (AA, BB, CC) passes within a few meters of several production platforms, and yet seismic line spacing, source-station spacing, and receiver-station spacing are uniform along the full extent of all of the lines. A circle having a diameter of 10 km is positioned atop this map of production facilities to illustrate the difficulty of towing a 10-km cable across the area in any azimuth direction. Regardless of which direction a 10-km cable is towed, the boat/cable combination will encounter obstructions that require course corrections and that may result in cable snagging and breakage. Recently (2005 and later), some seismic contractors claim to have improved their long-tow cable technology so that long cables can be steered and guided through areas of reasonable congestion. If this new towed-cable technology proves to be usable in a wide range of congestion areas, the advantage of OBC and OBS seismic technology in such areas may not be as great as it presently is.

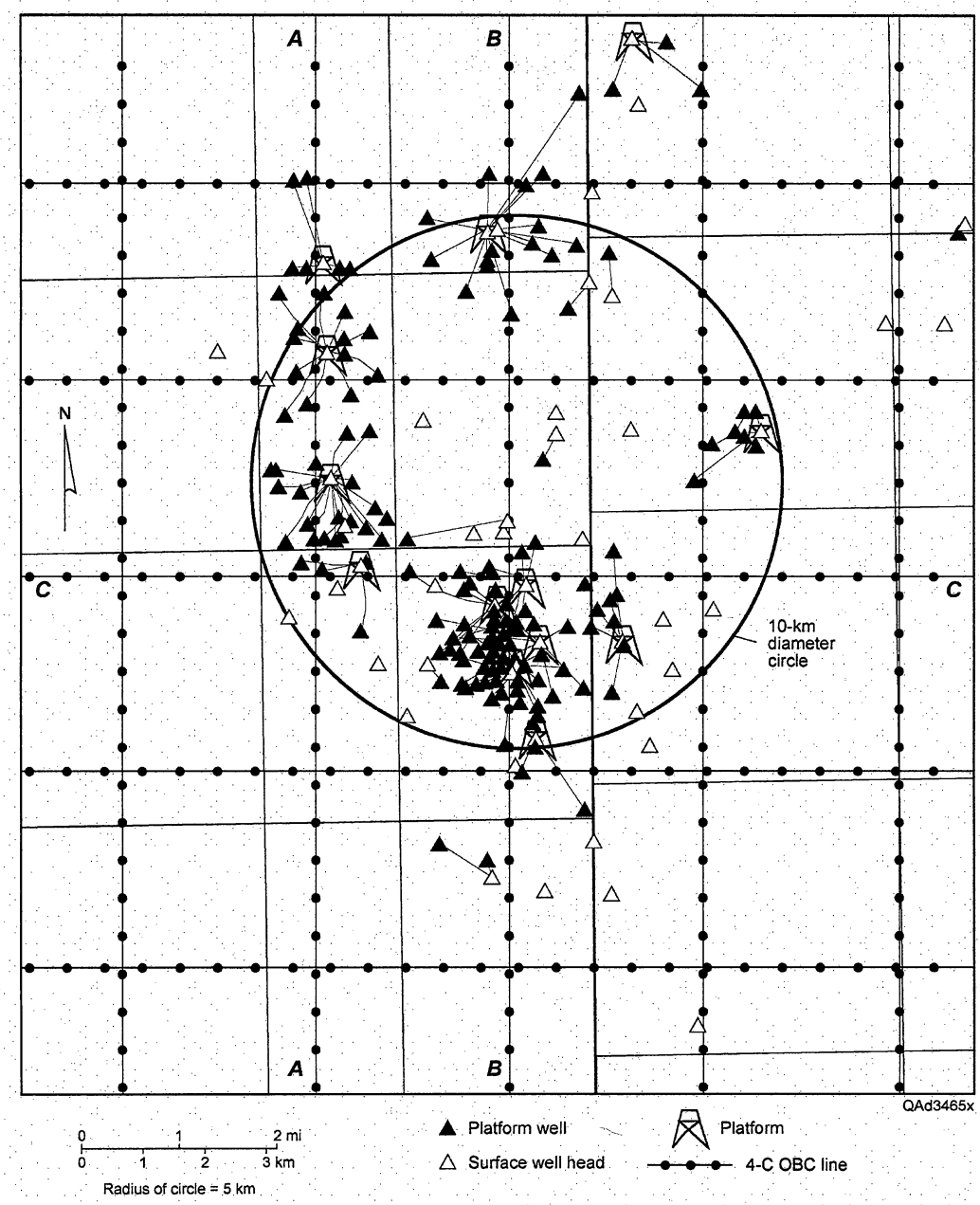

Figure 2. 4-C OBC data acquisition across congested areas. This map indicates the positions of actual OBC profiles used in this study. Note the positions of profiles AA, BB, and CC relative to production platforms. The diameter of the circle is 10 km.

Advantage 3 of Long-Offset 4C OBC Technology: Elastic Wavefield Stratigraphy

An additional appeal of OBC seismic technology over towed-cable technology is that 4C data can be acquired, which allows targeted reservoir intervals to be imaged with P-SV wavefields as well as with P-P wavefields. Parallel research to this project by our research team has demonstrated that one mode of an elastic wavefield may image stratal surfaces across some stratigraphic

intervals that are not seen by its companion wave modes and will thus provide different, but equally valid, information regarding depositional sequences and sedimentary facies within that interval (Hardage and others, 2006). We use the term **elastic wavefield straigraphy** to describe the methodology we use in which seismic sequences and seismic facies from all modes of an elastic wavefield are integrated into a seismic interpretation. Because 4C OBC seismic data are utilized in this deep-target study, we can integrate conventional P-P seismic sequences and facies with P-SV seismic sequences and facies to achieve greater insight into the deep geology that is imaged with these long-offset data. In our elastic wavefield stratigraphy analysis of these deep-target data, we employed rock-physics modeling to explain how and why certain geological conditions caused the differences that are observed between P-P seismic sequences and facies and P-SV sequences and facies.

For the data used in this study, some field records were acquired with offsets greater than 10 km. However, data offsets were limited to 10 km during data processing. Data examples will be illustrated and discussed that will document the imaging depths and image qualities of the P-P and P-SV modes embedded in these 10-km offset data.

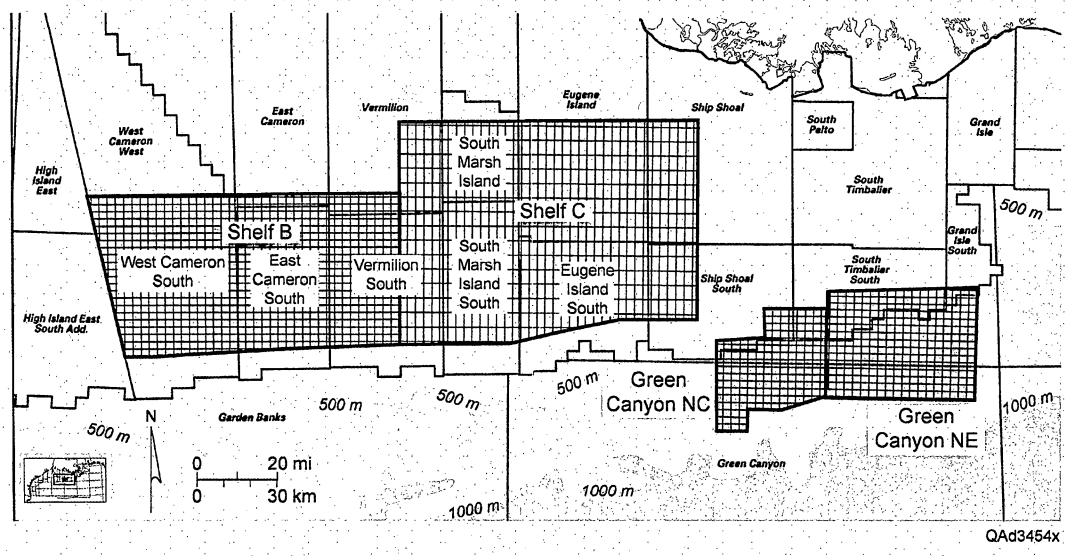

Figure 3. Location of WesternGeco's multi-component long-offset 4C2D seismic data surveys. Data used in this study come from the Shelf-B and Shelf-C surveys.

Study Area

WesternGeco allowed our research team to analyze and interpret some of their multi-client, long-offset, 4C OBC seismic data for this study. WesternGeco has acquired a considerable amount of long-offset 4C OBC data and segregates their multi-client data programs into the four survey areas shown in Figure 3. Data used in this study came from the Shelf-B and Shelf-C surveys that extend across portions of the following gas-prolific lease areas of the GOM:

- West Cameron South and West Cameron West,
- East Cameron South and East Cameron,
- Vermilion South and Vermilion,
- South Marsh Island South and South Marsh Island,
- Eugene Island South and Eugene Island, and
- Ship Shoal South and Ship Shoal.

Within these lease block areas, 4C OBC seismic data were acquired as parallel north-south and parallel east-west 2-D profiles that were spaced at intervals of 2 mi (3.2 km). East-west profiles, when extended across both surveys, were approximately 160 mi (~260 km) long. The lengths of north-south profiles in each survey varied from 50 to 65 miles (80 to 104 km).

Deep Geology across the Area

We use the term ***super deep*** to refer to the first strata that infilled the GOM basin as continental plate movements provided the initial accommodation space for sediment deposition. There are several published models of the super-deep geology across the GOM basin. All of these models involve some elements of conjecture because no wells yet penetrate super-deep strata underneath the GOM shelf, and previous seismic data have provided poor images of the deepest structure and stratigraphy. It is helpful to describe these basin models, even though they are based on seismic data that do not adequately image super-deep geology and on wells that do not penetrate the deepest strata, in order to appreciate the deep-imaging capabilities of the long-offset 4C OBC data that have been acquired across the Shelf-B and Shelf-C survey areas.

The mechanism that many plate-dynamics researchers think created the GOM basin was an angular rotation of the North American plate away from the

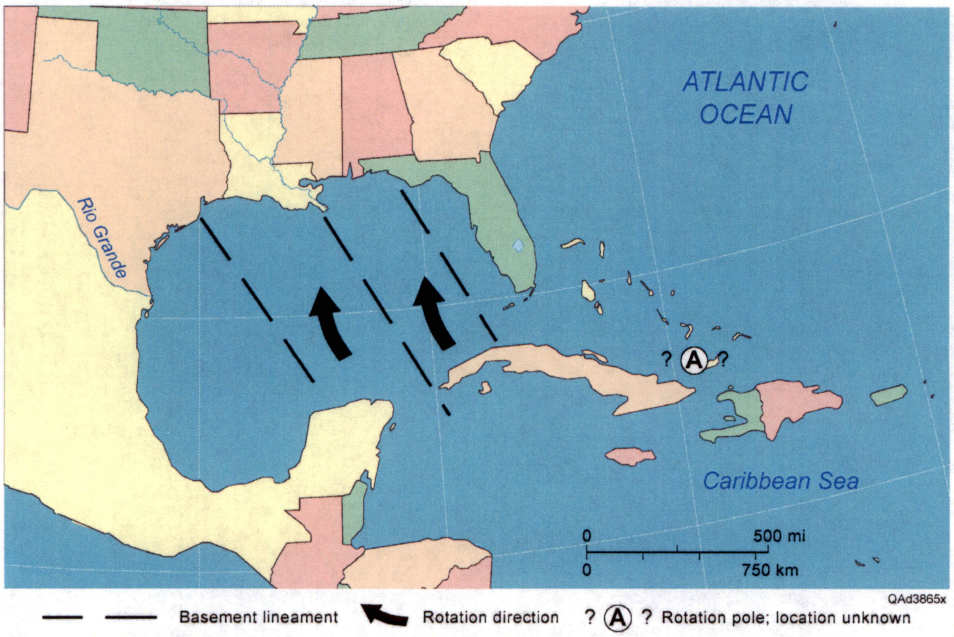

Figure 4. One model proposed for the opening of the GOM.

South American and Caribbean plates. The pole around which this rotation occurred is assumed to be located somewhere southeast of present-day Florida. This rotation pole and a hypothetical rifting action are shown in a generalized and simplified form in Figure 4. Such plate movement should produce basement-related lineaments trending northwest-southeast across the GOM basin, as illustrated by the dashed lines in this diagram.

An authoritative description of present-day plate and basement tectonic features is the *Tectonic Map of the World* developed by Exxon Production Research Company (1985) that is now distributed by the American Association of Petroleum Geologists. The portion of this worldwide map that spans the GOM basin is shown in Figure 5, together with an indication of the location and size of the Shelf-B and Shelf-C seismic surveys (labeled **Study area**). This map shows that a number of major basement lineaments do trend northwest-southeast across the GOM basin as implied by the model in Figure 4. These northwest-southeast-trending lineaments indicate lateral expansion of the basin to the northeast and southwest. Other lineaments trending northeast-southwest indicate basin expansion to the northwest and southeast. No lineaments are defined beneath the salt province north of the Sigsbee Deep (Fig. 5) because it has been difficult to acquire reliable potential-field data below these massive salt structures, and sub-salt seismic images of super-deep geology did not exist when this map was made in the early 1980's and are still difficult to create.

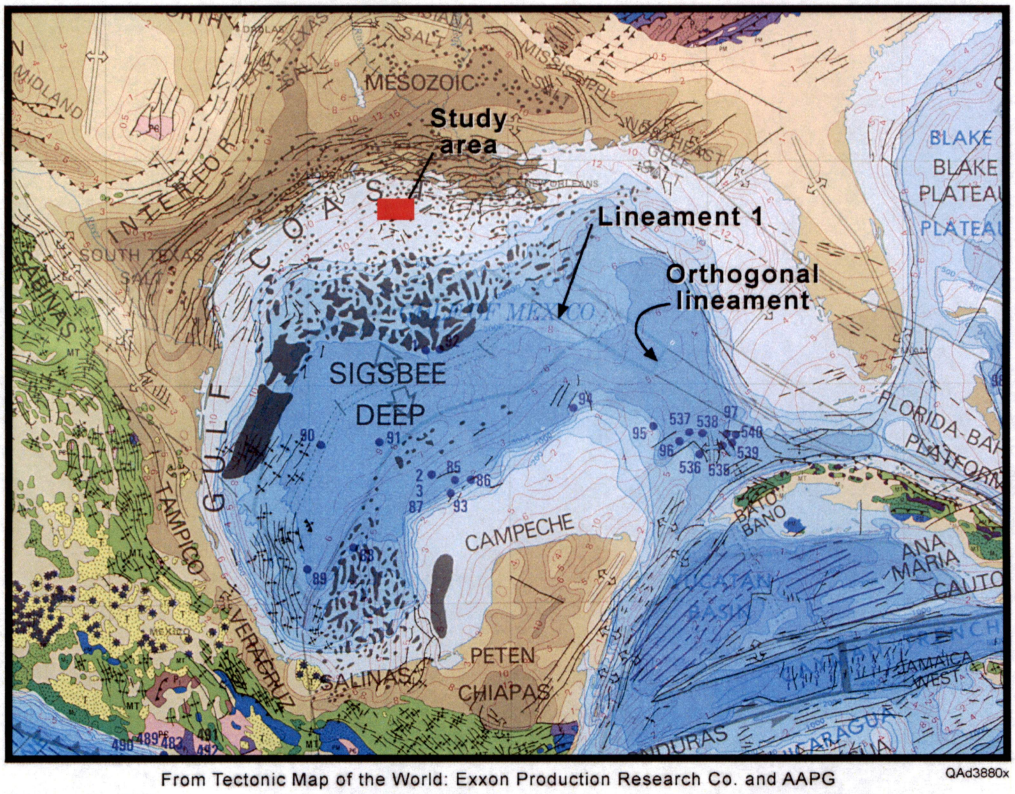

From Tectonic Map of the World: Exxon Production Research Co. and AAPG QAd3880x

Figure 5. Plate and basement tectonic elements across the GOM modified from Tectonic Map of the World produced by Exxon Production Research Company (1985) and distributed by AAPG.

The basement lineament labeled "**1**" should traverse the Shelf-B/Shelf-C survey area within this salt province if the linear feature continues northwest along the trend shown on the map. Short northeast-southwest-trending lineaments occur normal to the long northwest-southeast lineaments as a result of crustal movements parallel to these major-lineament trends. One of these short lineaments is labeled "**Orthogonal Lineament**" in Figure 5. Such a northeast-southwest lineament possibly underlies the Shelf-B/Shelf-C study area. Because these seismic surveys are positioned atop a salt province where basement information needed to construct this tectonic map was sparse, the long-offset data acquired with these surveys may provide information about the basement beneath the GOM salt province. A possible seismic-based interpretation of basement lineaments is presented later as Figure 29.

Geological Issues

Several geological issues need to be considered to establish a framework for evaluating the depth-imaging capability of the long-offset seismic data used in this study. Key questions that our research team investigated included:

1. How deep is the Moho beneath the Shelf-B and Shelf-C areas?
2. How thick is the sediment accumulation beneath the Shelf-B and Shelf-C surveys?
3. What is the conventional wisdom about the deepest depths that can be imaged with reflection seismic data available in the study area?

Depth of the Moho

The issue of **Moho** depth across the GOM basin was considered by Sawyer and others (1991). In their analysis, the Moho beneath the GOM basin was defined as "***a layer in which P-wave velocity V_P exceeds 7.6 km/s***," and they observed that V_P within the Moho is usually in the range of from 8.0 to 8.5 km/s. Figures 25 and 26 that follow show that the deepest layers imaged with the long-offset data used in this study have P-wave interval velocities that are considerably less than 8 km/s. Thus, the Shelf-B and Shelf-C long-offset data do not contain Moho reflections if the V_P velocity requirement used by Sawyer and others is imposed as a definition of a Moho interval. The estimated depth to Moho across the GOM basin developed by Sawyer and others (1991) is reproduced as Figure 6. The locations and physical sizes of the Shelf-B and Shelf-C surveys are indicated on the map and lead to the observation that Moho depth beneath the Shelf-B/Shelf-C area is 25 to 30 km. Subsequent seismic data examples will lead to the conclusion by our research team that the P-P mode extracted from the Shelf-B/Shelf-C long-offset data images to a depth of ~18 km in some portions of our study area.

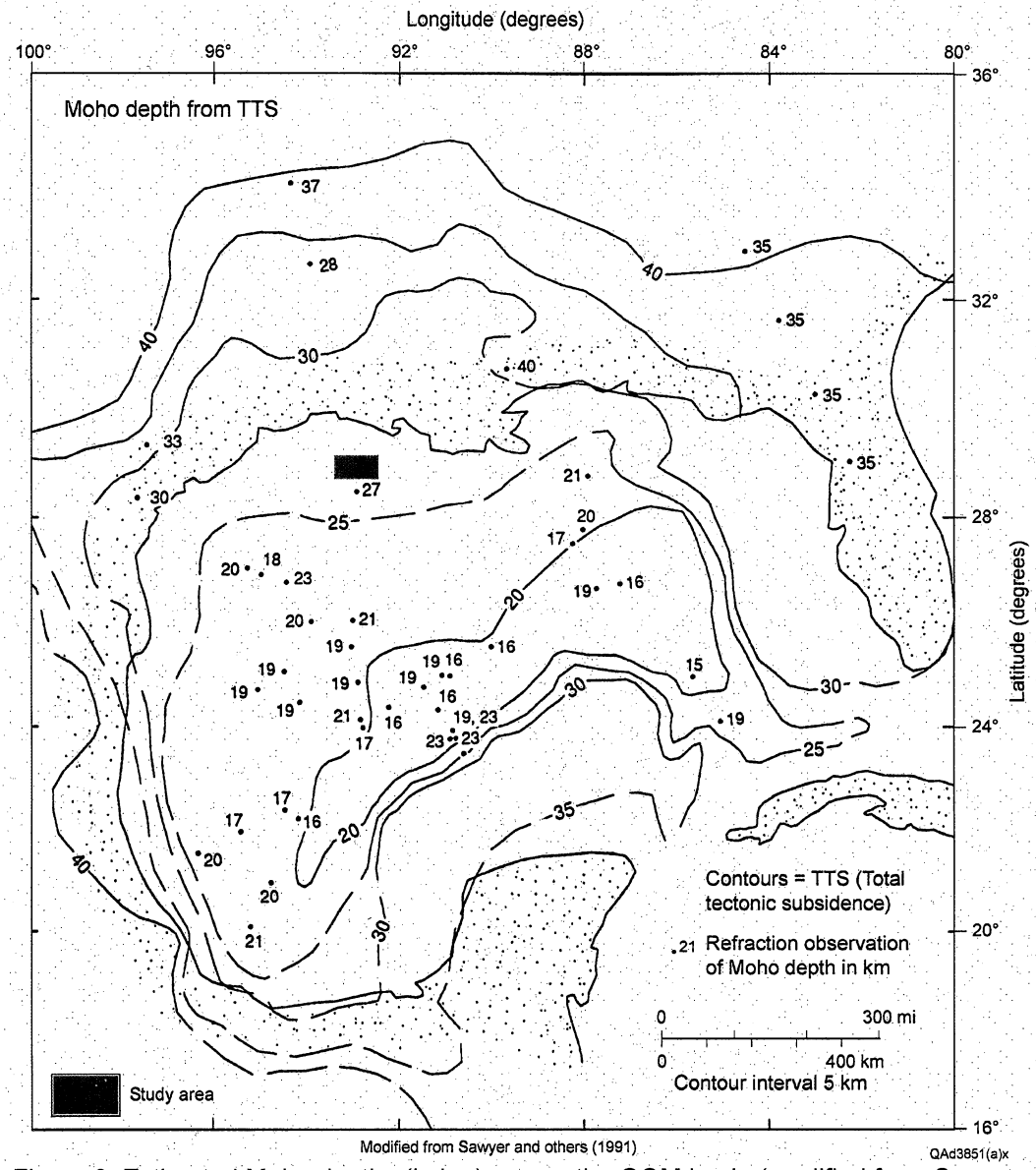

Figure 6. Estimated Moho depths (in km) across the GOM basin (modified from Sawyer and others, 1991). This map implies the Moho should be at a depth of 25 to 30 km beneath our study area.

Depth of Seismic Basement

Sawyer and others (1991) used a GOM-specific definition of seismic basement in which they stated **basement** to be, ***rock beneath an unconformity at the base of the marine Mesozoic section that is overlain by Middle Jurassic salt (and equivalents) and younger rocks and underlain by Lower Jurassic and older rocks***. Other researchers may use a different definition of crustal basement, but for the purposes of this study, we adopted this definition of Sawyer and others. A map showing basement depths and regional extents of crust types across the GOM basin that was published by Sawyer and his co-authors (1991) is shown in Figure 7 with the Shelf-B and Shelf-C survey areas highlighted. The labels *continental, oceanic, thick transitional,* and *thin transitional* on this map

refer to types of basement crust. Dashed contours are speculative basement depths. Depth contours in the vicinity of the Shelf-B and Shelf-C surveys are the deepest values on the map, but all of the contours across these survey areas are dashed (speculative). Taken at face value, this map suggests that the depth of seismic basement beneath the Shelf-B/Shelf-C surveys is about 16 km.

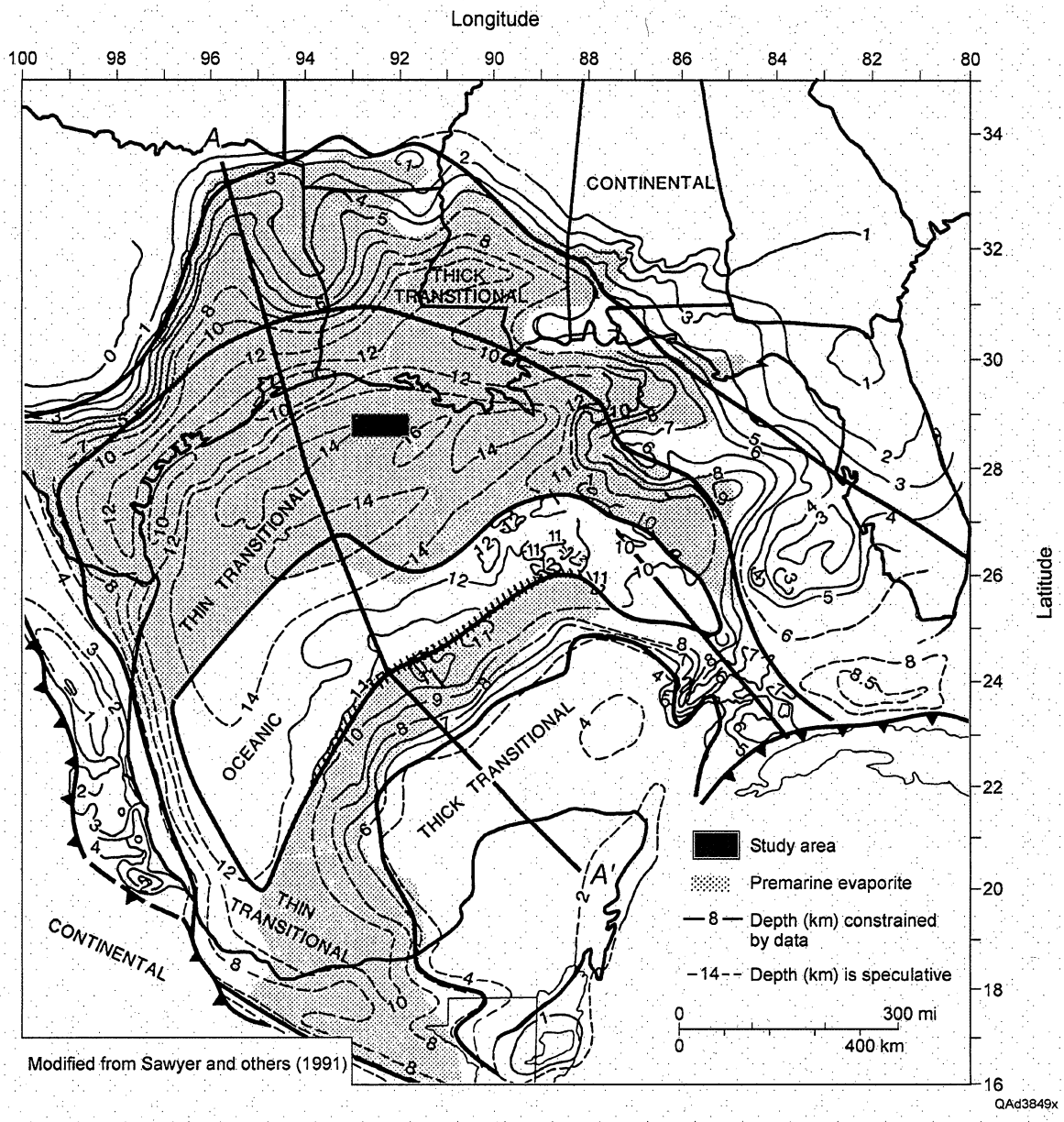

Figure 7. Depth to basement (in km) and types of basement crust across the GOM basin (modified from Sawyer and others, 1991). This map suggests seismic basement should be at a depth of ~16 km beneath our study area.

Conventional Wisdom: How Thick is the Sediment?

Several cross-section profiles traversed the original basement-depth map published by Sawyer and others (1991). The map in Figure 7 eliminates all of these profile locations except profile A-A′, the closest traverse to the Shelf-B/Shelf-C area. A reproduction of this published cross-section view of the geology along A-A′ is shown as Figure 8. A labeled arrow identifies the location of the seismic study area. This cross section tells the same story as the basement-depth map (Fig. 7): the thickest sedimentary section in the GOM basin is beneath the Shelf-B and Shelf-C surveys where the depth to basement is speculative but is probably at least 15 km.

A similar cross section across the GOM basin was published by Galloway and others (1991). A modified version of their cross section is shown as Figure 9. The location of this cross section is shown on the map inset and places the geology in the immediate vicinity of the Shelf-B/Shelf-C surveys. The position of the seismic surveys is labeled *Study area* on the cross section. This basin model also shows that the thickest sediment accumulation in the GOM basin is beneath the Shelf-B/Shelf-C area, and that although the thickness of the sediment beneath these seismic surveys is unknown, it is probably 15 km or more.

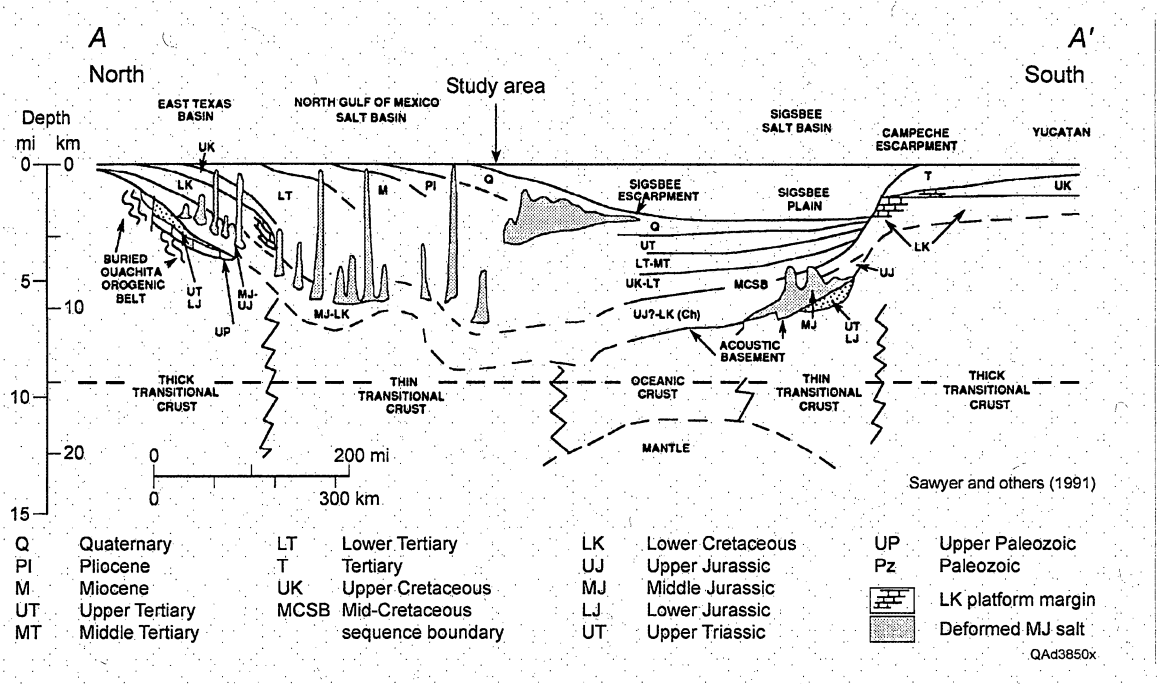

Figure 8. Schematic cross section A-A′ (Fig. 7) of geology near the Shelf-B/Shelf-C seismic survey (modified from Sawyer and others, 1991).

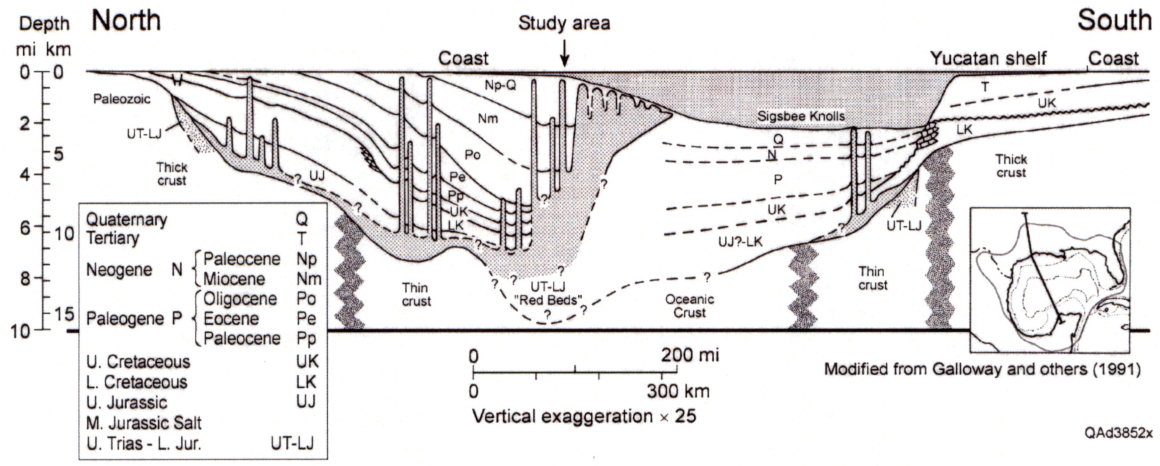

Figure 9. Generalized geologic cross section of the Gulf of Mexico basin in the vicinity of the seismic study area (modified from Galloway and others, 1991).

Conventional Wisdom: How Deep Do Seismic Data Image?

Two published studies have been selected to address the question of the maximum depths imaged by conventional P-P seismic data across the northern GOM basin. The first investigation was done by Diegel and others (1995). Their map of the tectonic and stratigraphic provinces of the northern GOM basin is reproduced as Figure 10. The numbered traverses across this map represent locations where seismic lines were spliced together to make long, regional

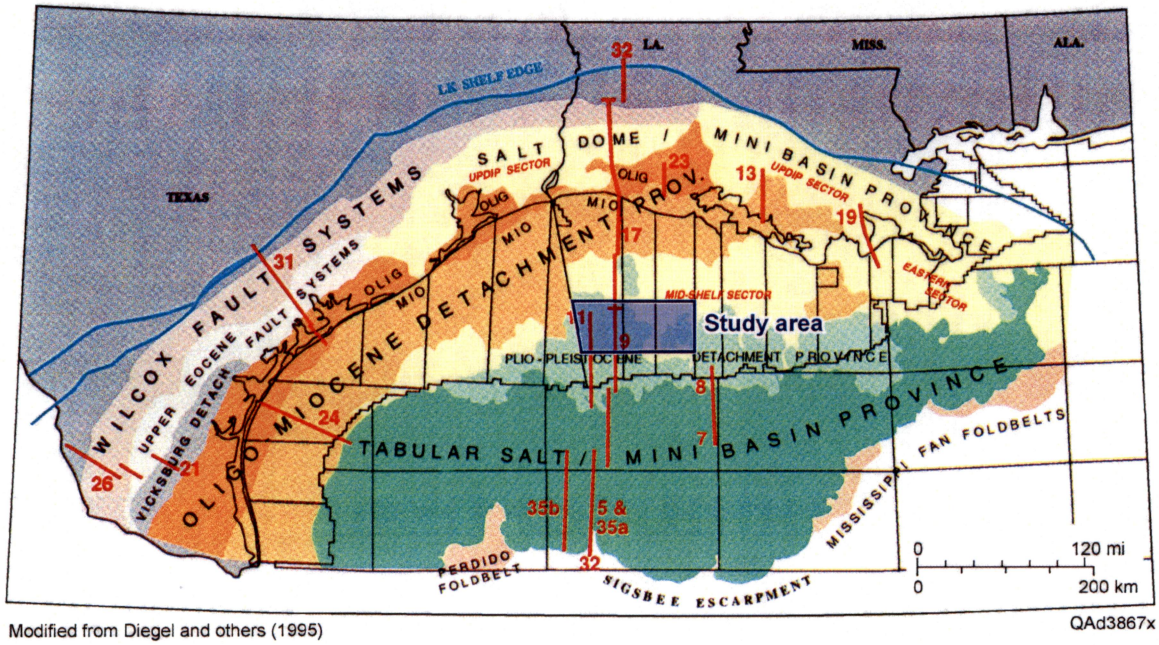

Figure 10. Tectonic and stratigraphic provinces of the northern Gulf of Mexico basin (modified from Diegel and others, 1995).

transects across the basin. Three of these seismic profiles (**9**, **11**, and **17**) traverse some portion of the Shelf-B and Shelf-C surveys. Profile **9** is displayed as Figure 11, profile **11** is shown as Figure 12, and profile **17** is reproduced in Figure 13. The position of the Shelf-B/Shelf-C area is labeled on each profile. These reflection data show that, at some locations along the profile, interpretable P-P reflections exist down to a maximum image time of 6 s. No doubt some GOM explorationists utilize P-P seismic data that image deeper than 6 s, but a 6-s seismic basement is typical of most conventional P-P seismic data across the northern GOM shelf. Later data examples will show that the long-offset P-P mode extracted from the Shelf-B/Shelf-C 4C OBC data have reflection events at two-way traveltimes of 10 s across some of the study area.

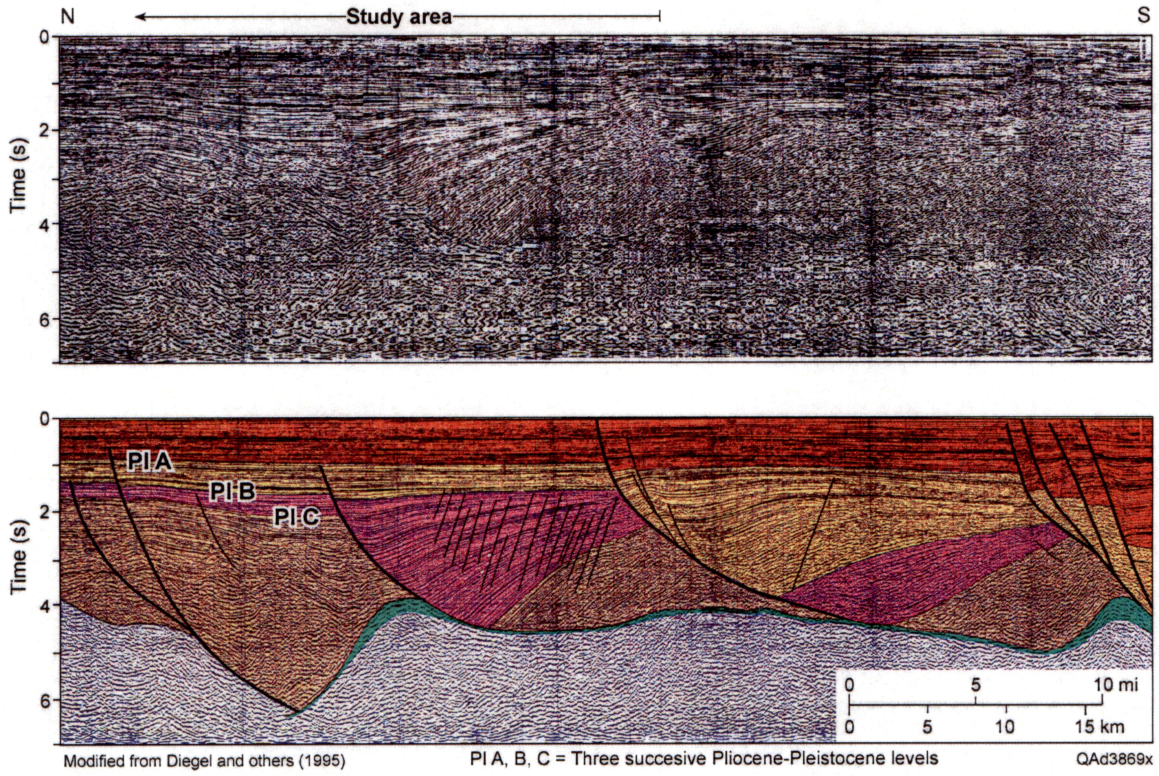

Figure 11. Seismic profile 9 traversing the study area. The location of the profile is defined in Figure 10 (modified from Diegel and other, 1995).

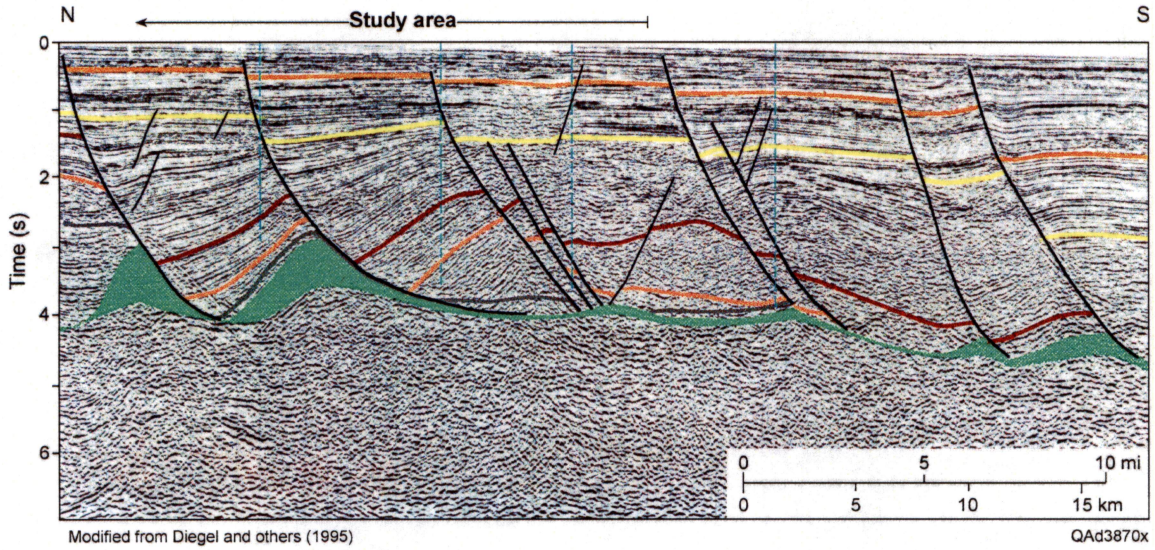

Figure 12. Seismic profile 11 traversing the study area. The location of the profile is defined in Figure 10 (modified from Diegel and others, 1995).

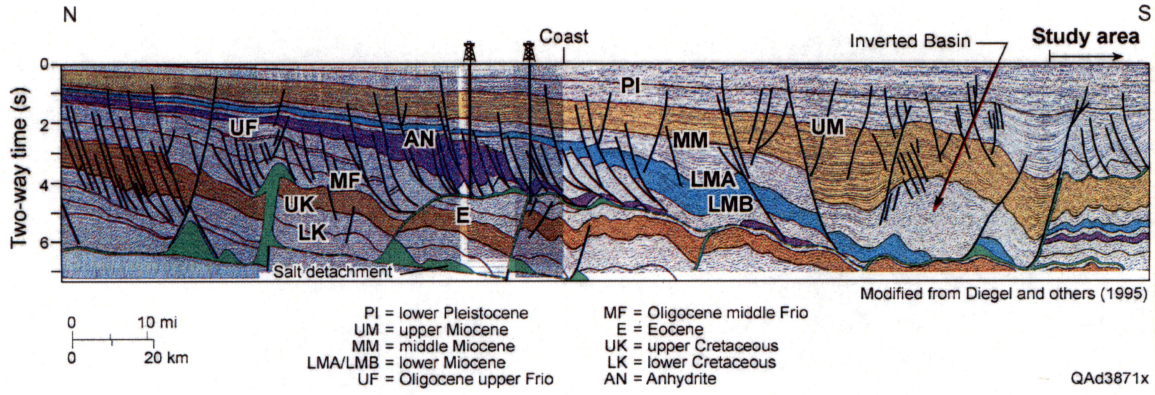

Figure 13. Seismic profile 17 traversing the study area. The location of the profile is defined in Figure 10 (modified from Diegel and others, 1995).

The second selected study was published by Peel and others (1995). These investigators developed models of sediment thicknesses across the GOM basin along several traverses that started onshore, crossed the GOM shelf, and ended at the oceanic crust in the center of the basin. Their map of the locations of these traverses is shown in Figure 14, together with a depositional model developed for profile **4** that crosses the Shelf-B/Shelf-C study area. This profile is significant in two respects: it implies that sediment is ~20 km thick beneath the Shelf-B and Shelf-C surveys, and it indicates that seismic data in the area image to depths of 10 to 12 km.

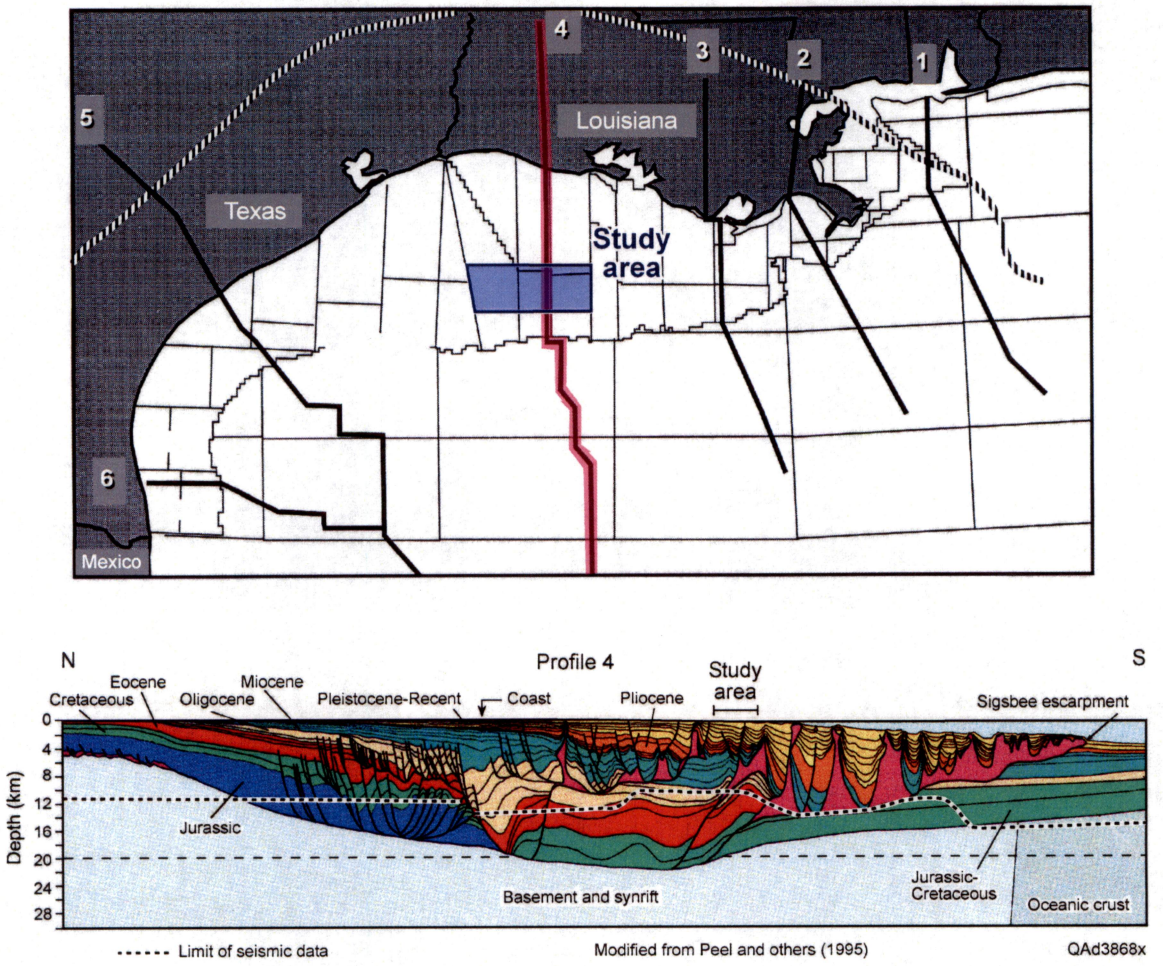

Figure 14. One proposed model of sediment thickness and maximum seismic imaging depth across the study area (modified from Peel and others, 1995).

Conventional Wisdom: A Summary

Other published studies could be considered, but the ones presented here were done by respected scientists and can be viewed as "conventional wisdom" about the deep geology beneath the Shelf-B/Shelf-C area. Key concepts provided by these studies can be summarized as

- The sediment accumulation in the GOM basin is thickest in the area of the Shelf-B/Shelf-C curves,
- The sediment beneath the Shelf-B/Shelf-C surveys is thought to be 15 to 20 km thick,
- Most P-P seismic reflection data image geology to a maximum two-way time of about 6 s, and
- The depth to the Moho is 25 to 30 km across the Shelf-B/Shelf-C area

No studies were found that illustrate or interpret converted-S (P-SV) seismic reflection data across the GOM basin. The long-offset P-SV data examples that follow will apparently be the first public documentation of the imaging capabilities of this important elastic wave mode across GOM basin plays.

Interpreted Horizons

The depth-imaging ability of the 10-km offset 4-C OBC data interpreted in this study will be illustrated using profiles that extend the full north-south or east-west extents of both the Shelf-B and Shelf-C surveys. Two horizons were interpreted along these profiles. Neither horizon is a structural horizon, which is a crucial point. Rather, each horizon is a convenient and subjective marker that indicates seismic reflection quality. **Horizon 1**, the shallower horizon, marks the ***base of continuous reflections***. As such, that horizon crosses geologic time lines and does not map geologic structure or indicate depth variations of a fixed formation. **Horizon 2**, a deeper horizon, defines the ***base of discontinuous reflections.*** This horizon also crosses geologic time lines and follows no fixed

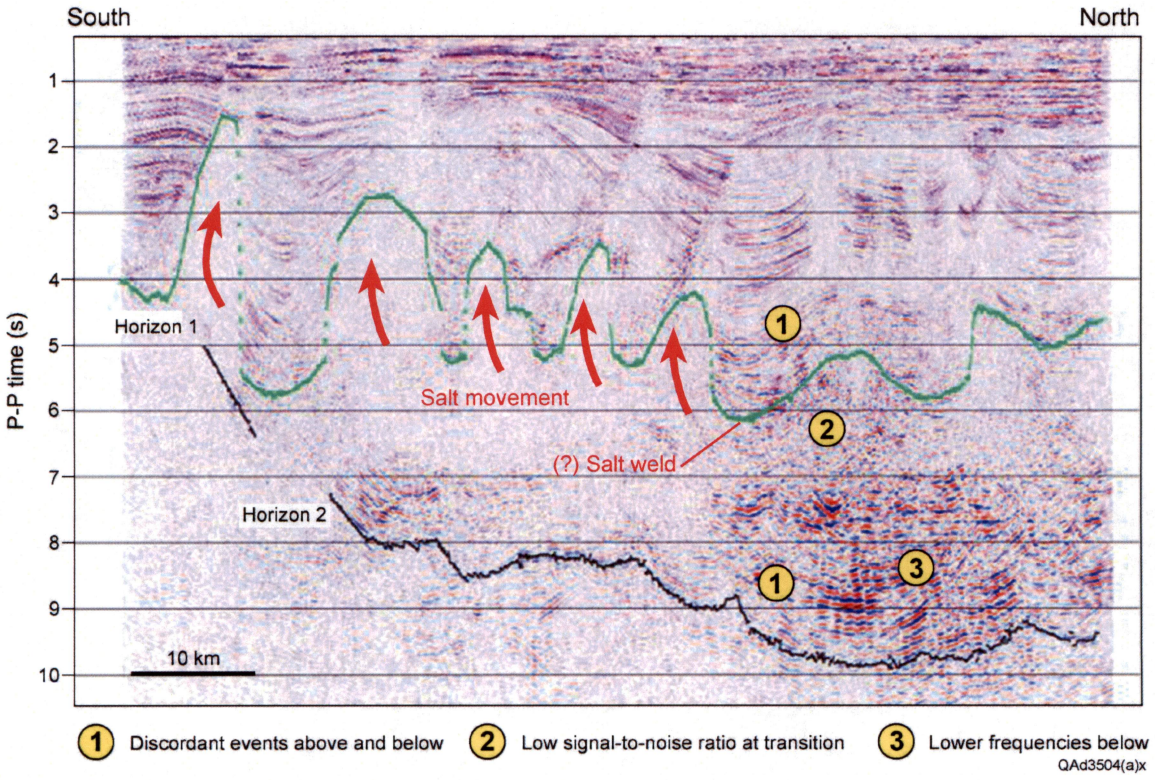

Figure 15. P-P image and interpreted **Horizon 1** and **Horizon 2** from the western portion of the Shelf-B survey.

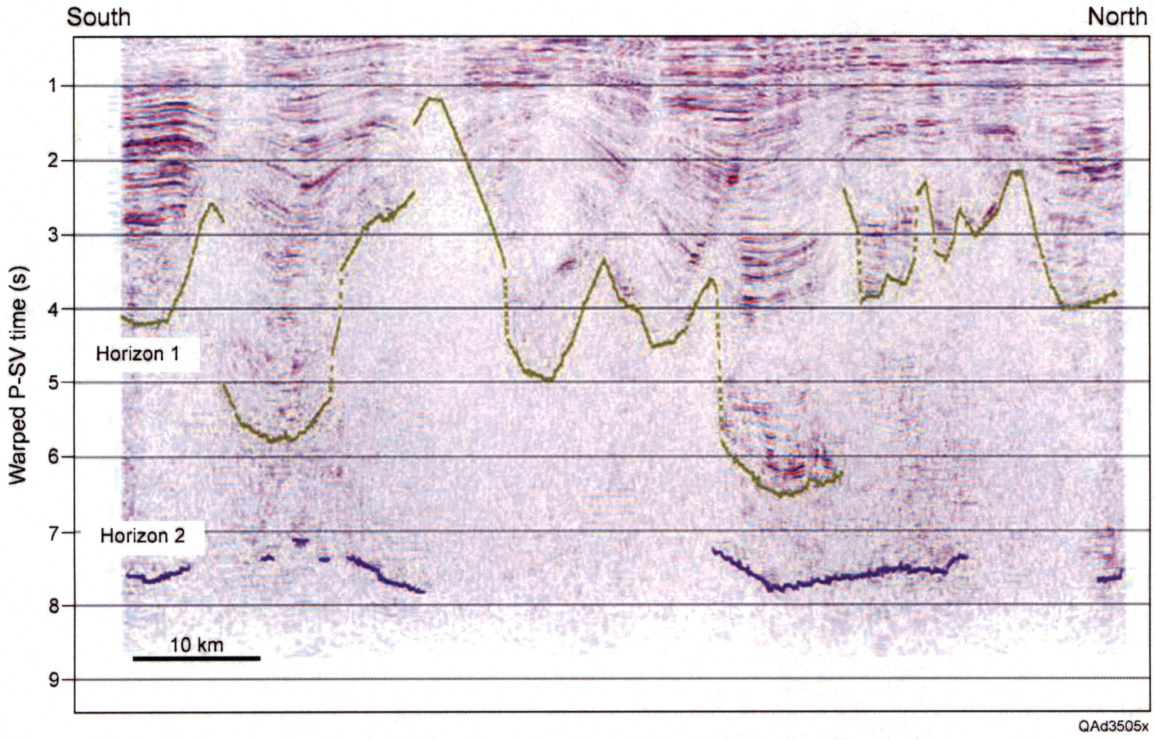

Figure 16. P-SV image and interpreted **Horizon 1** and **Horizon 2** from the western portion of the Shelf-B survey. This image should be compared with its companion P-P mode in Figure 15.

geologic structure; it is only a subjective and qualitative estimate of the maximum depth of usable reflection signal. When the following interpreted data are inspected, Horizons 1 and 2 must be viewed only as indicators of seismic reflection quality, never as geologic-time surfaces. Examples of the interpretation of these horizons along a profile that traverses the western part of the Shelf-B survey are shown on Figure 15 for the P-P image and on Figure 16 for the companion P-SV image.

Time-Warping Function: Shelf-B

All P-SV data examples used in this discussion will be displayed as **time-warped** data. With P-P data and time-warped P-SV data displayed side by side, depth-equivalent geology can be recognized in P-P and P-SV image spaces with more confidence. The critical data needed to transform P-SV image-time coordinates to P-P image-time coordinates are Vp/Vs velocity ratios across the seismic image space. A single, space-invariant Vp/Vs function, shown in Figure 17, was used to transform P-SV image time to P-P image time across the total Shelf-B survey. This simplifying assumption that Vp/Vs behavior was laterally invariant over the large area spanned by Shelf-B data was made for expediency so that P-SV data could be compared quickly with P-P data. The assumption of spatially invariant Vp/Vs dependency causes the transformation of P-SV time to P-P time to have an embedded error that varies vertically and laterally across the

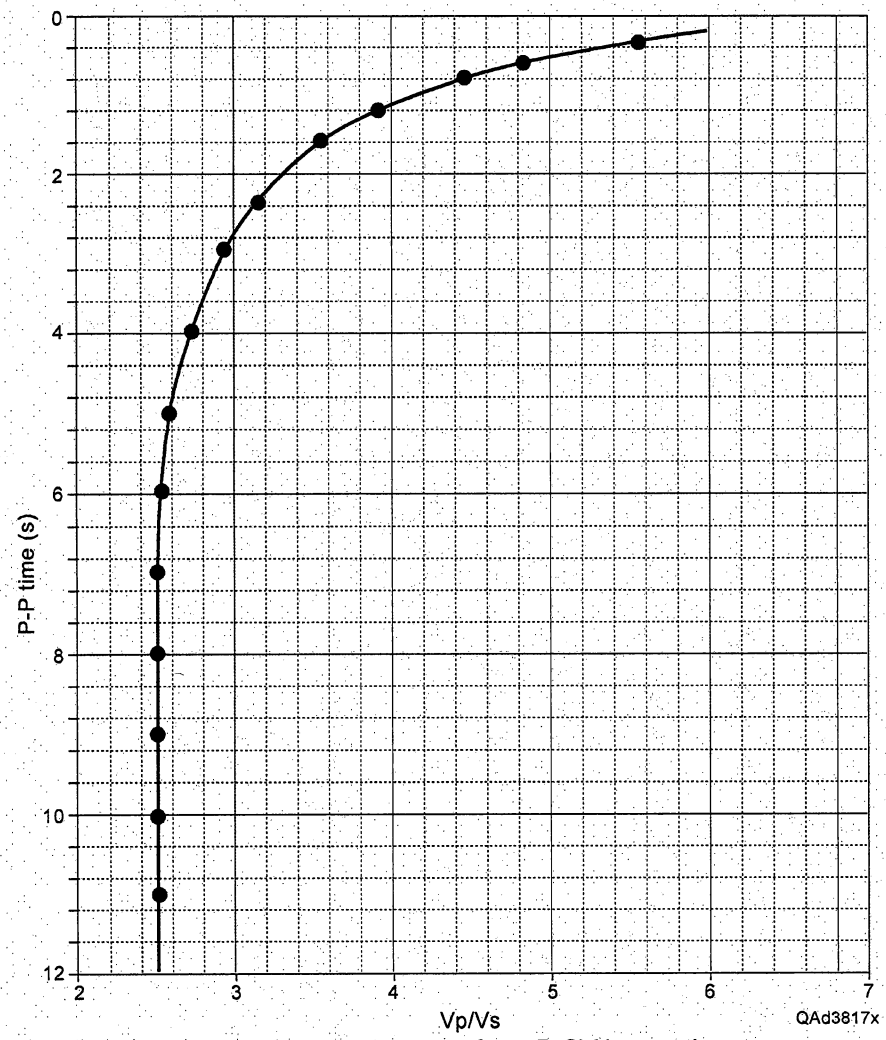

Figure 17. Time-variant Vp/Vs function used to transform P-SV image time to P-P image time across the Shelf-B survey.

survey. However, time-warped P-SV data are still adjusted to their companion P-P data to an accuracy that allows depth-equivalent P-P and P-SV structure and stratigraphy to be recognized.

Only the radial component of the time-warped P-SV wavefield will be used to illustrate the depth-imaging capability of these long-offset, P-SV data. For brevity, the adjective "radial" will be dropped when referring these P-SV data.

Interpretation Effort: Shelf-B

The depth positions of Horizon 1 and Horizon 2 were interpreted along a total of 3,700 line miles (~5,900 km) of OBC profiles across the Shelf-B survey. Because two images (P-P and P-SV) were interpreted along each profile, our research findings across the Shelf-B area represent 7,400 mi (~11,800 km) of data interpretation. The positions and lengths of the long-offset OBC profiles interpreted across Shelf-B are defined on the map displayed as Figure 18.

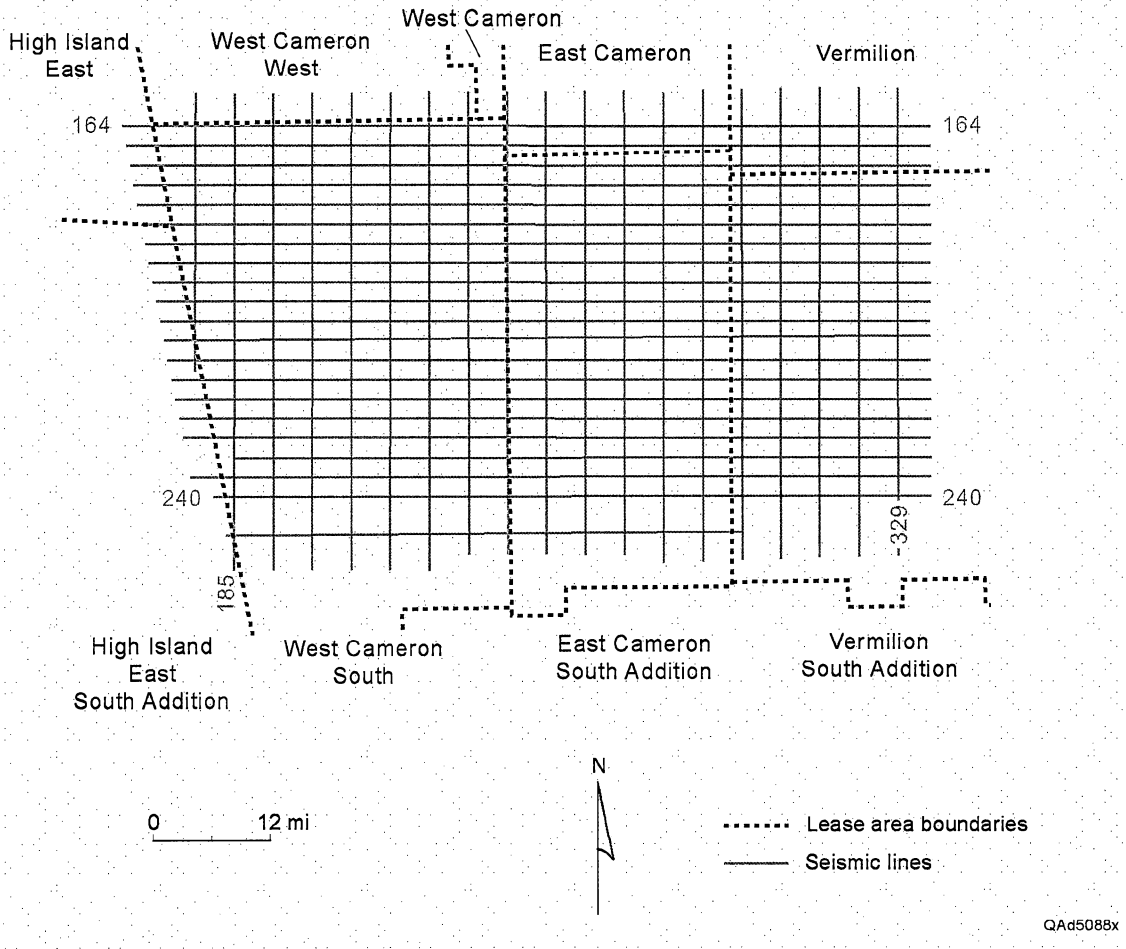

Figure 18. Interpreted OBC profiles across the Shelf-B survey.

Selected Seismic Profiles: Shelf-B

Profile 1: P-P and P-SV Data

Image quality of long-offset Shelf-B data will be illustrated along profiles that traverse the full east-west and north-south dimensions of the Shelf-B survey. The first example is a north-south profile in the west part of the Shelf-B survey. The P-P image along this profile is displayed in Figure 15. The profile is 45 mi (72 km) long, and a 10-km scale bar is positioned on the image to represent the dimension of the longest source-receiver offset used in processing the data. This maximum-offset scale bar can be compared with the physical sizes of the salt structures and rotated fault blocks along the profile to identify locations where the seismic propagation velocity can be expected to change laterally over distances similar in magnitude to the maximum data-processing offset and thus affect the accuracy of deep imaging.

The profile shows that there is a thick sediment accumulation in the northern one-third of the image space where Horizon 2 drops down to

approximately 10 s. This sediment load squeezes the Jurassic salt southward, causing several salt structures to punch upward through overlying, younger strata as shown by the salt-flow arrows. This salt movement creates numerous en echelon, rotated fault blocks. The depth of shallower Horizon 1 is controlled to a great extent by the vertical depth to the tops of the various salt structures along the profile. The definition of the base of continuous P-P reflections (Horizon 1) in the north portion of the profile is arbitrary. If desired, Horizon 1 could be positioned deeper at the north end of the seismic line than where it is shown in Figure 15. The exact vertical position of Horizon 1 in P-P image space is not too critical because the surface is a data-quality indicator, not a geologic horizon.

The 10-s image times of the deepest P-P reflections on this profile are considerably deeper than the maximum P-P seismic imaging depths observed with "conventional" seismic data in the area (Figs. 11 through 14). Interpreters have to acknowledge that these long-offset OBC data image much deeper geology than do seismic reflection data acquired to date over the northern GOM shelf.

In the north portion of this profile, a **salt weld** should be located somewhere near Horizon 1, where underlying salt has evacuated and flowed south. Common seismic attributes of a salt weld are labeled with the numbers **1**, **2**, **3** on the data display and have the following meanings:

1. Events above the weld are usually discordant with events below the weld,
2. The signal-to-noise ratio is often low in the data window that encompasses the weld, and
3. Events below the weld tend to be lower frequency.

The P-SV image along example Profile 1 is illustrated in Figure 16. If this image is compared with its companion P-P image (Fig. 15), P-SV Horizon 1 is approximately at the same image-time depths as P-P Horizon 1 (about 5 s) across the profile. Locally, P-P Horizon 1 and P-SV Horizon 1 differ. The important point is that in a broad perspective, the two horizons are essentially depth equivalent. This observation is a key principle. Many explorationists do not yet know how deep P-SV data can be applied. This data comparison provides critical information suggesting that P-SV data provide continuous, mappable reflections to the same depths as P-P data. A second point to emphasize is that local differences between P-P Horizon 1 and P-SV Horizon 1 are important only if these horizons are structural surfaces. Because the horizons are indicators of reflection quality (specifically indicating the base of deepest continuous reflections) and not structure surfaces, local differences between P-P Horizon 1 and P-SV Horizon 1 are not critical.

A different situation exists for Horizon 2. It is difficult to find an appreciable number of P-SV events at image times significantly below P-SV Horizon 1. Only a few short segments of deep P-SV events are labeled on Figure 16. In contrast, the P-P data contain numerous deep Horizon 2 events (Fig. 15). The lack of P-SV events near the super-deep depths of P-P Horizon 2 does not reduce the value of P-SV data for evaluating deep drilling targets in the GOM basin. After the image times of Horizon 1 are converted to depth (Fig. 27), Horizon 1 will turn out to be

located at the deepest depths (~9 km [30,000 ft]) that operators now wish to drill across the northern shelf of the GOM shelf.

Profile 2: P-P and P-SV Data

A second data comparison is a north-south profile in the east part of the Shelf-B grid. P-P and P-SV images along this profile are shown as Figures 19 and 20, respectively. This profile is located about 60 mi (96 km) east of the profile shown in Figures 15 and 16. Comparison of these new P-P and P-SV images leads to the same conclusions as for the first profile, namely

- Good-quality continuous reflections extend down to 5 and 6 s for both the P-P and the P-SV modes (Horizon 1 in the figures),
- A thick section of sediment extends down to 10 s along the north quarter of the profile,
- P-P data image deeper strata within the northern, thick, sediment mass than do the P-SV data, and
- The thick sediment load at the north end of the profile causes deep Jurassic salt to flow south and to form numerous salt structures and salt-driven, rotated fault blocks.

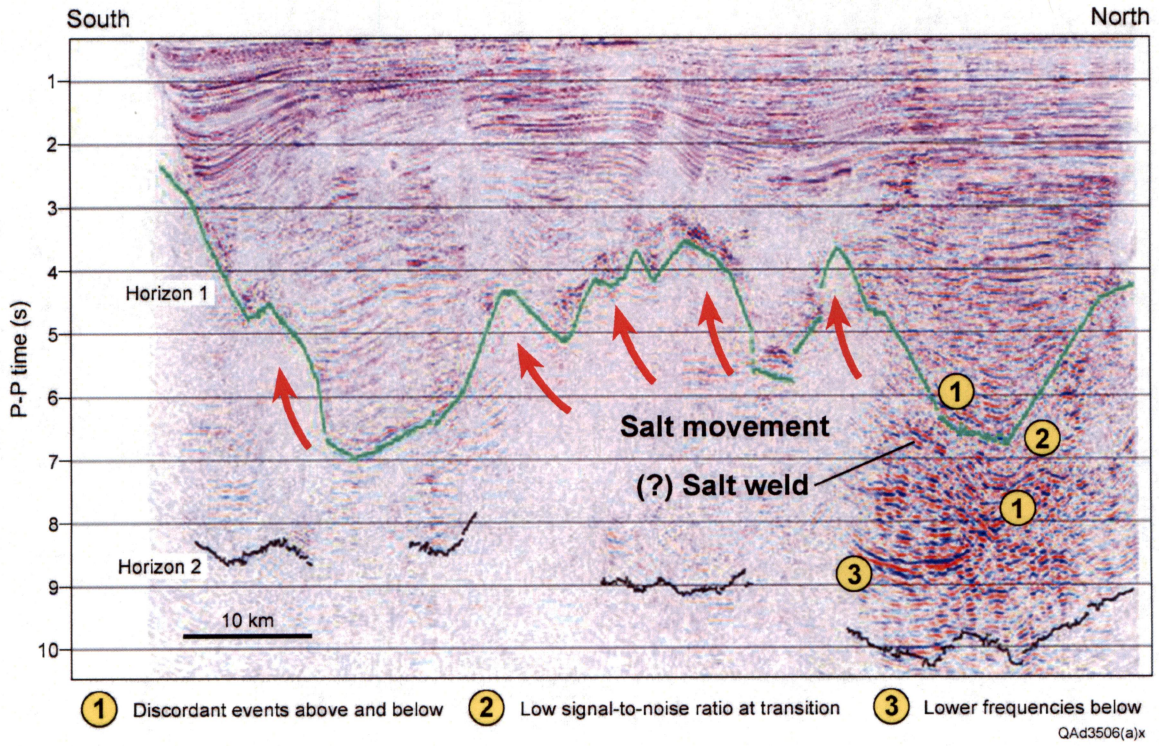

Figure 19. P-P image from the eastern portion of the Shelf-B survey.

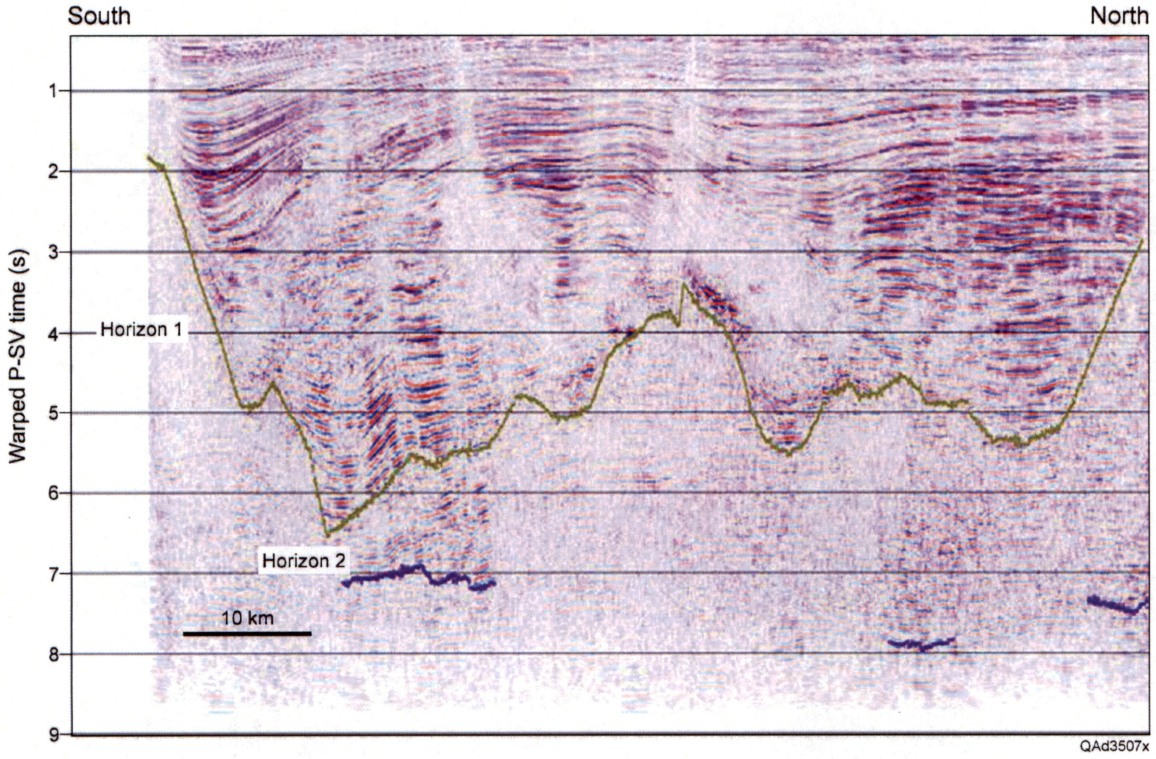

Figure 20. P-SV image from the eastern portion of the Shelf-B survey. This image should be compared with its companion P-P mode in Figure 19.

Profile 3: P-P and P-SV Data

A third illustration of the deep-imaging capability of Shelf-B long-offset data is an east-west profile across the north part of the survey, where the two preceding profiles indicate that there is a thick sedimentary section extending to 10 s image time. The P-P and P-SV images produced along this profile are exhibited as Figures 21 and 22. This profile is about 75 mi (120 km) long. Again, a 10-km scale bar is added to each image to indicate the maximum source-receiver offset used in processing the data. The position of Horizon 1 on each image is subjective, as previously stated. Four interpreters at the Bureau of Economic Geology reviewed all of the interpreted profiles, debated where to position Horizon 1, and ended up with the surfaces positioned as shown in Figures 15 through 22. Note that good-quality P-SV reflections extend to deeper depths at the east end of this profile (Fig. 22). Horizon 2 is rather definitive for the P-P data and oscillates between 9 and 10 s across the entire length of the profile. As was the case for the preceding north-south profiles (Figs. 15 – 20), a deep Horizon 2 is difficult to find in the P-SV data. Short intervals of deep P-SV events are shown in Figure 22 at image times of 7 to 8 s, which places these reflections at depths of about 13 km (42,000 ft).

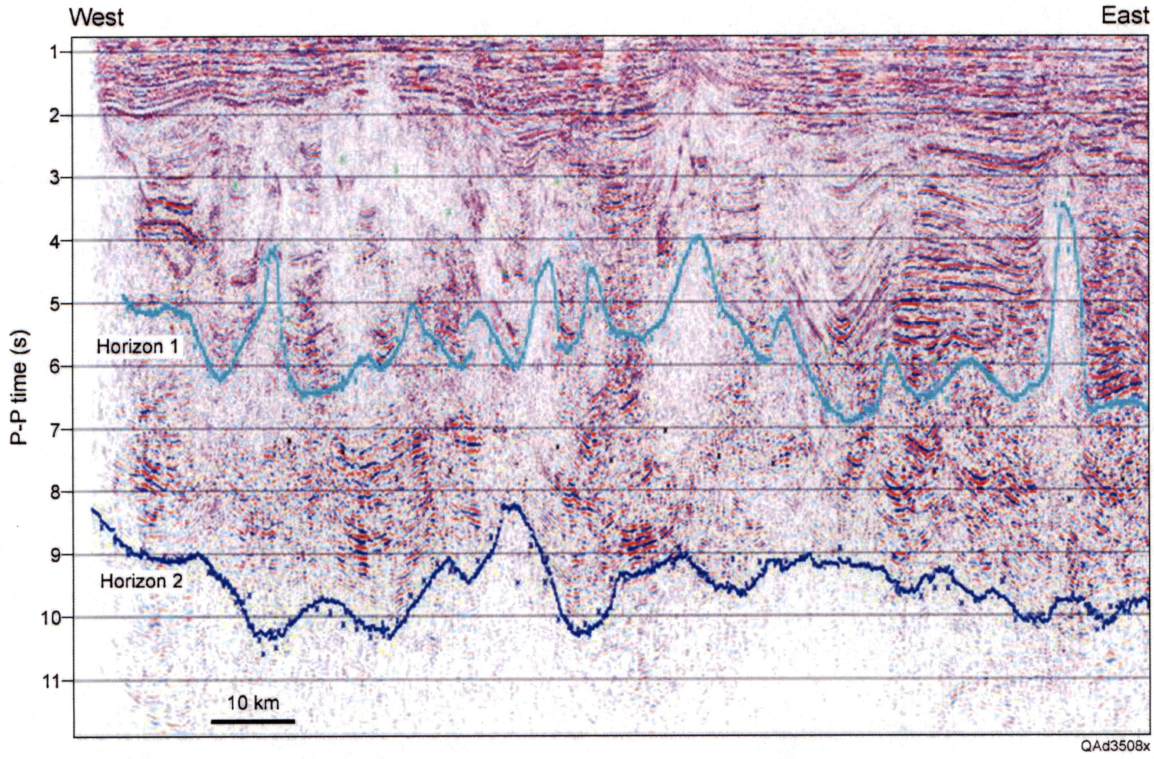

Figure 21. P-P image from the northern area of the Shelf-B survey.

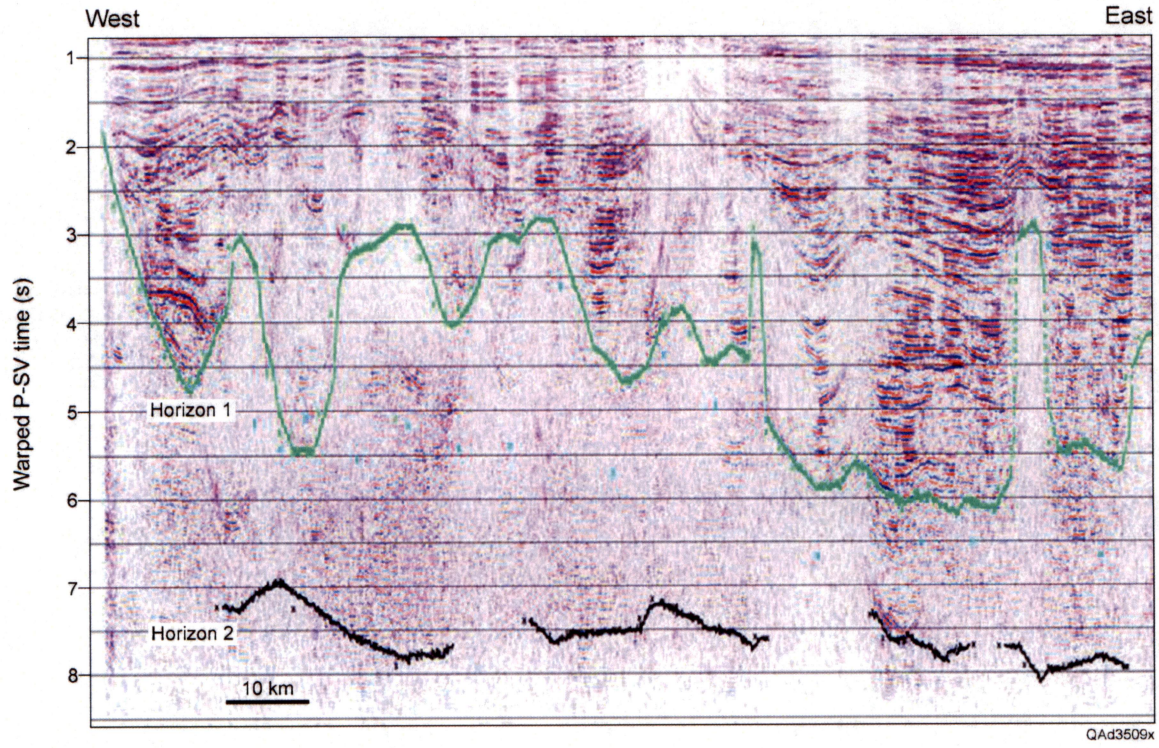

Figure 22. P-SV image from the northern area of the Shelf-B survey. This image should be compared with its companion P-P mode in Figure 21.

Time-Based Maps of Seismic Data Quality: Shelf-B

North-south and east-west lines were interpreted across the Shelf-B survey so that maps of seismic data quality could be constructed across the complete survey area. The maps that should be of most interest to GOM-basin drillers are those that indicate depths to the base of continuous, good-quality reflections because this information can assist the planning of seismic programs across GOM prospects. Image times to the base of continuous P-P reflections are displayed in Figure 23. The equivalent image-time map to the base of continuous P-SV reflections is shown as Figure 24.

Comparing these maps confirms that P-P and P-SV data image GOM geology to equivalent depths, in a general sense, across the entire Shelf-B survey. Locally there are differences in the depths to which each mode produces continuous reflection events. It must be stressed again that these maps are not structure maps. Rather, they are simply map depictions of Horizon 1 illustrated on the preceding seismic profiles, which is a horizon that cuts across geologic time surfaces. The maps are what the captions say they are: maps that indicate the P-P image-time coordinates of good-quality P-P and time-warped P-SV reflection signals.

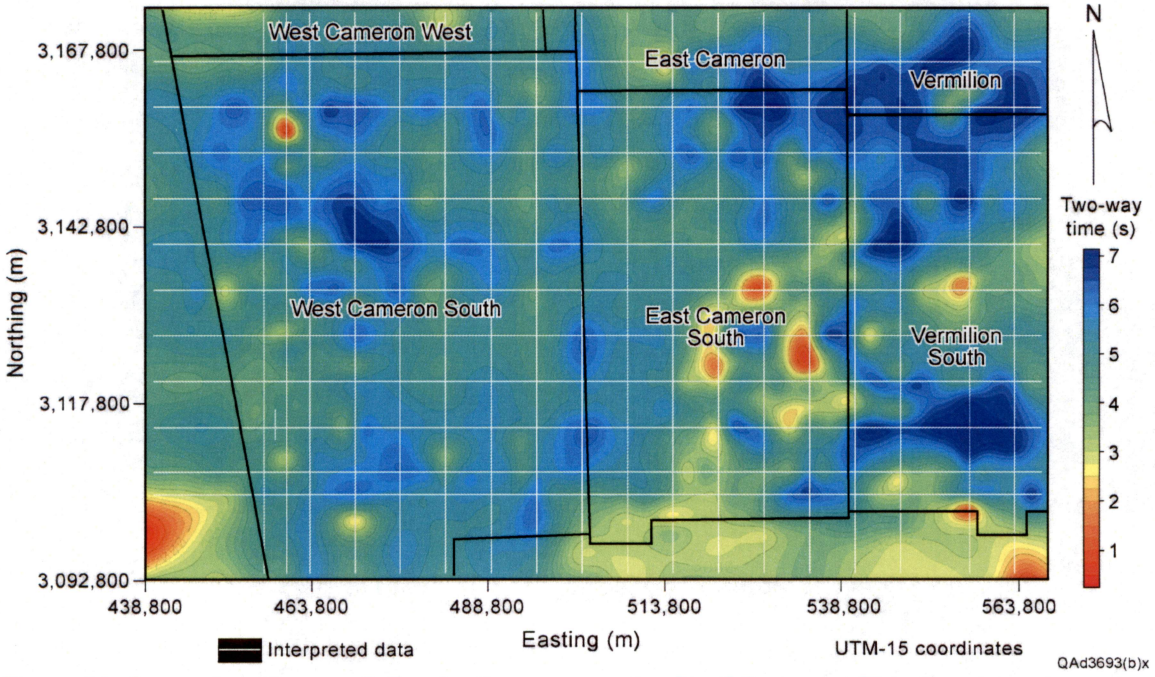

Figure 23. Base of continuous P-P reflections across the Shelf-B survey. This time-based map is not a structure map. The mapped horizon (Horizon 1, Figs. 15, 19, 21) crosses geologic time lines. The map indicates only seismic data quality.

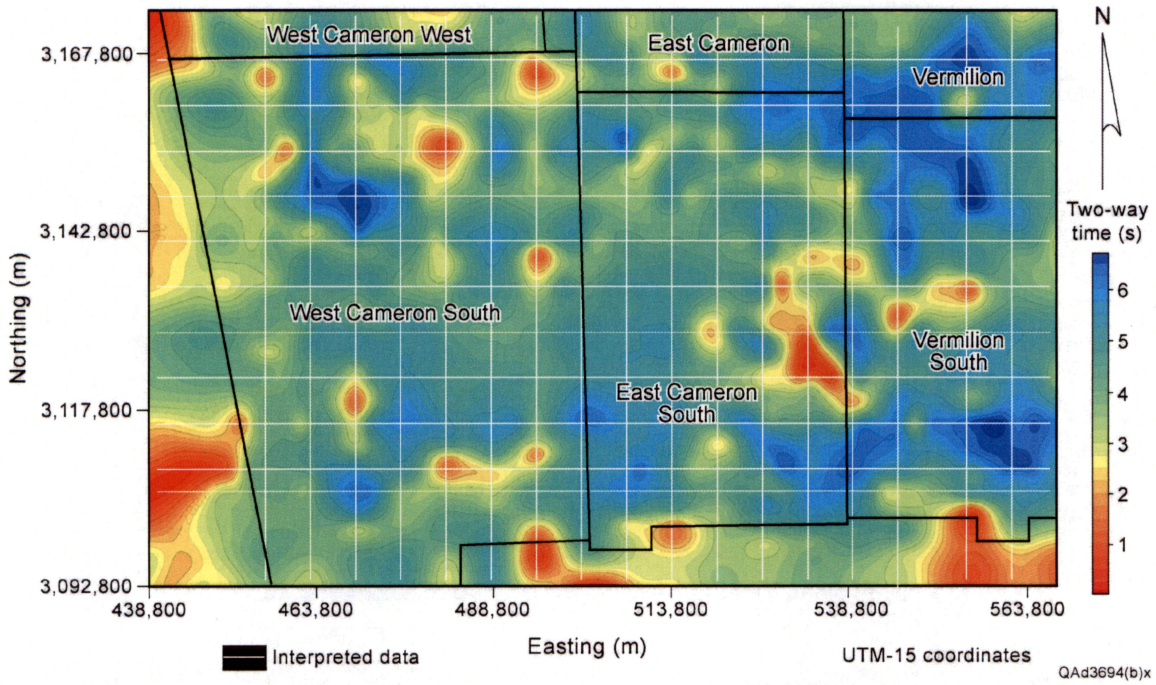

Figure 24. Base of continuous P-SV reflections across the Shelf-B survey. This time-based map is not a structure map. The mapped horizon (Horizon 1, Figs. 16, 20, 22) cuts across geologic time boundaries. The map should be used only as an indicator of seismic data quality.

P-P Seismic Velocities: Shelf-B

The time-based maps in Figures 23 and 24 need to be converted to depth maps for the depth imaging capabilities of long-offset P-P and P-SV data to be better appreciated. The transformation from image time to depth was done using seismic velocities determined during seismic data processing. Examples of P-P rms velocities determined across the Shelf-B survey area are shown in Figures 25 and 26. Arbitrary north-south and east-west profiles of these seismic-based velocities are displayed to give a sense of the velocity behavior beneath the Shelf-B seismic grid. The velocity values for the deeper velocity layers on these profiles do not approach the V_P value of 7.6 km/s (23,000 ft/s) that Sawyer and others (1991) used to define the Moho. The velocity layering exhibits major vertical oscillations and thickness changes in the image-time interval between 3 and 6 s, where propagating wavefields first encounter salt-related structures.

The 10-km scale bar on each velocity profile is helpful for recognizing locations along the profile where lateral velocity variations occur over distances of the same dimensions as the positive-offset and negative-offset ranges used in processing the Shelf-B data. Lateral velocity changes of this physical scale will complicate deeper imaging. Below 6 s, the velocity layering is reasonably smooth and uniform. All velocity layers drop deeper at the north end of the profile (Fig. 25), where the thickest sediment accumulation is encountered and no high-velocity salt is present (Figs. 15 and 19).

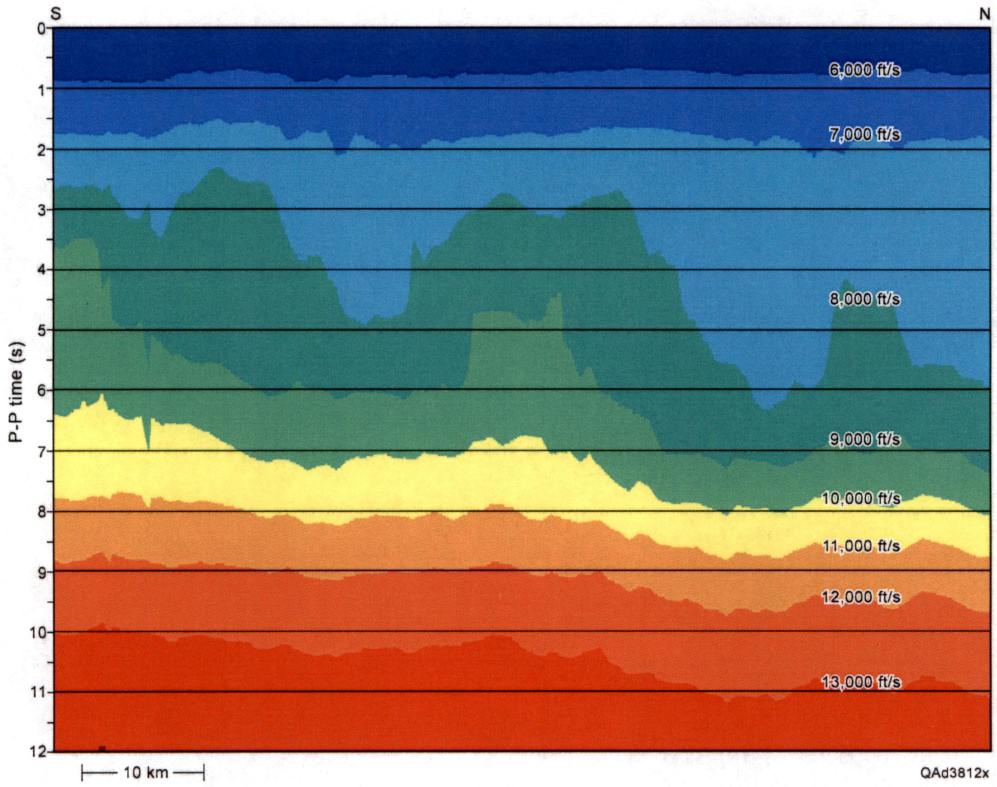

Figure 25. Arbitrary north-south profile showing P-P rms velocities across the Shelf-B survey.

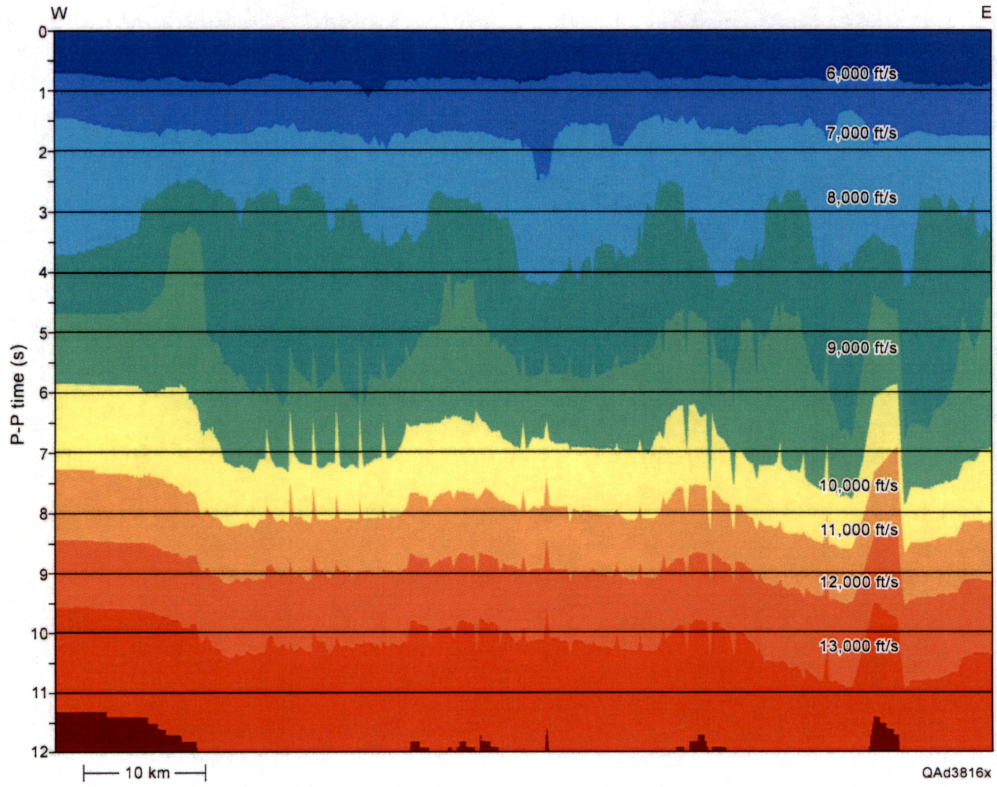

Figure 26. Arbitrary east-west profile showing P-P rms velocities across the Shelf-B survey.

Depth Maps of Seismic Data Quality: Shelf-B

Seismic-derived rms velocities like those illustrated in Figures 25 and 26 were available for every seismic line of the Shelf-B survey. The complete velocity database was input to Landmark's TVD software package to convert the time-based maps of seismic reflection quality (Figs. 23 and 24) to depth maps. The resulting depth-converted maps are displayed as Figures 27 and 28.

The basic message provided by these depth maps is critical information for explorationists operating in the GOM basin; namely, long-offset 4-C OBC data can provide good-quality P-SV and P-P reflection images of GOM geology to depths of 30,000 ft (9 km). The fact that good-quality, continuous P-P reflections extend down to 30,000-ft targets is not surprising. The fact that equivalent-quality P-SV reflections are obtained for these same target depths is new and important information.

It is again important to emphasize that these depth maps are not structure maps. Each mapped surface cuts across geologic ages. The maps must be viewed only as definitions of the depths to the base of continuous, good-quality, P-P and time-warped P-SV seismic reflection events.

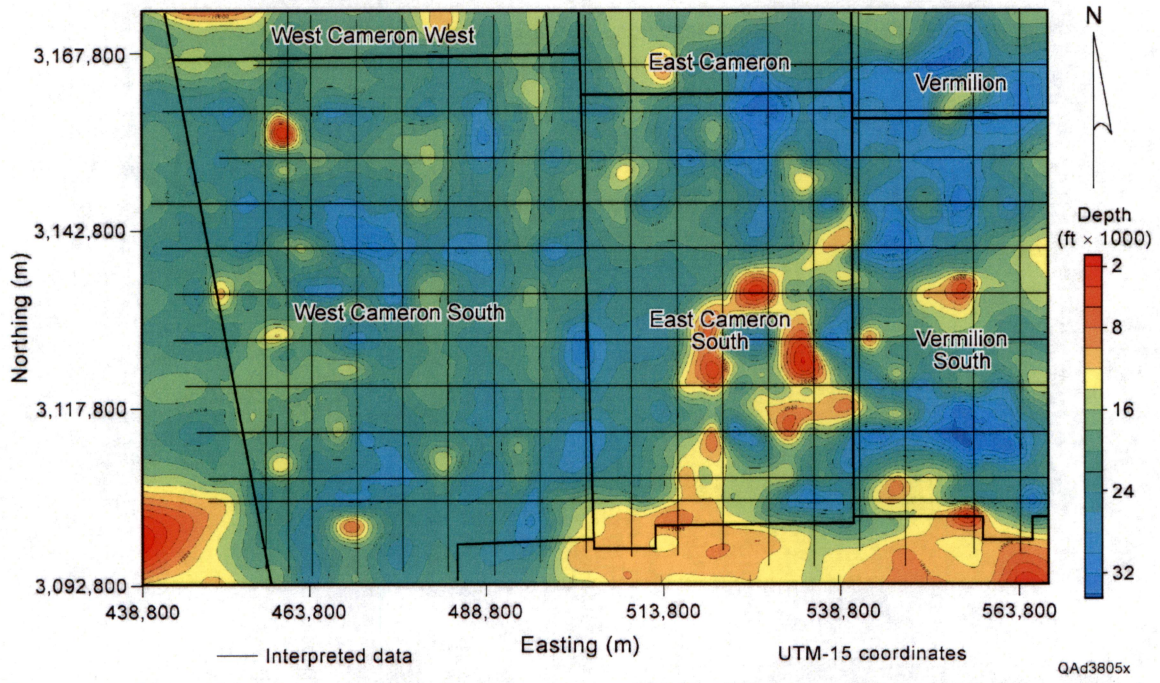

Figure 27. Base of continuous P-P reflections across the Shelf-B survey. This depth-based map is not a structure map. The mapped surface (Horizon 1, Figs. 15, 19, 21) crosses numerous geologic time boundaries. The map indicates only depths to which continuous, good-quality P-P data can be acquired.

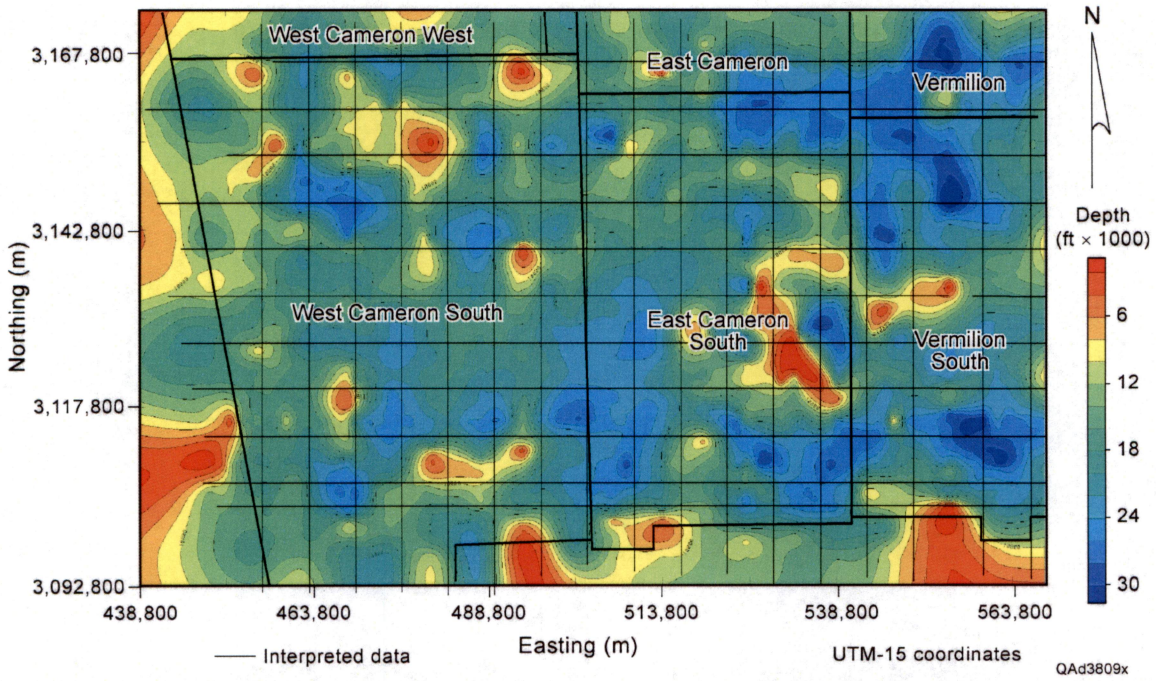

Figure 28. Base of continuous P-SV reflections across the Shelf-B survey. This depth-based map is not a structure map. The mapped horizon (Horizon 1, Figs. 16, 20, 22) follows no fixed geologic time or formation. The map indicates only depths to which continuous, good-quality P-SV data can be obtained.

Super-Deep Imaging: Shelf-B

The Shelf-B long-offset seismic data provide a unique opportunity to image super-deep GOM geology beneath the salt province where the Shelf-B survey is located. The illustration of this super-deep imaging will be limited to the P-P seismic mode because the preceding examples of image quality along the selected Shelf-B profiles show that although the P-SV mode provides some super-deep information, that information is restricted to smaller, more-segregated patches than is the super-deep information provided by the P-P mode.

The time-based map of P-P Horizon 2, the base of *discontinuous* P-P reflections, is illustrated in Figure 29. The blank patches are areas where the deepest P-P reflection signal occurs above 7 s, the shallowest image-time value allowed with the color bar selected for this display. These earlier-time terminations of P-P reflection signal are caused by shallow, vertically extensive salt bodies, not by seismic data-acquisition or data-processing limitations.

The corresponding depth map of the base of super-deep P-P reflections is shown as Figure 30. Reflections from depths of 60,000 ft (18 km) occur at numerous locations beneath the Shelf-B survey. An east-west trend of 60,000-ft reflection depths extends across the north edge of the survey, corresponding to the deep 10-s image times of P-P Horizon 2 noted on the example profiles (Figs. 15, 19, and 21).

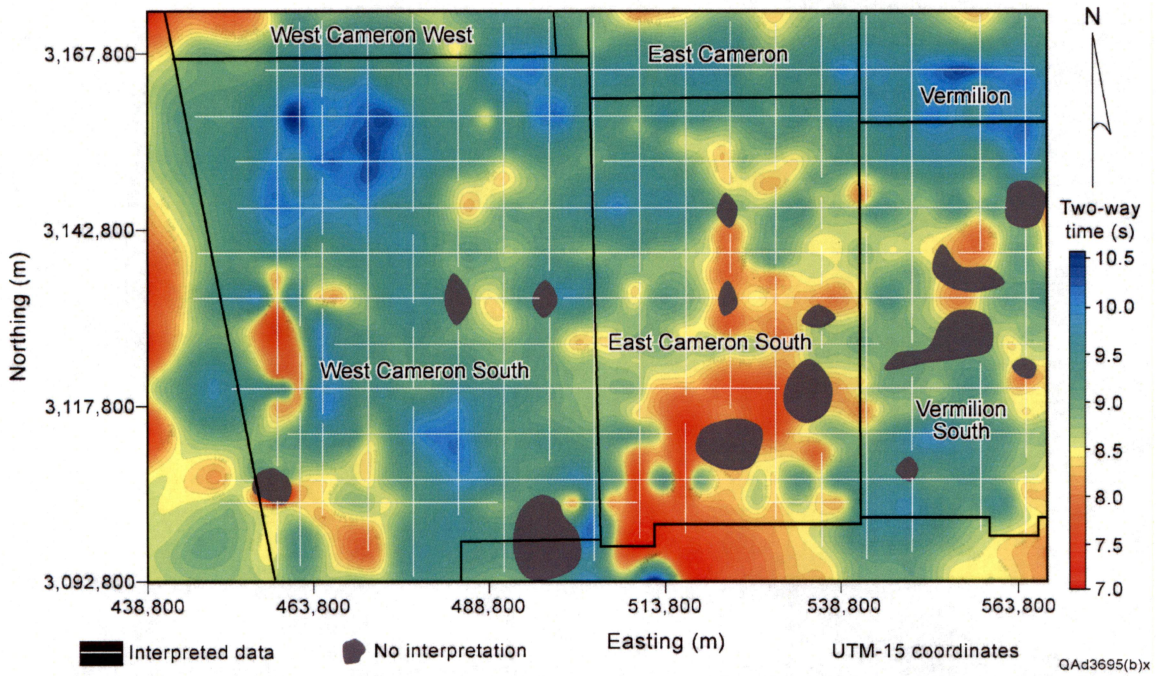

Figure 29. Base of discontinuous P-P reflections across the Shelf-B survey. This time-based map of Horizon 2 (Figs. 15, 19, 21) is not a structure map. It indicates only the traveltimes from which the deepest discontinuous P-P reflection signal was acquired.

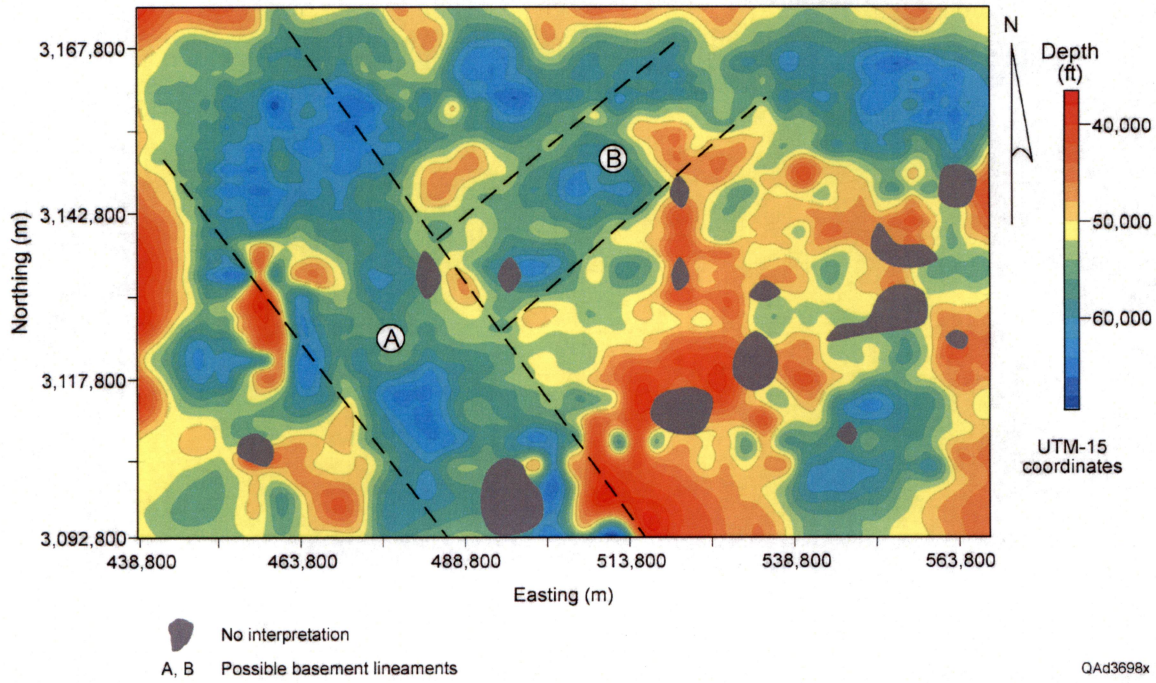

Figure 30. Base of discontinuous P-P reflections across the Shelf-B survey. This depth-based map of Horizon 2 (Figs. 15, 19, 21) is not a structure map. It indicates only the depths from which the deepest discontinuous P-P reflection signal was acquired. Compare deep, linear trends **A** and **B** with the labeled basement lineaments in Figure 5.

Seismic-Imaged Basement Lineaments

Dashed lines bracketing two trends of deepest reflection depths are drawn across the map in Figure 30. Corridor **A** trends northwest-southeast; corridor B trends northeast-southwest. Corridor **A** aligns with "**Lineament 1**" labeled on the Tectonic Map of the World (Fig. 5). Corridor **B** is aligned in the same way as is the feature labeled "**Orthogonal Lineament**" on the map. Do these deepest P-P reflection trends indicate basement lineaments beneath the Shelf-B survey? This question cannot be answered with certainty, but the possibility that they do is intriguing.

Deep-Imaging Summary: Shelf-B

In summary, the Shelf-B long-offset data image deeper strata in the GOM basin than what previous investigators thought was possible. Conventional wisdom has been that deepest P-P reflections extend to 6 s and maybe 7 s (Figs. 11 and 13) and that the thickest sediment is about 15 km thick or maybe as much as 20 km (Figs. 7, 8, 9, and 14). The Shelf-B long-offset P-P data image to 10 s and show sedimnentary strata to depths of 18 km. Even the long-offset P-SV data image geology to depths of 7 s or 42,000 ft (~13 km) in some areas, which is beyond the maximum image times and imaging depths proposed by conventional wisdom (Figs. 8 through 14).

Elastic Wavefield Stratigraphy and Seismic Facies: Shelf-B

Super-deep geology at the depths described by the P-P Horizon 2 map of Figure 30 is beyond current drilling interest. Even the depths of P-SV Horizon 2 reflections (~42,000 ft) exceed the drilling depths now planned by GOM operators. Most (all?) deep-drilling targets across the Shelf-B area of the GOM shelf are at depths near or above P-P and P-SV Horizon 1. Several examples of P-P and P-SV images at deep, but drillable, target depths will be illustrated in this section to document that long-offset 4C OBC seismic data allow **elastic wavefield stratigraphy** to be applied to deep drilling targets (Hardage and others, 2006).

This documentation will be done by positioning P-P and time-warped P-SV data side-by-side to aid comparisons of P-P and P-SV **seismic facies**. In these data comparisons, either one feature (labeled **A**) or two features (**A** and **B**) in both image spaces will be interpreted to be depth-equivalent and are highlighted. Comparing these labeled-letter features will demonstrate the accuracy to which time warping has adjusted the P-SV data to the same image-time coordinates as the P-P data. Several seismic facies features across the P-P and P-SV image spaces will then be labeled with numbers (**1**, **2**, **3**, . . .). These labeled-number features emphasize some type of stratigraphic or structural information that is obvious in one image space but not in the companion image space, which is the fundamental principle of elastic wavefield stratigraphy. The physical basis for a P-

P mode imaging different stratal surfaces and facies than does the P-SV mode will be discussed in the section *Rock Physics*.

Seismic Facies: Example 1

The first example of the application of elastic wavefield stratigraphy and seismic facies principles to deep GOM geology is chosen from the west part of the Shelf-B survey. The selected data window, displayed in Figure 31, has a base at a depth of about 5.6 km (18,500 ft). The dipping strata defined by reflection package **A** in each image space are interpreted to be depth-equivalent geology. In this instance, the spatially invariant time-warping function (Fig. 17) positions **A** about 200 ms too early in time-warped P-SV image space. Even so, depth-equivalent P-P and P-SV structure and stratigraphy can be identified between the two image spaces. Event **1** indicates a facies that is better imaged by the P-P mode than by the P-SV mode. Events **2** through **5** are facies that are better imaged by the P-SV mode than by the P-P mode. The fact that one mode of a multicomponent seismic wavefield images stratal surfaces that are not seen by its companion wave modes is the attraction for acquiring multicomponent seismic data across a prospect area and is the fundamental principle of elastic wavefield stratigraphy (Hardage and others, 2006).

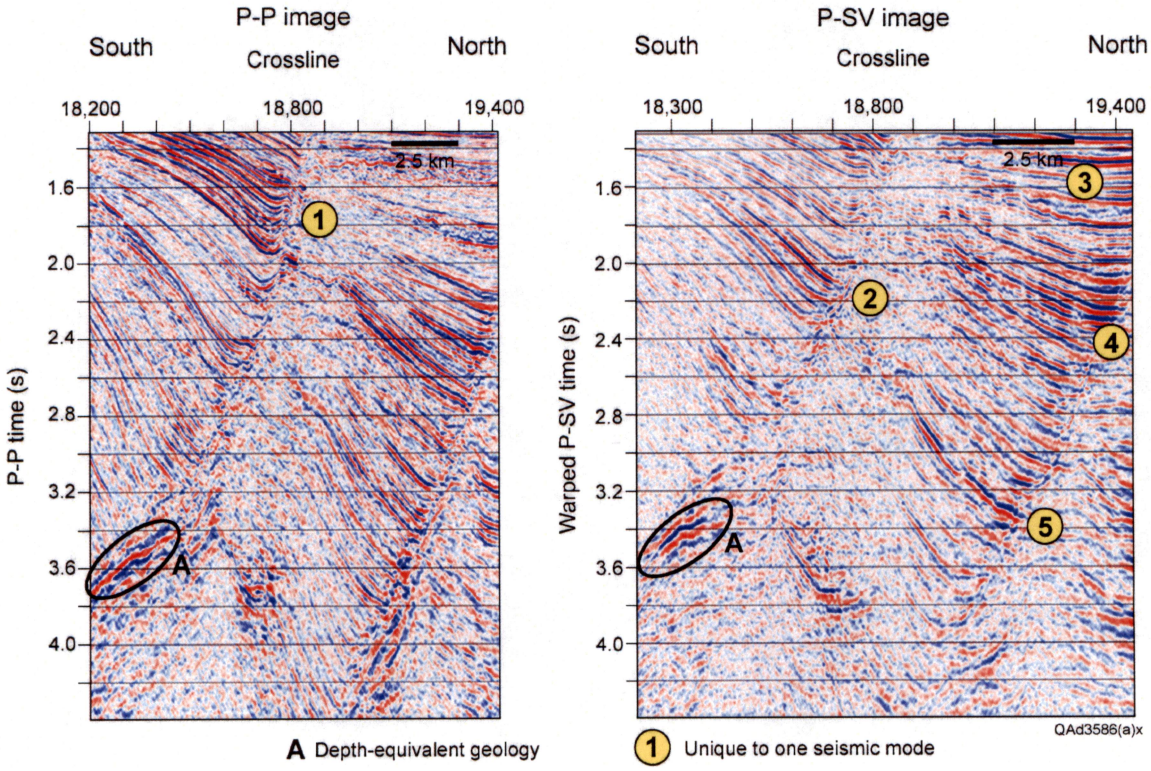

Figure 31. Comparison of deep, depth-equivalent, P-P and P-SV seismic facies in the western part of the Shelf-B survey.

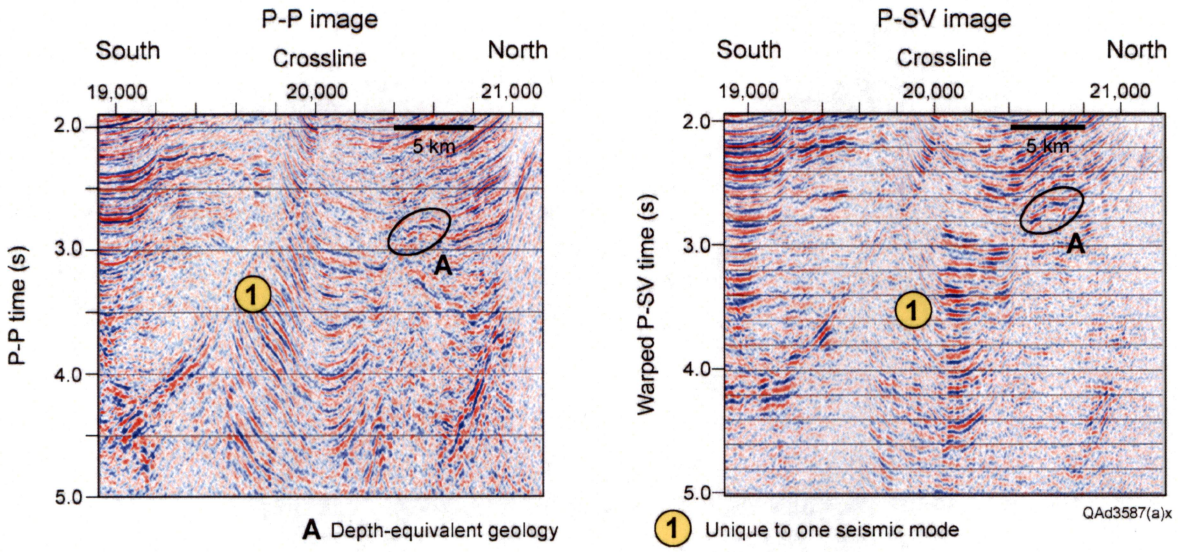

Figure 32. Comparison of deep, depth-equivalent, P-P and P-SV seismic facies in the central part of the Shelf-B survey. Compare this steep-dip imaging with that of Figure 36.

Seismic Facies: Example 2

Example 2 (Fig. 32) used to illustrate the application of elastic wavefield stratigraphy to deep geology and seismic facies concepts is from the central part of the Shelf-B survey. This data window extends to a depth of about 6.3 km (21,000 ft). The small anticline-like feature defined by reflection package **A** in each image space is interpreted to be depth-equivalent geology. Again, the time-warping function places event **A** in P-SV image space about 200 ms higher than where it is in P-P image space. Event **1** demonstrates an important aspect of P-P and P-SV wave physics for steep-dip imaging. Positive-offset P-SV data often provide an image of steep-dip strata that differs from the image provided by negative-offset P-SV data. In the processing of P-SV data, positive-offset data and negative-offset data are processed separately and imaged separately. Near the end of the data-processing sequence, positive-offset and negative-offset images are summed to make a total-offset image. It is not uncommon for one of these half-offset P-SV images, either the positive-offset data or the negative-offset data, to image some steep-dip strata better than the other half-offset image does. Neither is it uncommon for this particular half-offset image to show the steep-dip target better than the total-offset image does. All P-SV images used in this discussion are total-offset images. Feature **1** in Figure 32 is an example in which a total-offset P-SV image does not depict steep dips in the same way as do P-P data. For a more acceptable depiction of structural dip to be inserted into P-SV image space, the solution is sometimes as simple as inspecting the positive-offset P-SV image and the negative-offset P-SV image and selecting the half-offset image that optimizes

the P-SV steep-dip strata. This example may cause some interpreters to assume that CMP-based P-P data provide a more reliable image of dipping strata than do CCP-based P-SV data. However, a later example (Fig. 36) will illustrate a situation where P-SV data show dipping strata better than P-P data do.

Seismic Facies: Example 3

Example 3 is from the north part of the Shelf-B survey and is shown in Figure 33. The base of this data window is about 18,000 ft (~5.5 km). Reflection packages **A** and **B** are interpreted to be depth-equivalent geology. Here the time warping places **A** and **B** in P-SV time-warp space within 100 ms of their positions in P-P image space. Interval **1** indicates a lithofacies pattern that is better seen by the P-P data than by the P-SV data. Reflection sequences **2** and **3** are important examples because they document a situation in which P-SV data image deep lithofacies contrasts better than P-P data do.

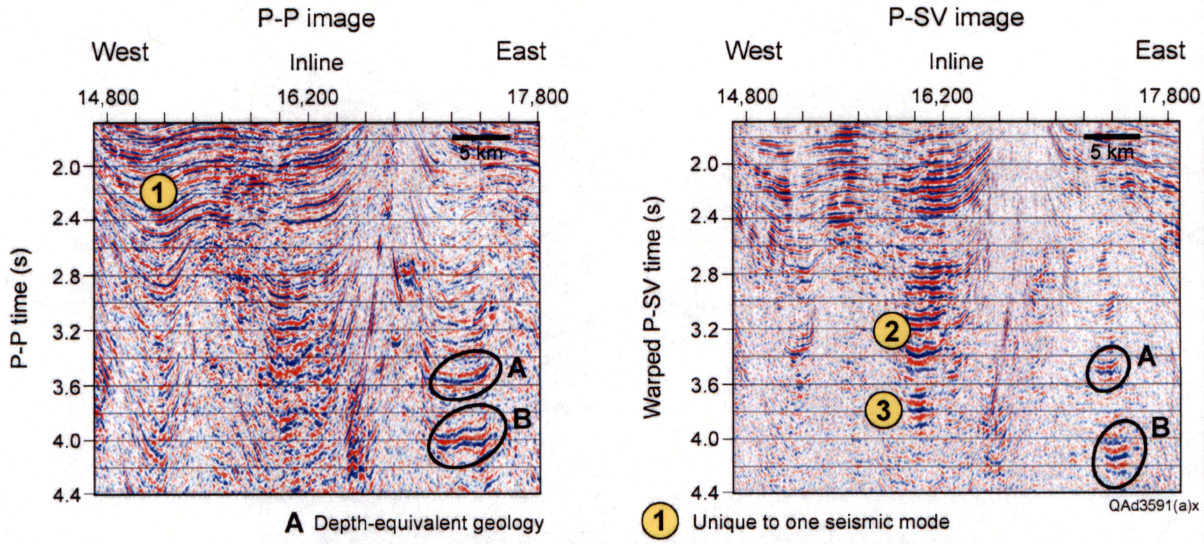

Figure 33. Comparison of deep, depth-equivalent P-P and P-SV seismic facies in the northern area of the Shelf-B survey.

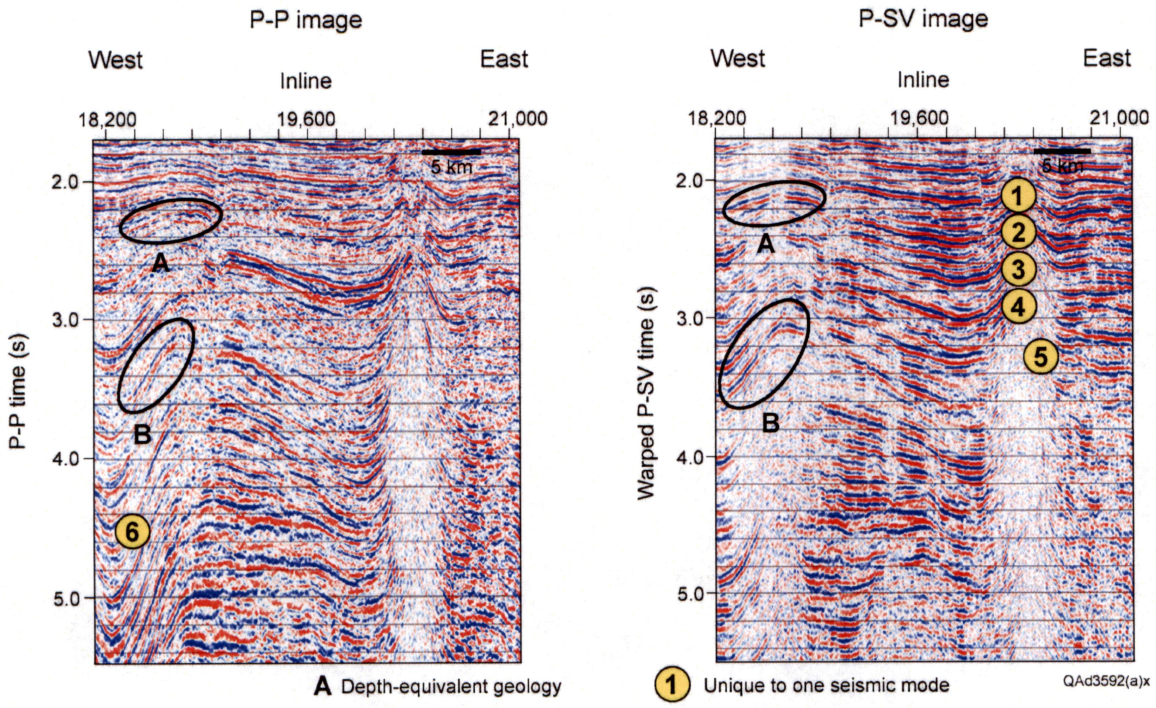

Figure 34. Comparison of deep, depth-equivalent P-P and P-SV seismic facies in the northern area of the Shelf-B survey.

Seismic Facies: Example 4

Example 4 is from a second area in the north part of the survey. The selected data window (Fig. 34) extends to almost 24,000 ft (~7.3 km). Structural features **A** and **B** are interpreted to be depth-equivalent. The time-warping process positions **A** and **B** in time-warped P-SV space to within 100 ms of their positions in P-P image space. A narrow, vertical salt structure blanks out both P-P and P-SV images between CDP coordinates 19,600 and 21,000. Features **1** through **4** on the P-SV image indicate a cyclic depositional process that is not obvious in the P-P image. Feature **5** is an example of P-SV data showing a facies interval that is not present in the P-P data.

Seismic Facies: Example 5

Example 5 in Figure 35 is from the south part of the survey and images to a depth of about 18,000 ft (~5.5 km). Reflection package **A** labeled on each image is interpreted to be depth-equivalent geology. In this part of the survey, the time-warp transform is quite accurate, and reflection **A** is at the same image coordinate in both data spaces. High-amplitude event **1** in P-P image space is caused by a pore-fluid variation, and the event is absent in the P-SV image, as it should be. Strata packages **2** through **5** are examples of P-SV data imaging deep sequences better than P-P data do.

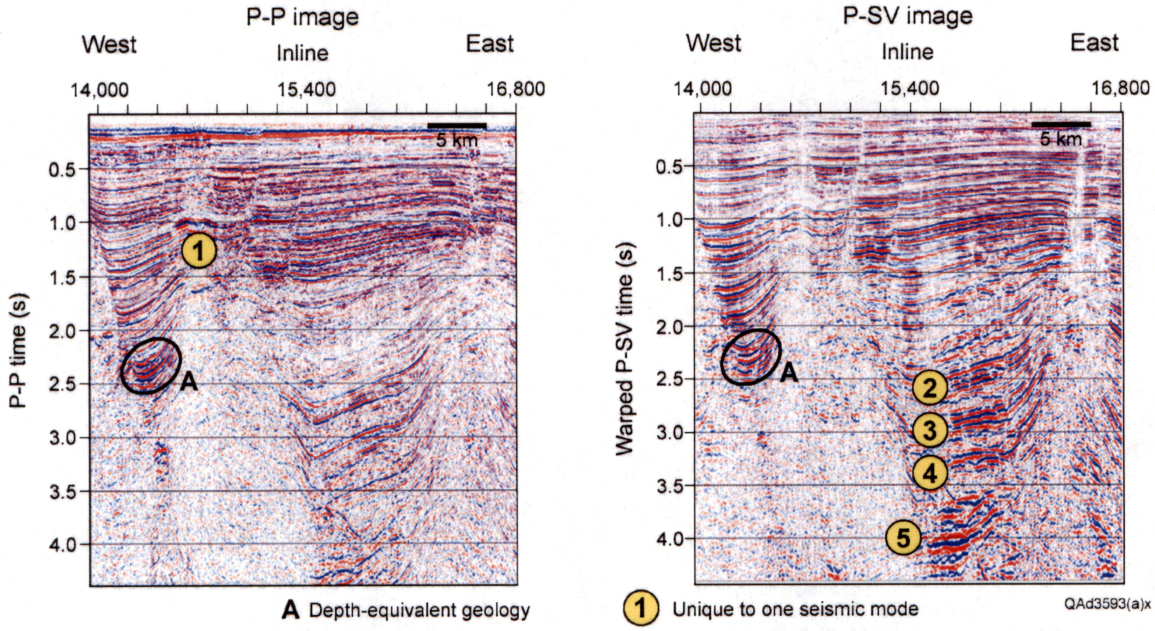

Figure 35. Comparison of deep, depth-equivalent P-P and P-SV seismic facies in the southern part of the Shelf-B survey.

Seismic Facies: Example 6

Example 6 is taken from a second target area in the south part of the survey and is shown as Figure 36. This data window is shallower, about 13,000 ft (~4 km) and is not a "deep" target. However, these data show steep-dip imaging that is needed to balance the observations about steep-dip imaging that were made for Example 2 (Fig. 32). Syncline features **A** and **B** are interpreted to be depth equivalent. The central part of each image is affected by a local salt structure. The P-SV image provides more geologic information east of this salt structure than does the P-P image, as indicated by labeled features **1** through **5**. Note that in this case, the P-SV data image steep dips on the east flank of the salt structure better than the P-P data do. This steep-dip imaging contrast between P-P and P-SV data is opposite that illustrated in Figure 32.

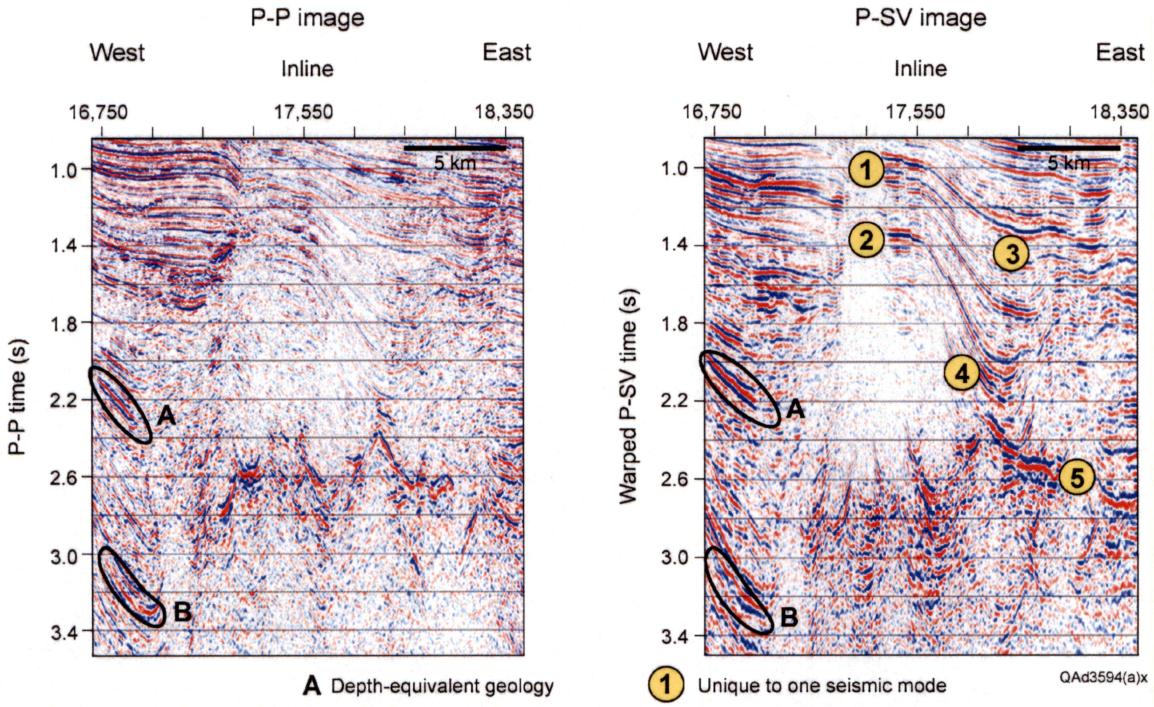

Figure 36. Comparison of shallower, depth-equivalent P-P and P-SV seismic facies in the southern part of the Shelf-B survey. Compare this steep-dip imaging to that in Figure 32.

Seismic Facies: Example 7

The last example is from the east side of the survey. This selected data window in Figure 37 extends to a depth of only 8,000 ft (2.4 km) and does not image deep geology. This shallow window was chosen because it contains an excellent example of the distinction between P-P seismic stratigraphy and P-SV seismic stratigraphy. Reflections **A** and **B** are interpreted to be depth-equivalent stratal surfaces. The time-warp transform positions **A** and **B** in time-warp P-SV data space at the same positions where they occur in P-P image space. P-SV features **1** and **2** define a sequence geometry that is absent in the P-P data. An interpreter using only P-P seismic data would construct a system architecture at this depth that differs fundamentally from the system architecture that would result if both P-P and P-SV data were used in a seismic-stratigraphy analysis. The fact that over some stratigraphic intervals, one seismic mode of a multicomponent seismic wavefield sometimes images different stratal surfaces, different seismic sequences, or different seismic facies than do other modes of that wavefield is the basis of the new seismic interpretation science, elastic wavefield stratigraphy, promoted by the Bureau of Economic Geology (Hardage and others, 2006). Feature **3** is an example of the P-SV mode imaging a facies system not easily seen in the P-P image.

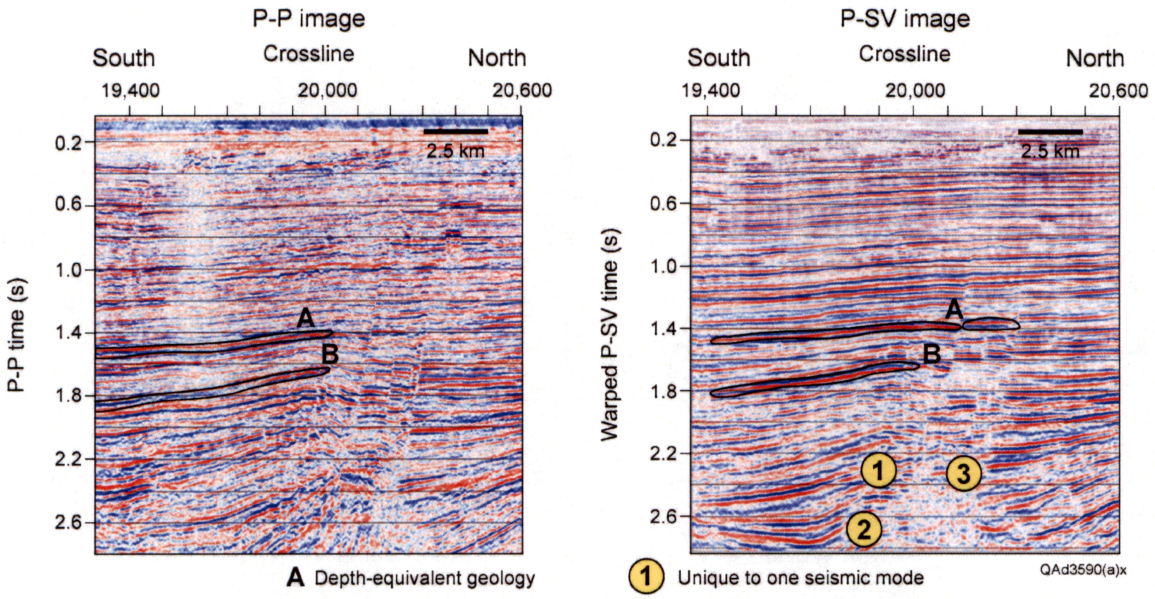

Figure 37. Comparison of shallow, depth-equivalent P-P and P-SV seismic facies in the eastern part of the Shelf-B survey. These data are a classic example of the principle of elastic-wavefield seismic stratigraphy.

Interpretation Effort: Shelf-C

The positions and lengths of OBC seismic lines interpreted across the Shelf-C survey are shown in Figure 38, with the boundaries of major lease block areas superimposed. Collectively, these lines total to 3,700 mi (~5,900 km). Both P-P and P-SV images were interpreted along each profile, making a total of 7,400 mi (~11,800 km) of line interpretations. Although the Shelf-C survey spans a larger are area than the Shelf-B survey, the number of line miles of data in each survey is essentially identical. The Shelf-C survey has a greater north-south dimension than the Shelf-B survey because the east-west profiles across Shelf-C are spaced at intervals of 4 mi (6.4 km); whereas, they are spaced at intervals of 2 mi (3.2 km) across Shelf-B (Fig. 18). Profiles through the central part of the survey will be used to illustrate data quality and the depth positions of Horizon 1 and Horizon 2 in P-P and P-SV image spaces.

Selected Seismic Profiles: Shelf-C

Data across Shelf-B and Shelf-C were processed by different data-processing teams. The Shelf-B team extended the P-P and P-SV images to 12 s. The Shelf-C team also extended the P-P image time along each profile to 12 s, but they arbitrarily muted all P-SV images below 8 s of P-SV warped time. Although we would prefer that this muting of the P-SV images had not been done, the muted data do not negatively impact our objective of determining the depth imaging limit of continuous P-SV reflections across the Shelf-C area for two reasons. First, 8 s of P-P image time equates to a depth range of 40,000 to 45,000 ft (12 to 14 km),

which is far below the maximum drilling depth now being considered across the northern shelf of the GOM (~30,000 ft [~9km]). Second, massive salt deposits beneath the Shelf-C area limit the effective image time to 5 s or 6 s across most of the survey.

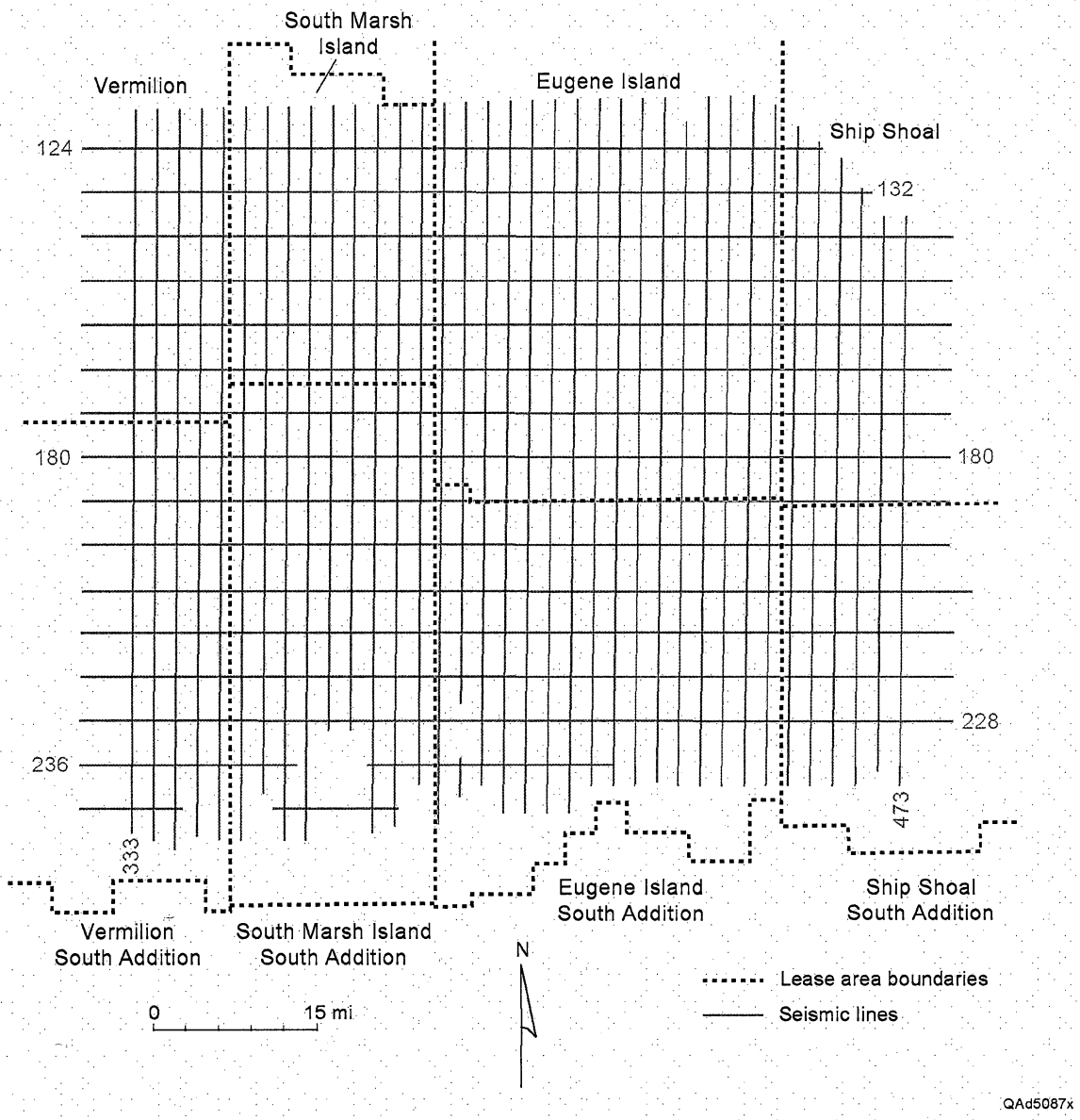

Figure 38. Interpreted OBC profiles across the Shelf-C survey.

Sub-salt reflections are not well imaged by either the P-P or the P-SV wave mode because studying deep sub-salt geology was not an objective of the Shelf-C data acquisition and processing. Even so, there are occasional glimpses of subsalt reflections that allow the depths of Horizon 2 to be estimated across the survey coverage.

Profile 1: P-P and P-SV Data

Uninterpreted and interpreted versions of the P-P image along Profile 1 are exhibited as Figure 39. The equivalent P-SV data are illustrated as Figures 40. In general, the depth position of Horizon 1 in P-SV image space is equivalent to its depth position in P-P image space. Locally, the position of Horizon 1 in P-P image space differs from its position in P-SV image space by small amounts. Our fundamental research finding is that, in general, P-SV data across Shelf-C provide good-quality images to the same depths as P-P data, which along this profile is ~5 s or about 22,500 ft (~6.8 km).

Evidence for Horizon 2 could be found at deeper depths in P-P image space than in P-SV image space as is shown by the positions of Horizon 2 in Figures 39 and 40. However, in each image space, Horizon 2 was too fragmented to conclude if there is an imaging advantage of either wave mode over its companion wave mode at the deep sub-salt depths of that horizon.

Profile 2: P-P and P-SV Data

The preceding comments about Profile 1 apply also to the P-P and P-SV images along Profile 2 shown in Figures 41 and 42. One distinction between Profile 2 and Profile 1 is that Horizon 1 along Profile 2 is, in general, slightly deeper than it is along Profile 1. For Profile 2, Horizon 1 in both P-P and P-SV image space was interpreted to be at an image time of ~6 s (~28,500 ft [~8.7 km]). This deeper imaging along Profile 2 occurs because the top of salt is a bit deeper beneath Profile 2 than it is below Profile 1.

Time-Based Maps of Seismic Data Quality: Shelf-C

Horizon 1 was interpreted along the full extent of each of the Shelf-C OBC profiles shown on the map in Figure 38. These horizon interpretations were done for both the P-P image and for the P-SV image along each line, similar to the manner these interpretations are demonstrated in Figures 39 through 42. These interpretations defined the depths of both P-P Horizon 1 and P-SV Horizon 1 in terms of P-P image time across the Shelf-C survey. From these interpretations, we then constructed the time-based maps of P-P Horizon 1 shown as Figure 43 and its companion time-based map of P-SV Horizon 1 displayed as Figure 44.

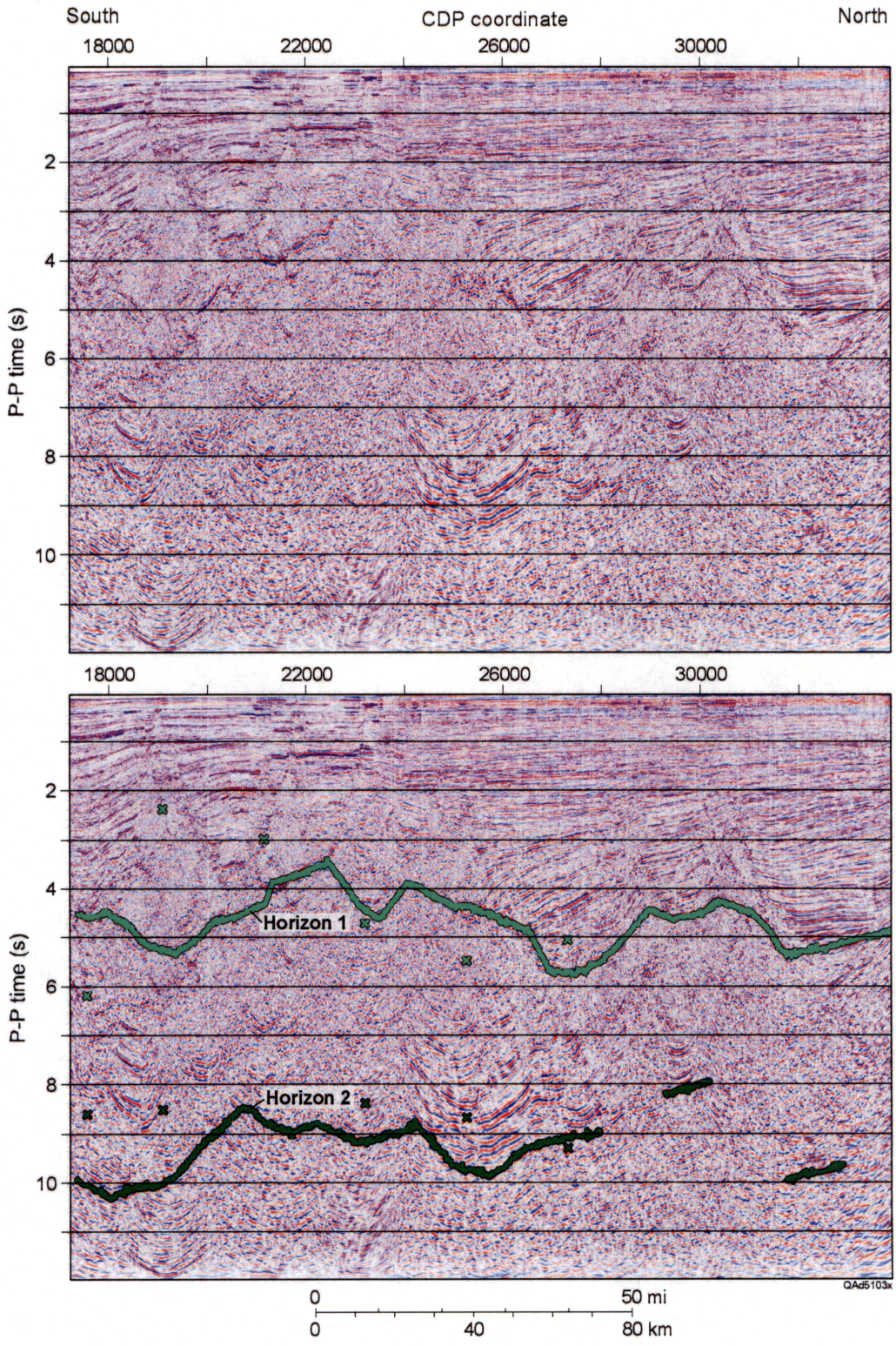

Figure 39. P-P image along Profile 1, east-central portion of the Shelf-C survey. (Top) Uninterpreted data. (Bottom) Interpreted data.

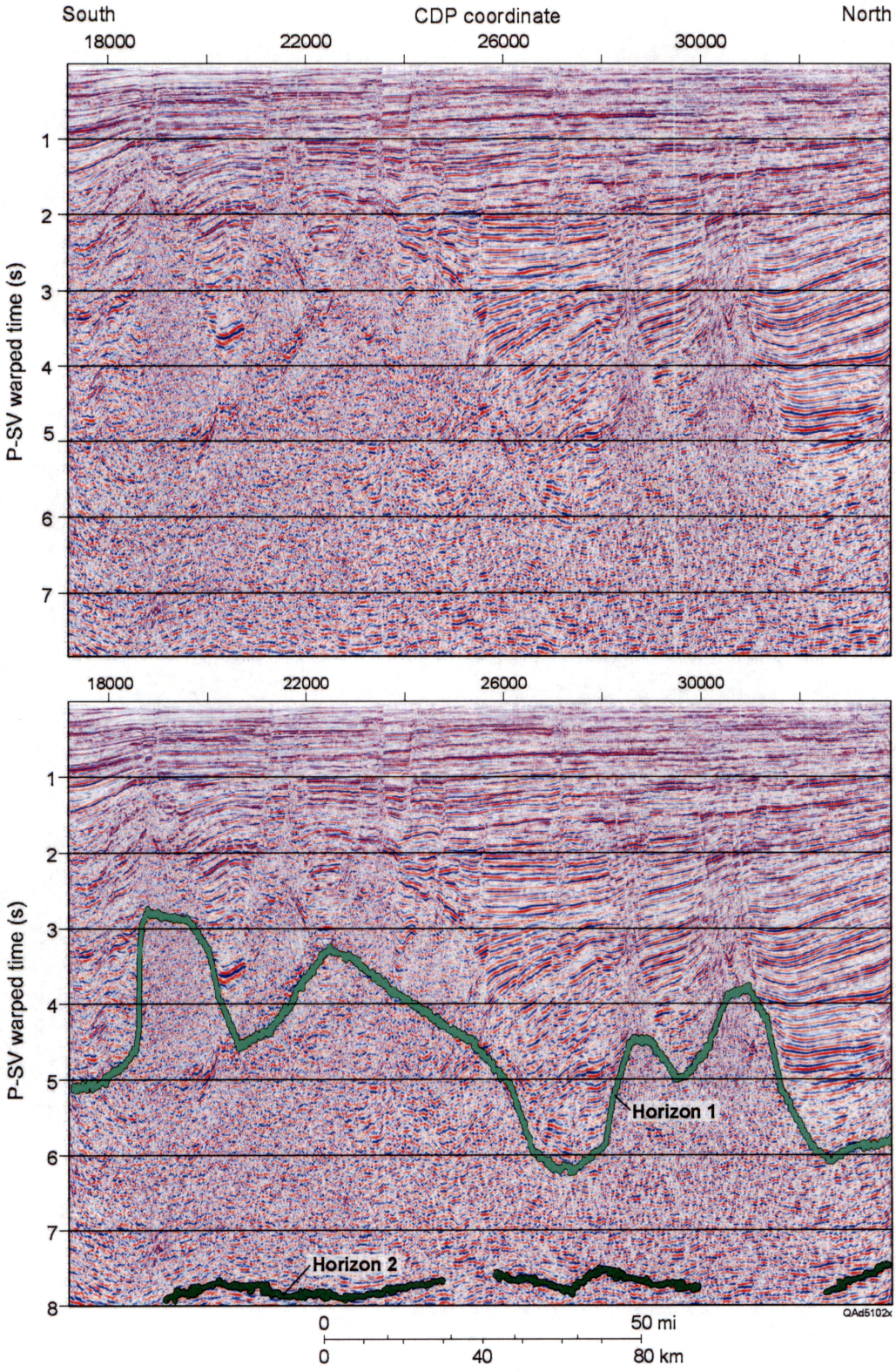

Figure 40. P-SV image along Profile 1, east-central portion of the Shelf-C survey. (Top) Uninterpreted data. (Bottom) Interpreted data.

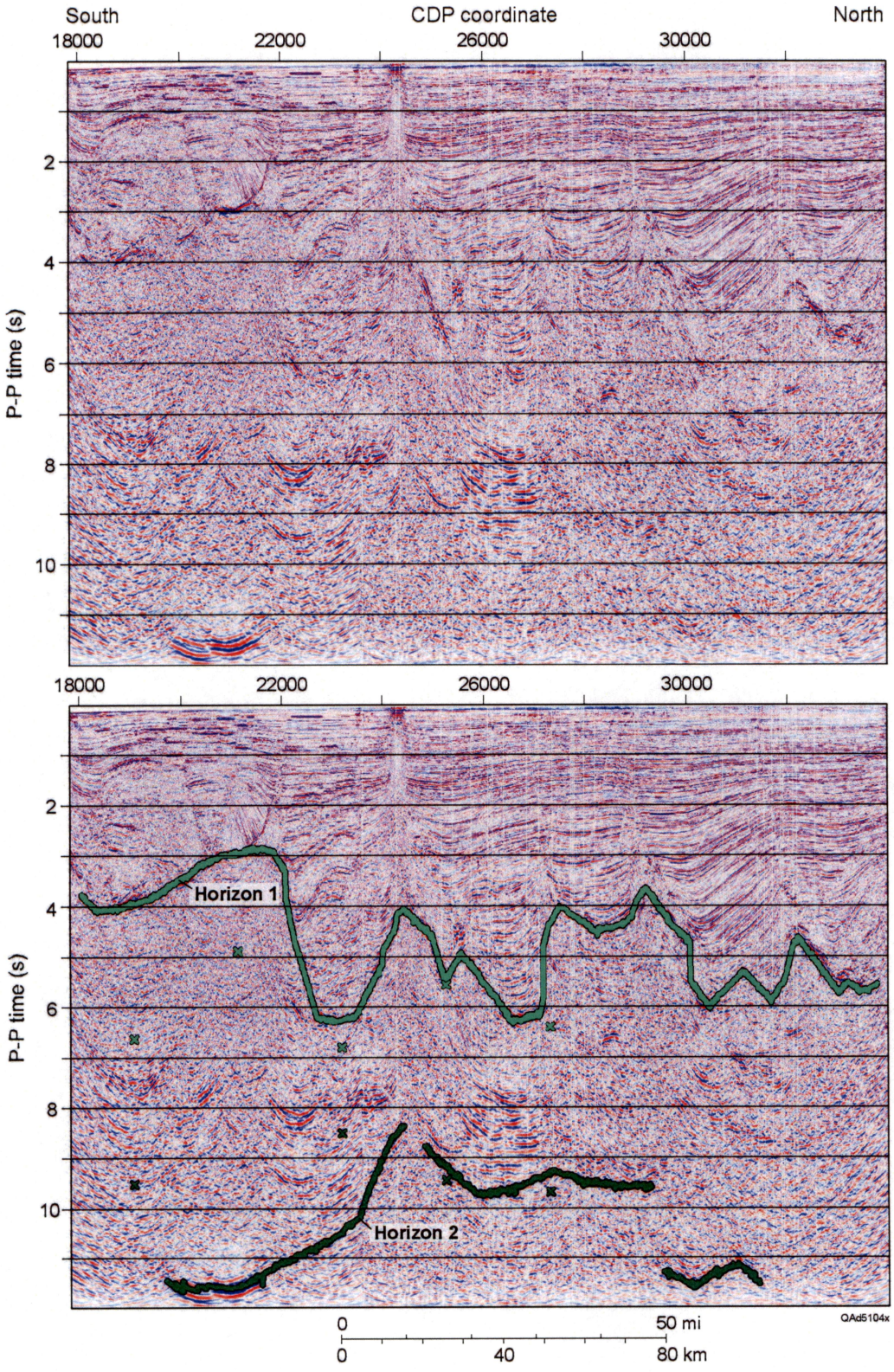

Figure 41. P-P image along Profile 2, west-central portion of the Shelf-C survey. (Top) Uninterpreted data. (Bottom) Interpreted data.

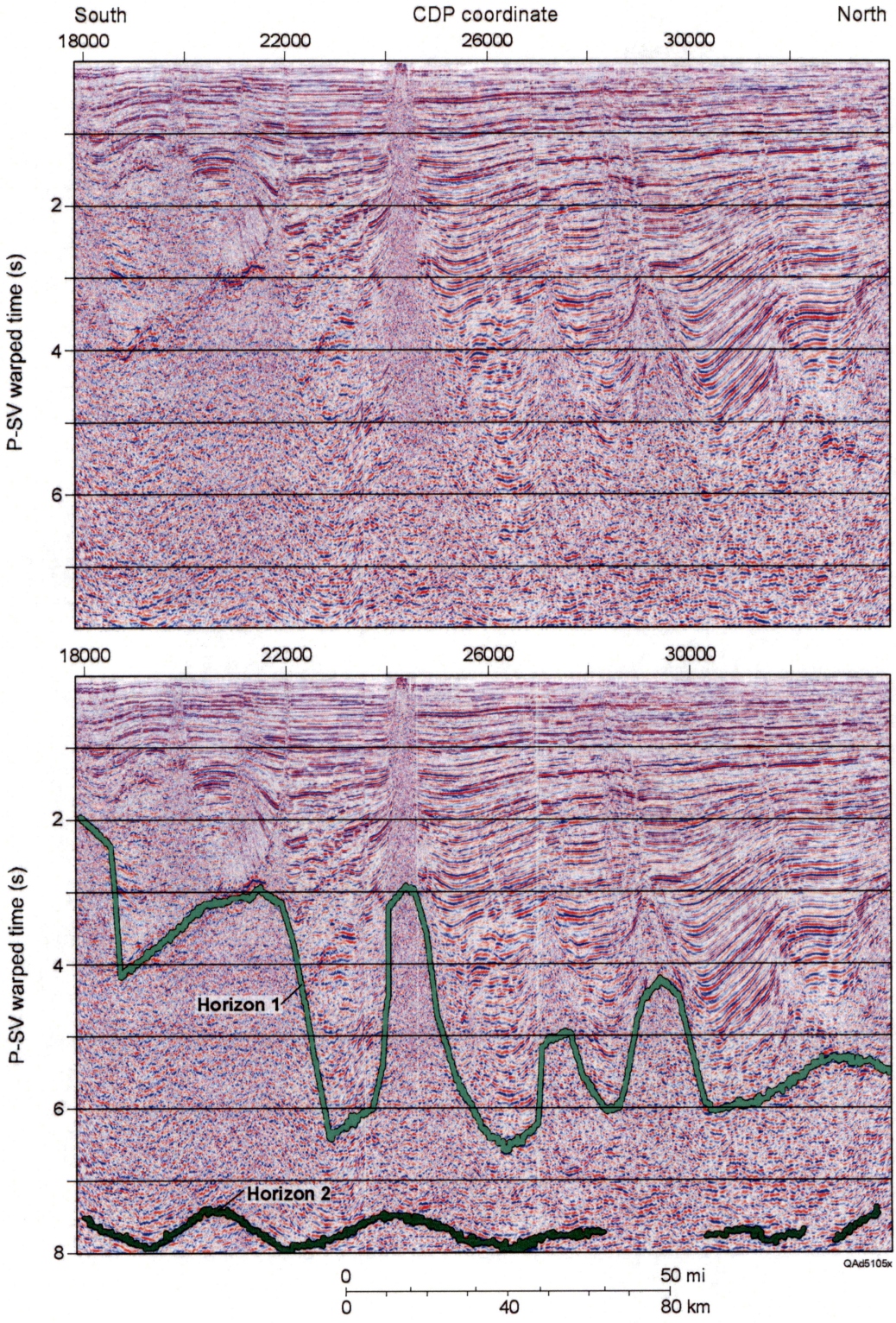

Figure 42. P-SV image along Profile 2, west-central portion of the Shelf-C survey. (Top) Uninterpreted data. (Bottom) Interpreted data.

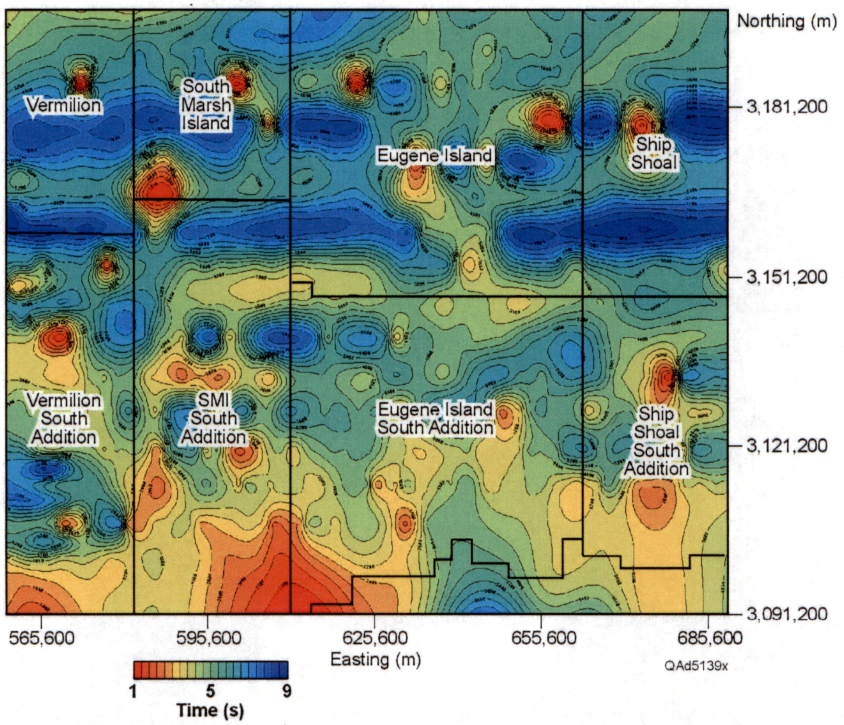

Figure 43. Time structure map, base of continuous P-P reflections, Shelf-C.

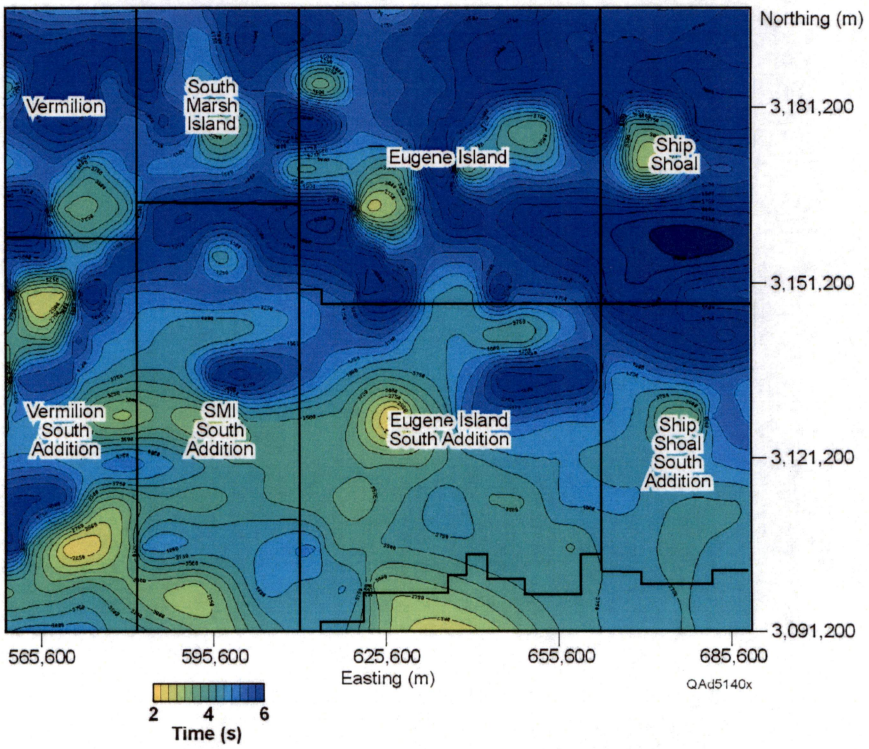

Figure 44. Time structure map, base of continuous P-SV reflections, Shelf-C.

By comparing these maps with their equivalents across Shelf-B (Figs. 23 and 24), we make two conclusions.

1. In general, continuous P-SV events extend to the same depths as continuous P-P events, and
2. the depths of Horizon 1 across each image space (P-P and P-SV) of the Shelf-C survey are approximately the same as they are across the Shelf-B area.

Both the P-P map (Fig. 43) and the P-SV map (Fig. 44) show there is a deep sediment trough extending east-to west near the southern boundaries of the Ship Shoal, Eugene Island, South Marsh Island, and Vermilion leased areas. Only along this deep-trough trend do P-P data provide significantly deeper continuous images (~8 s) than do P-SV data (~6 s). The base of continuous reflections becomes much shallower (up to ~3 to 4 s) in both P-P and P-SV image spaces across the south half of the Vermilion South Addition, South Marsh Island South Addition, Eugene Island South Addition, and Ship Shoal South Addition lease areas where the top of the regional salt layer is closer to the seafloor. This shallower depth to the top of salt is caused by the weight of the sediment load in the deep east-west trough just mentioned (shown ~60 km to the north on these time-structure maps). This sediment load has squeezed salt to the south and caused the top of salt to punch upward toward the seafloor in several locations as is indicated by the seismic profiles in Figures 15 and 19.

A time-based map of Horizon 2 in P-P image space is plotted on Figure 45. This map was constructed from the sparse, sporadic segments of Horizon 2 that could be estimated across a few segments of each OBC line, similar to the appearance of Horizon 2 shown in Figures 39 through 42. The accuracy and validity of this Horizon 2 map is questionable. The evidence of a deep Horizon 2 was so weak in P-SV image space, that no P-SV time structure map of the base of discontinuous P-SV reflections was made. We include the P-P map in this report only to document the thoroughness of our investigation. We do not intend to use this map to reconstruct super-deep geology beneath the Shelf-C area

P-P Seismic Velocities: Shelf-C

Horizon 1 defines the maximum depth of continuous reflection signal for the two elastic wave modes, P-P and P-SV. The time-based maps of Horizon 1 plotted in Figures 43 and 44 need to be converted to depth maps in order for gas operators in the Shelf-C area to know if P-P and P-SV data acquired with long-offset OBC technology will define geology at the deepest target depths that they wish to drill. Accurate P-P rms velocities are required to convert these maps from the P-P image-time domain to the depth domain. These rms velocities were determined along all of the OBC profiles defined on the map displayed as Figure 38. Collectively, all of these velocities form a 3D P-wave velocity volume that can convert any time-based surface such as Horizon 1 to a depth-based surface. Examples of the P-P rms velocity behavior along two profiles of this 3D P-wave velocity volume are displayed as Figures 46 and 47.

Depth Maps of Seismic Data Quality: Shelf-C

Depth maps of P-P and P-SV Horizon 1 were created using Landmark's TVD software package. This mapping algorithm creates a depth map of an interpreted time surface by the simple process of multiplying the time coordinate of each data point of that surface by the P-P rms velocity value located at the same coordinate point in the 3D P-P rms velocity volume. Depth-based versions of P-P Horizon 1 and P-SV Horizon 1 are shown as Figures 48 and 49, respectively. The equivalent maps constructed across Shelf-B are defined in Figures 27 and 28. The maps in these four figures show that, in general, the P-SV mode creates continuous reflection events to the same depths as does the P-P mode across the area spanned by the Shelf-B and Shelf-C surveys.

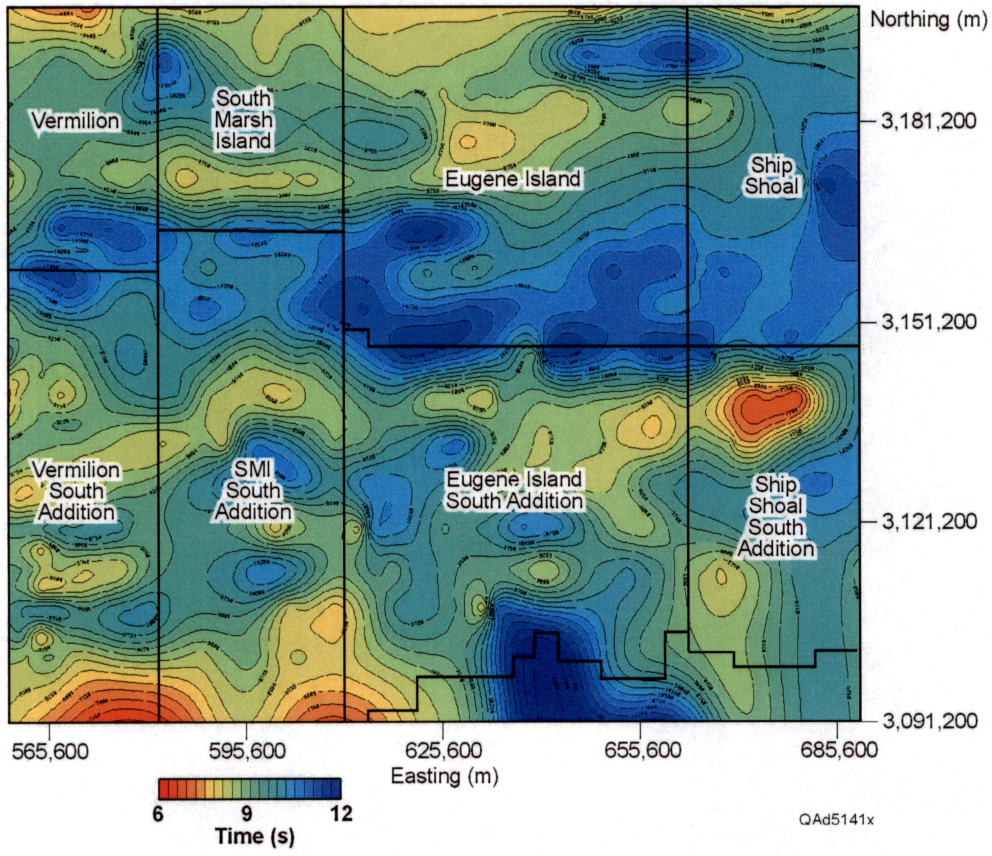

Figure 45. Time structure map, base of discontinuous P-P reflections, Shelf-C.

Task not finished because project funding was eliminated for Year 3 of the project.

Figure 46. East-west profile of P-P rms velocities across the central portion of the Shelf-C survey.

Task not completed because project funding was eliminated for Year 3 of the project.

Figure 47. North-south profile of P-P rms velocities across the central portion of the Shelf-C survey.

Task not completed because project funding was eliminated for Year 3 of the project.

Figure 48. Depth map, base of continuous P-P reflections, Shelf-C.

Task not completed because project funding was eliminated for Year 3 of the project.

Figure 49. Depth map, base of continuous P-SV reflections, Shelf-C.

Elastic Wavefield Stratigraphy and Seismic Sequences: Shelf-C

Data examples from the Shelf-B survey were used earlier in this report (Figs. 31 through 37) to illustrate **Principle 1** of elastic wavefield stratigraphy: **P-P seismic facies differ from P-SV seismic facies, and both facies images are correct descriptions of geologic facies conditions**. In this section, we will use comparisons of P-P and P-SV images from the Shelf-C survey to illustrate **Principle 2** of elastic wavefield stratigraphy: **P-P seismic sequences differ from P-SV seismic sequences, and both sequence images are correct descriptions of geologic sequence conditions**. Following these Shelf-C examples, the physical basis for these two principles will be explained using appropriate rock physics theory.

In the following data examples, depth-equivalent P-P and P-SV images are shown adjacent to each other with no interpretations overlain on either image so that readers can impose their own interpretations of the data if they wish. Each example is then followed by the same data windows with a few selected sequences labeled by letters **A**, **B**, **C**, . . . and with sequence boundaries marked with colored horizons. Geologic features that are interpreted to be depth-equivalent and that are unique enough to be used to indicate the accuracy of the P-SV time warping are circled, labeled **DR** (for "depth registration"), and emphasized by an arrow pointer.

Seismic Sequences: Example 1

Our first example of P-P and P-SV seismic sequences is illustrated in Figure 50 (uninterpreted data) and Figure 51 (interpreted data). These data windows extend to a depth of ~28,500 ft (~8.7 km). Comparing depth-registration features **DR** (Fig. 51) shows that the time-warping process adjusts the P-SV data so that PSV-defined geology is ~100 ms above PP-defined geology. This depth registration is sufficiently accurate for visual comparisons of depth-equivalent P-P and P-SV sequences.

The sequences in Figure 51 were defined by picking a **prominant** reflection as a sequence boundary in P-SV image space and then marking the P-P reflection that was the nearest depth-equivalent "**prominant**" P-P event to the chosen P-SV sequence boundary. If a P-P sequence boundary and a P-SV sequence boundaries are truly depth-equivalent, the 100-ms time shift between P-P and P-SV depth-registration features **DR** would cause each P-P sequence boundary to be ~100 ms below its corresponding P-SV sequence boundary along this particular profile.

Several sequence boundaries are labeled in each image space to demonstrate that for each P-SV sequence boundary, an equivalent P-P sequence boundary is either not present at a time delay of ~100 ms, or is a much fainter event. Intervals **A** through **D** are good examples of the concept that P-P and P-SV modes often image different sequence boundaries.

Seismic Sequences: Example 2

Our second comparison of P-P and P-SV seismic sequences is displayed in Figure 52 (the uninterpreted data) and Figure 53 (with interpreted sequences). These data windows reach to depths of ~28,500 ft (~8.7 km). Time warping positions the P-SV data at the same image coordinates as the P-P data down to an image time of almost 3 s, as indicated by the equivalent position of the shallow **DR** feature shown just above 2 s in each image space in Figure 53. Below 3 s, the time-warping has a dynamic positioning error that causes P-SV registration event **DR** in the lower-left corner of the data window to be ~100 ms deeper than the equivalent P-P **DR** event. Thus the boundaries of P-P sequences **A**, **B**, **C** should be at the same time coordinates as the boundaries of P-SV sequences **A**, **B**, **C**, and the boundaries of P-P sequences **D** and **E** should be ~50 ms earlier than the boundaries of P-SV sequences **D** and **E**.

Using these time shifts to compare the P-P sequences in Figure 53 with their corresponding P-SV sequences shows that several P-SV sequence boundaries have no equivalent P-P sequence boundary, or a much fainter sequence boundary.

Seismic Sequences: Example 3

Figure 54 illustrates the uninterpreted data windows that will be used as Example 3 of P-P and P-SV seismic sequences. The interpreted versions of these data are displayed as Figure 55. These data windows extend to a depth of ~22,500 ft (~6.8 km). Time-warping creates minimal displacement of P-SV depth-registration feature **DR** relative to P-P depth-registration feature **DR**. This time-warping means that the boundaries of all labeled P-P sequences should be at the same image coordinates as the boundaries of the equivalent P-SV sequences. Comparing the images in Figure 55 shows that P-P sequence **A** is different than P-SV sequence **A**; whereas, P-P sequence **B** and much of P-P interval **C** are the same as their P-SV equivalents.

Seismic Sequences: Example 4

Example 4 of P-P and P-SV seismic sequences is shown as Figures 56 and 57. Depth-registration geology **DR** is ~100 ms earlier in P-SV image space than it is in P-P image space (Fig. 57). That depth-registration time shift will be assumed to be appropriate across the total image space. This assumption means that the boundaries of P-P sequences **A**, **B**, **C** should be ~100 ms later than the boundaries

of P-SV sequences **A**, **B**, and **C**. Rarely is there a robust P-P sequence boundary ~100 ms later than any of the robust P-SV sequence boundaries.

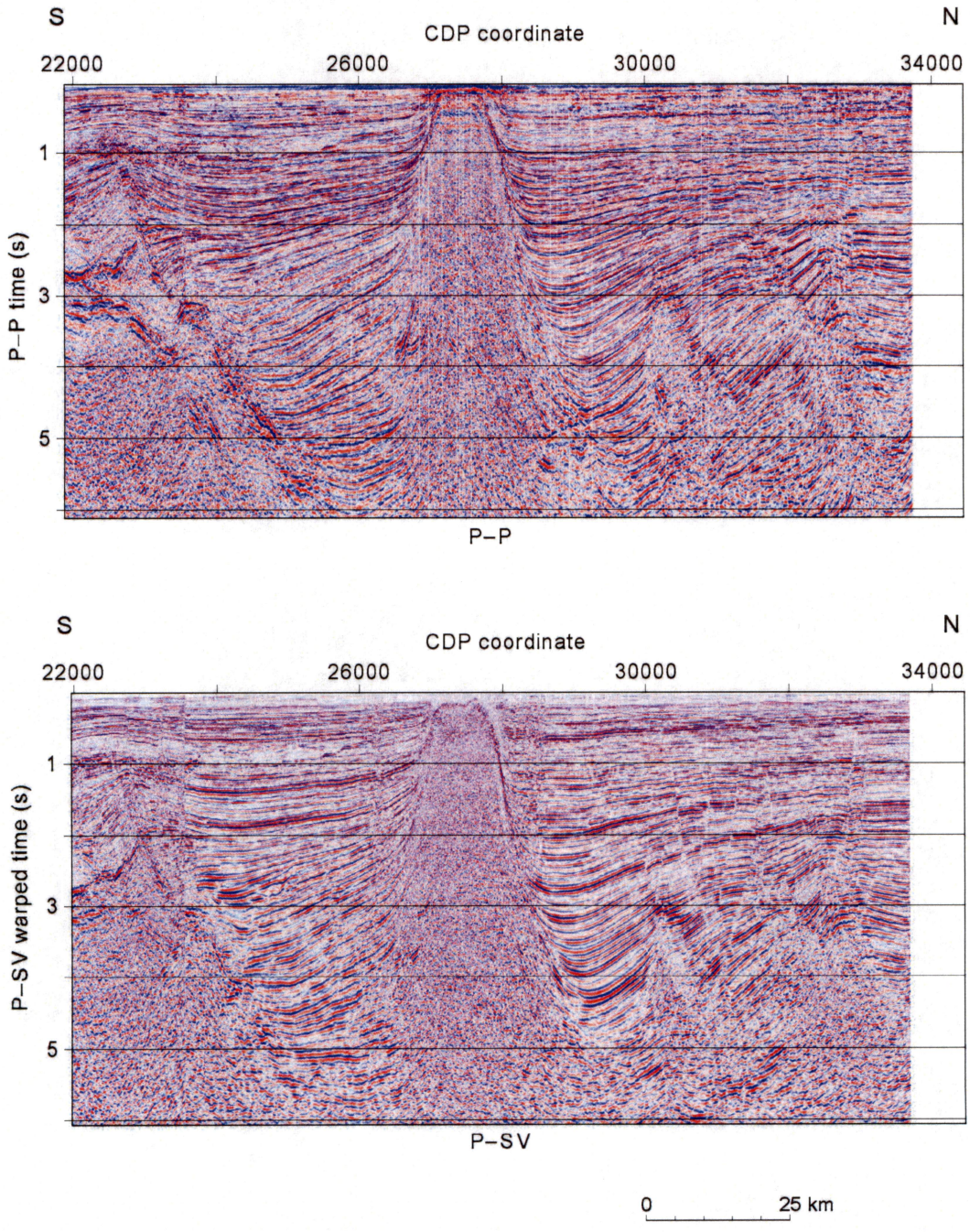

QAd5089(a)x

Figure 50. Uninterpreted P-P image (top) and P-SV image (bottom) along Example Line 1.

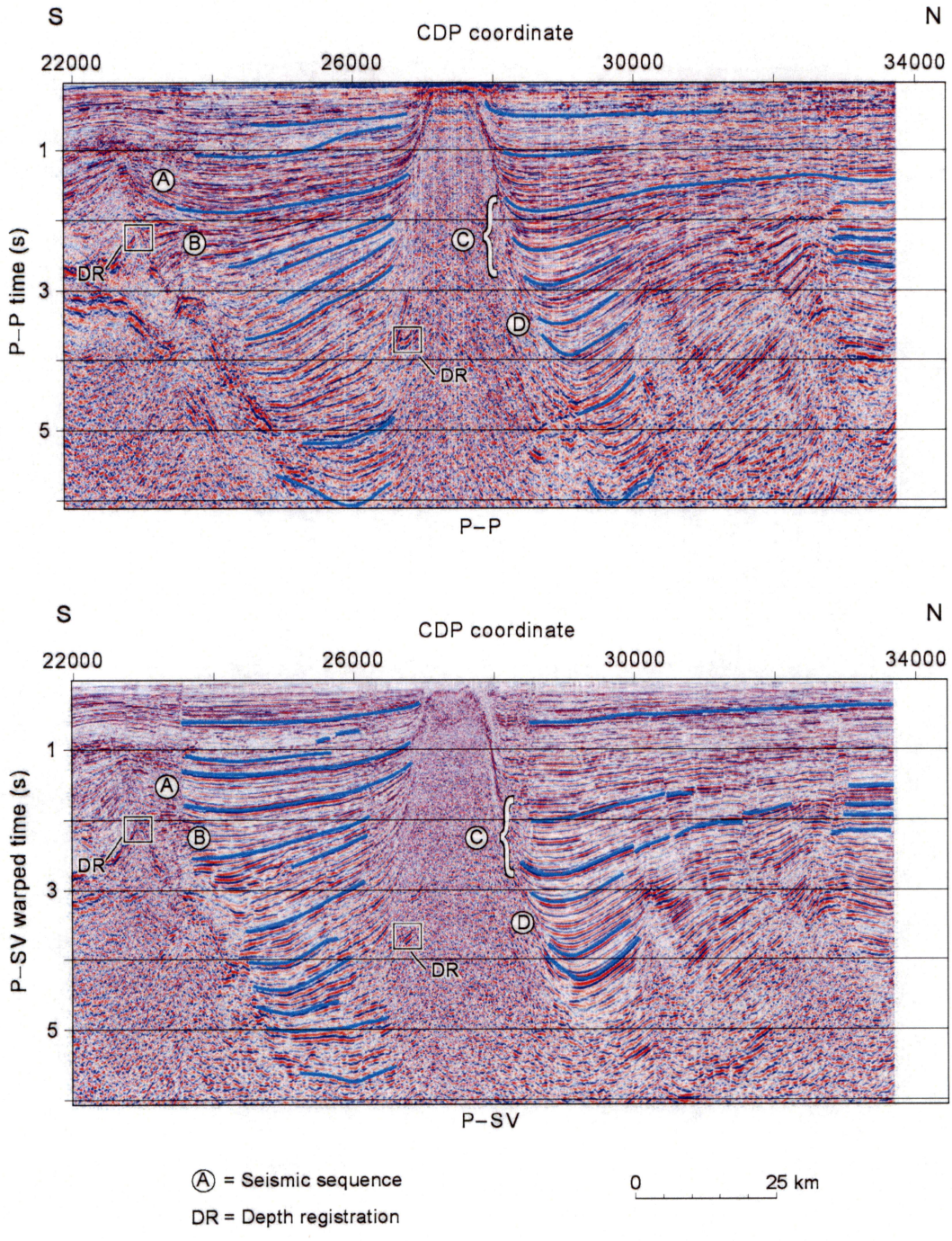

QAd5089(b)x

Figure 51. Interpreted P-SV sequences (bottom) and their equivalent P-P sequence intervals (top) along Example Line 1. **DR** = depth-registration feature showing P-SV geology is positioned 100 ms earlier than P-P geology. Intervals **A** through **D** are depth equivalent and show that a P-SV sequence boundary often has no equivalent P-P sequence boundary, or that the depth-equivalent P-P event is much fainter than its companion P-SV boundary.

Seismic Sequences: Example 5

An example of P-P and P-SV seismic sequences from the central portion of the Shelf-C survey is displayed as Figures 58 and 59. Geologic feature **DR** chosen as a depth-registration indicator shows that time-warping adjusts P-SV image space to be depth-equivalent to P-P image space with no additional time shifting required to align geological features. Each P-P seismic sequence and its equivalent P-SV sequence should be at identical image coordinates across the complete image space. Comparing the interpreted images (Fig. 59) shows that there is rarely a robust P-P event at the same image coordinates as the interpreted P-SV sequence boundaries. The depth-equivalent P-P sequence boundaries are either (1) absent or (2) much fainter events than the P-SV sequence boundaries.

Seismic Sequences: Example 6

Our last example comparing P-P and P-SV seismic sequences is an east-west profile documented in Figures 60 and 61. These data extend to a depth of ~28,500 ft (~8.7km). Two depth-registration features **DR** are labeled and show that time-warping has adjusted P-SV image time to be ~100 ms earlier than P-P image time over the total image window. P-P sequence boundaries that are depth equivalent to the marked P-SV sequence boundaries should be ~100 ms later than their companion P-SV boundaries. Note that P-P sequence **A** is not well imaged in P-SV image space, and conversely, P-SV sequence **B** is not well imaged in P-P image space. The sequences across interval **C** are much different in P-P image space than in P-SV image space.

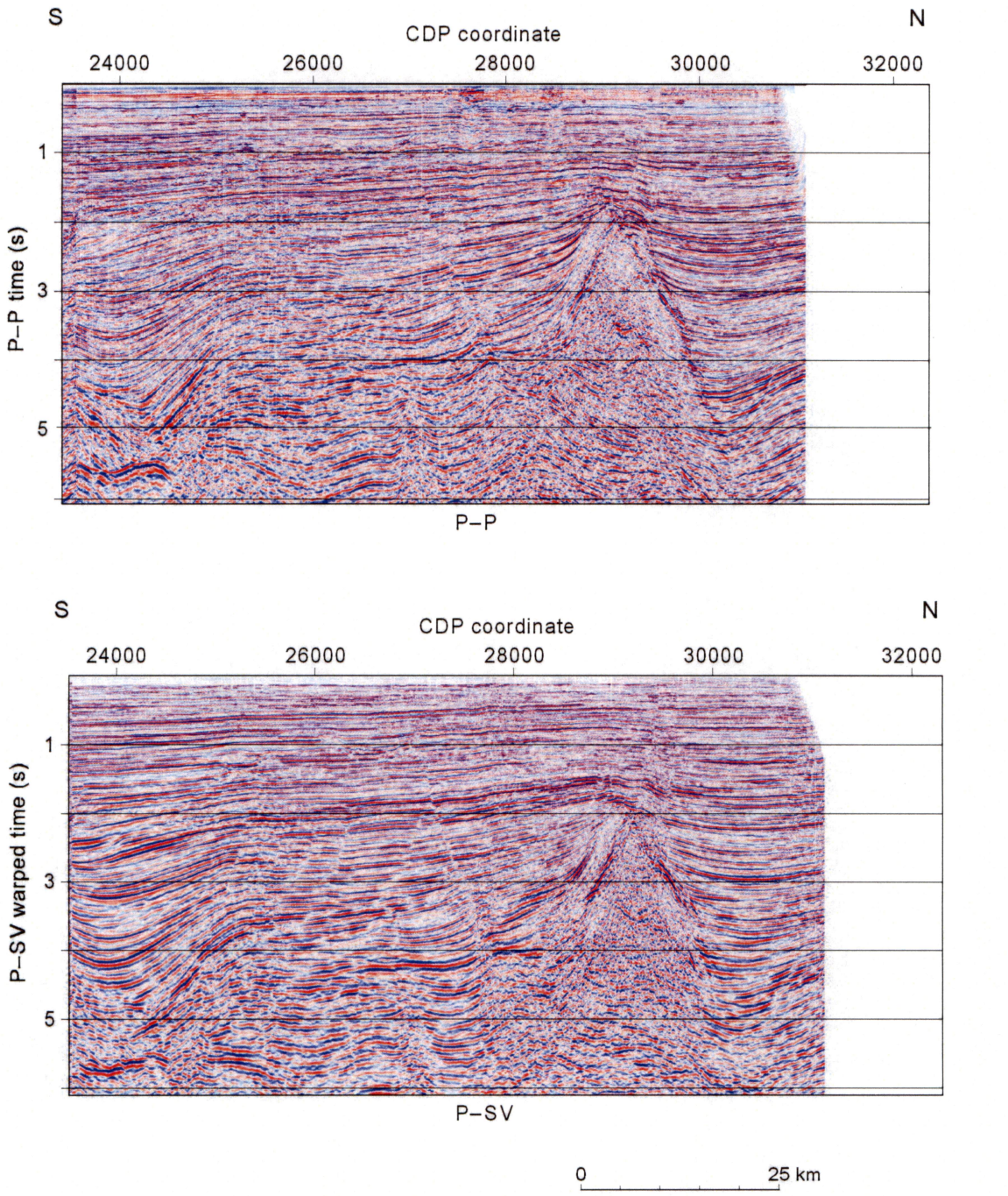

Figure 52. Uninterpreted P-P image (top) and P-SV image (bottom) along Example Line 2.

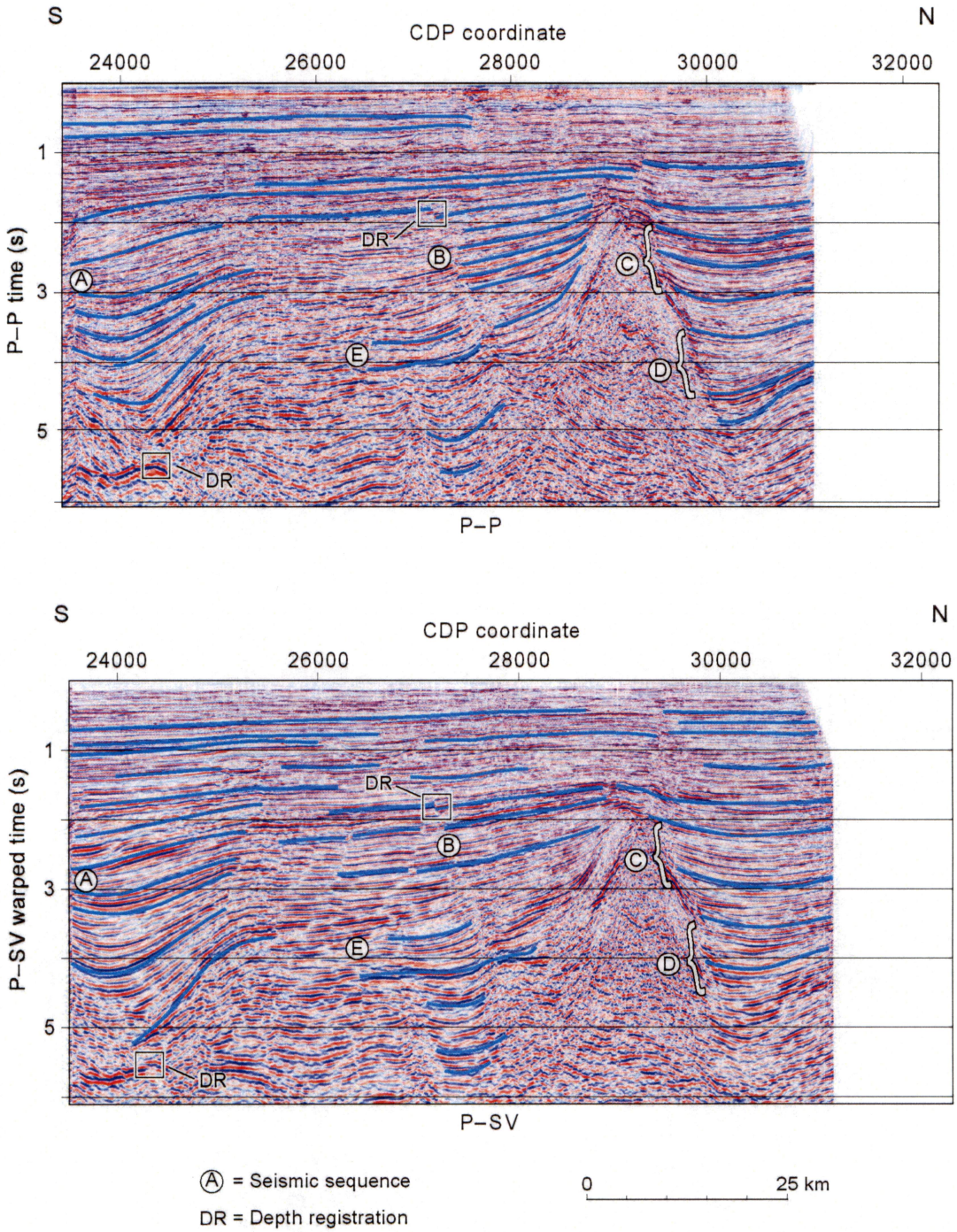

QAd5093(b)x

Figure 53. Interpreted P-SV sequences (bottom) and their equivalent interpreted P-P sequences (top) along Example Line 2. **DR** = depth-registration feature showing time-warping positions P-SV geology at the same image coordinates as P-P geology above 3 s, and then slowly delays P-SV geology to be ~100 ms later than P-P geology at 5.5 s. Intervals **A** through **E** are depth equivalent and shown that a P-SV sequence boundary often has no equivalent P-P sequence boundary, or that the depth-equivalent P-P event is much fainter than its companion P-SV boundary.

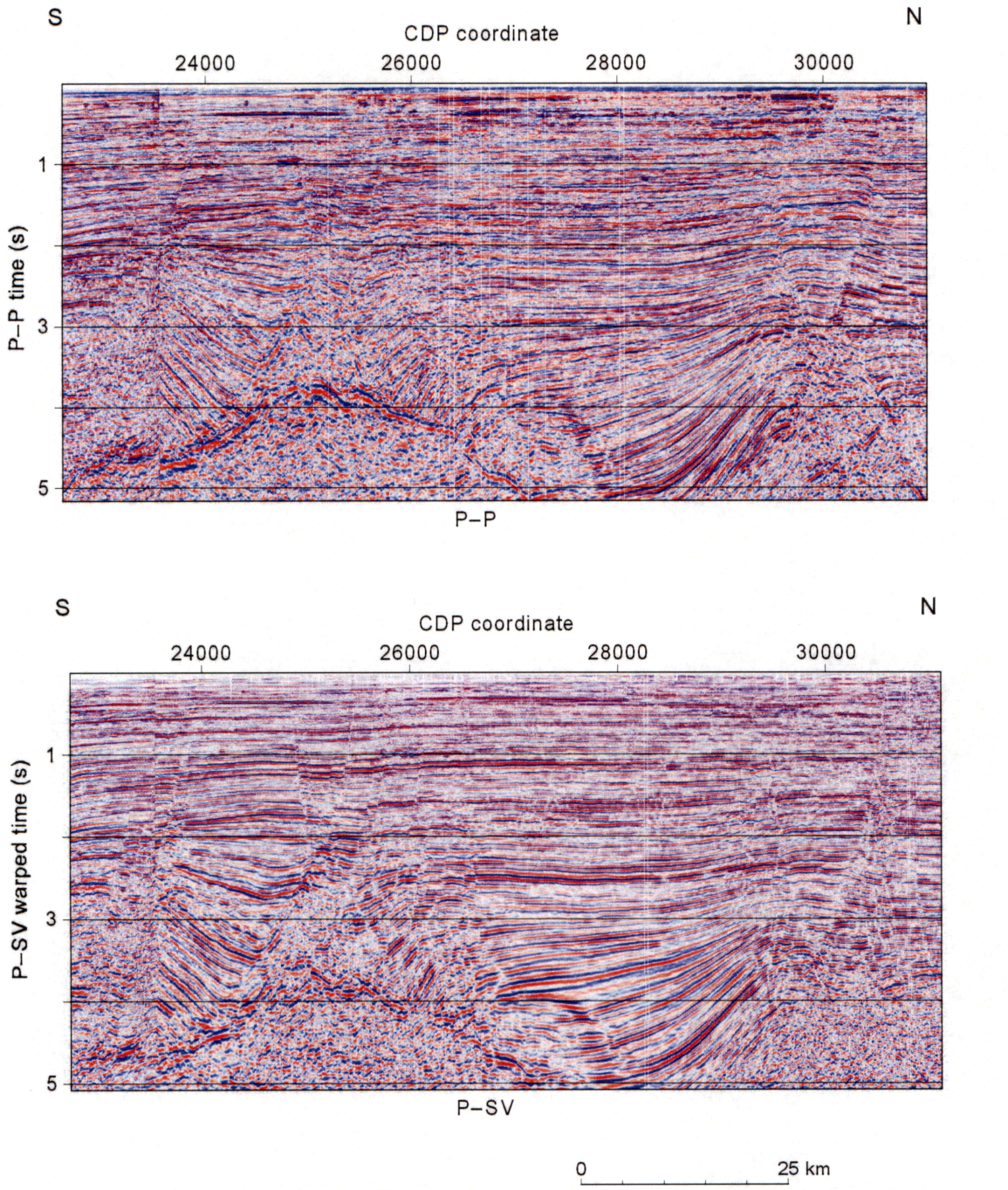

Figure 54. Uninterpreted P-P image (top) and P-SV image (bottom) along Example Line 3.

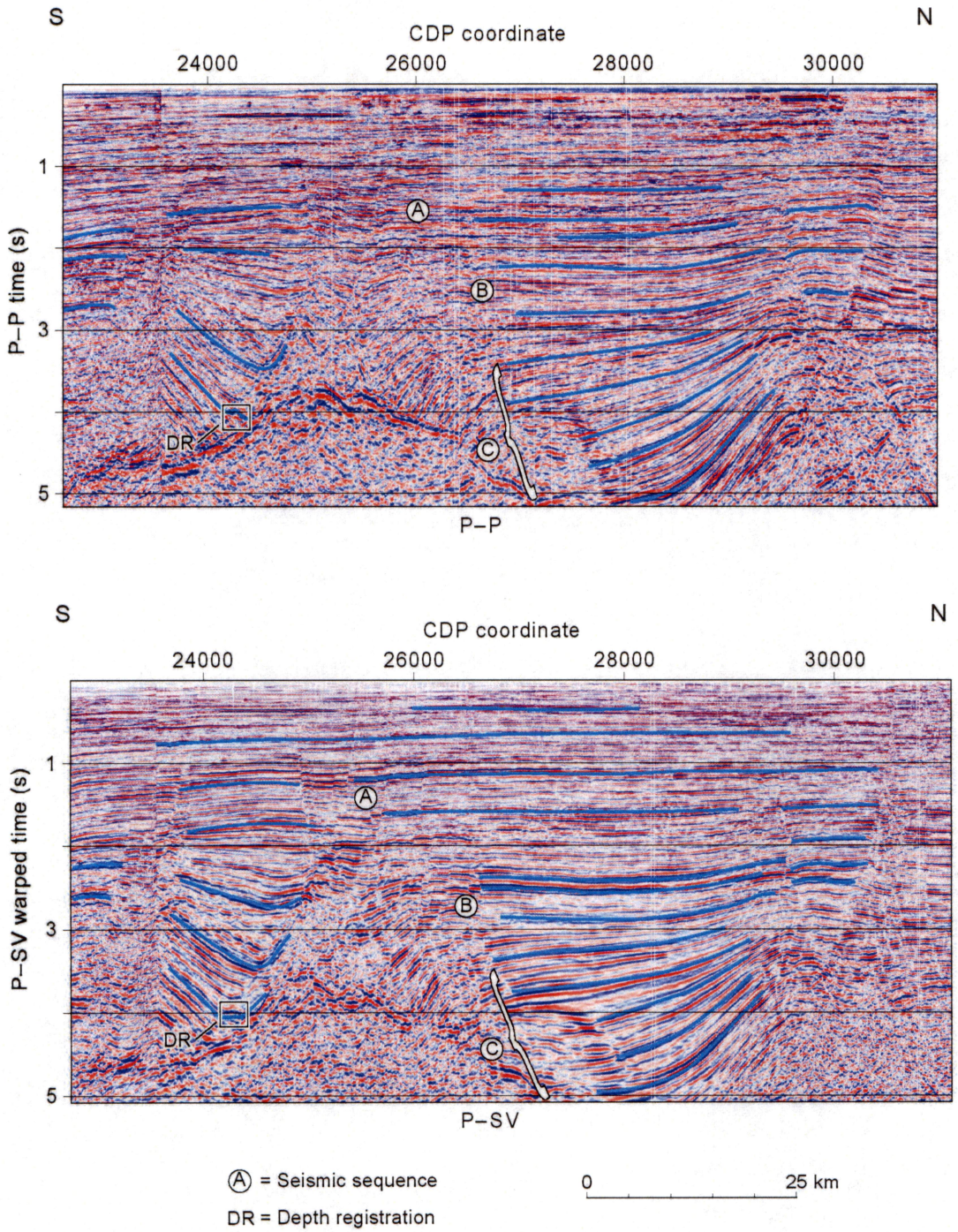

QAd5094(b)x

Figure 55. Interpreted P-SV sequences (bottom) and their equivalent interpreted P-P sequences (top) along Example Line 3. **DR** = depth-registration feature showing that P-SV geology is at the same image-time coordinates as P-P geology over the entire data window. Intervals **A** through **C** are depth equivalent and show that a P-SV sequence boundary often has no equivalent P-P sequence boundary, or that the depth-equivalent P-P event is much fainter than its companion P-SV boundary.

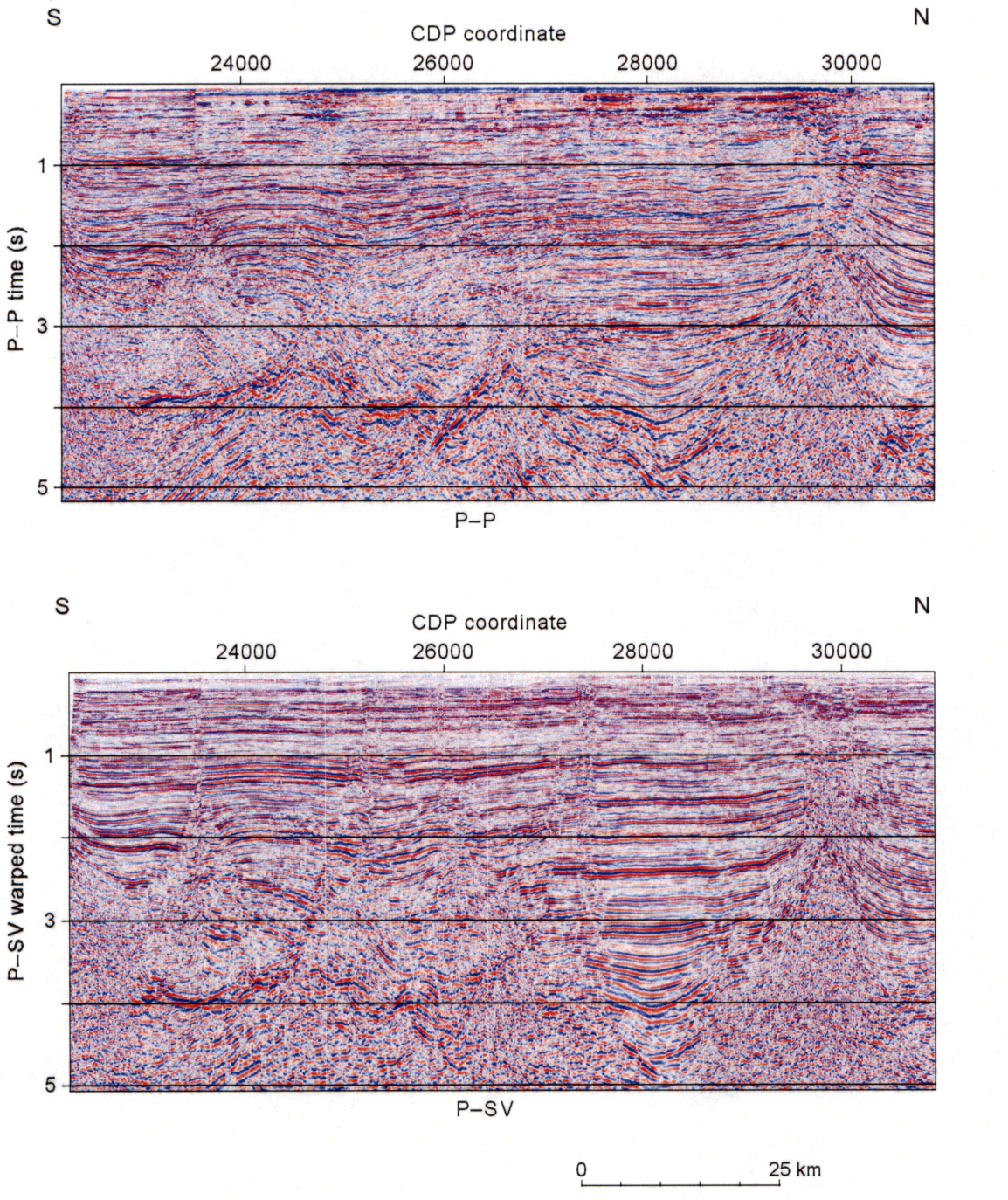

Figure 56. Uninterpreted P-P image (top) and P-SV image (bottom) along Example Line 4.

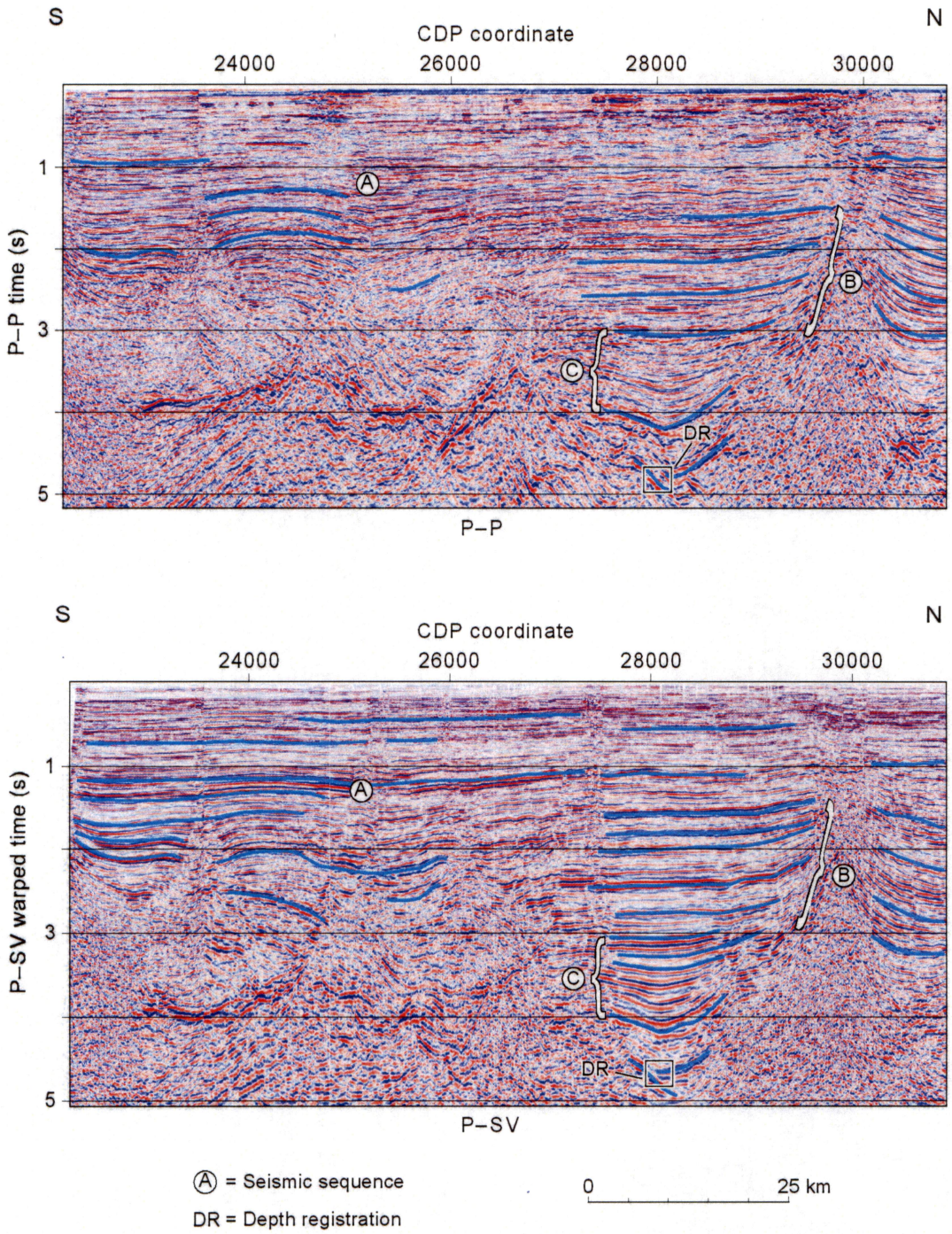

Figure 57. Interpreted P-SV sequences (bottom) and their equivalent interpreted P-P sequences (top) along Example Line 4. **DR** = depth-registration feature showing that P-SV geology is positioned ~100 ms earlier than P-P geology. Intervals **A** through **C** are depth equivalent and show that a P-SV sequence boundary often has no equivalent P-P sequence boundary, or that the depth-equivalent P-P event is much fainter than its P-SV companion boundary.

Rock Physics

Variable Clay Content

Work by Han and others (1986) provides a rock-physics theory that is helpful in understanding P-P and P-SV reflection phenomena that occur in the clay-dominated lithofacies that are imaged in Figures 31 through 37 and in Figures 50 through 61. Han and co-workers did a detailed laboratory analysis of 70 samples of consolidated rocks obtained from deep GOM cores. Their core measurements established the following relationships between seismic velocities (V_P and V_S), porosity, and clay content:

(1) $V_P = 5.59 - 6.93\Phi - 2.18c$, and

(2) $V_S = 3.52 - 4.91\Phi - 1.89c$.

In these equations, V_P is P-wave velocity (in km/s), V_S is S-wave velocity (in km/s), Φ is porosity, and c is clay content ($0<c<1$). Constants in the equations are appropriate for rocks subjected to an effective pressure of 40 MPa or more, which would be a pressure regime of targets such as are shown in Figures 50 through 61. To calculate example reflectivities across super-deep data windows, we set Φ equal to 4 and 10 percent. Coupling these velocity equations with the density equation

(3) $\rho = [c\rho_{cl} + (1 - c)\rho_Q](1 - \Phi) + \rho_{fl}\Phi$,

where ρ_{cl} is the density of clay, ρ_Q is the density of quartz, and ρ_{fl} is the density of the pore fluid, allows P-P and P-SV reflectivities at deep interfaces to be analyzed for targets having variable clay content.

These rock-physics equations are important because (a) they are based on real laboratory measurements made on real rocks and are not synthetic models, (b) rock samples come from geology imaged by the seismic data illustrated in this report, and (c) rocks that were analyzed had a wide range of clay content. To illustrate the value of this rock-physics theory, we used a simple, two-layer Earth model (Fig. 62) to represent deep-target conditions across the northern shelf of the GOM.

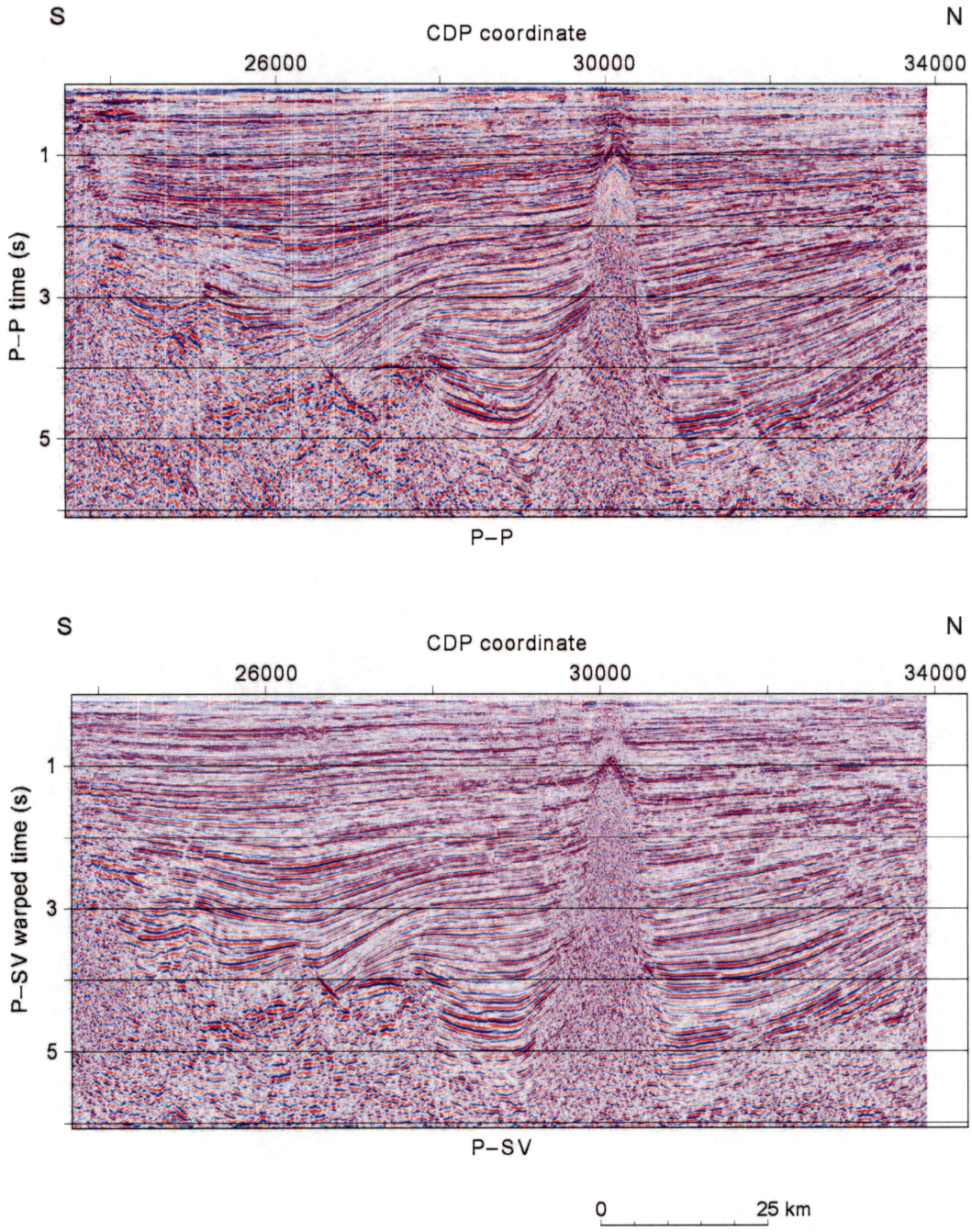

Figure 58. Uninterpreted P-P image (top) and P-SV image (bottom) along Example Line 5.

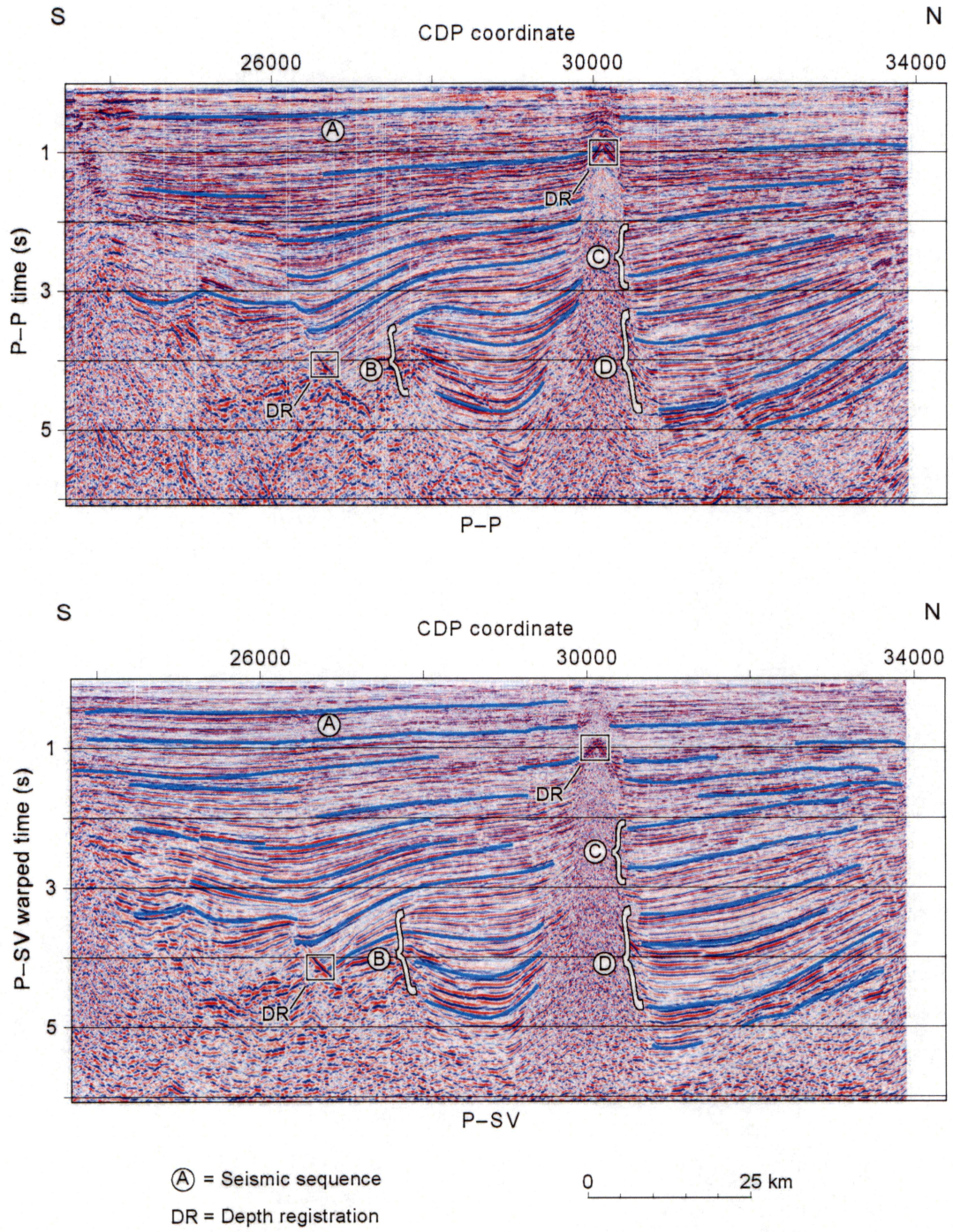

QAd5090(b)x

Figure 59. Interpreted P-SV sequences (bottom) and their equivalent interpreted P-P sequences (top) along Example Line 5. **DR** = depth-registration feature showing time-warped P-SV geology is at the same image coordinates as P-P geology. Intervals **A** through **D** are depth equivalent and show that a P-SV sequence boundary often has no equivalent P-P sequence boundary, or that the depth-equivalent P-P event is much fainter than its companion P-SV boundary.

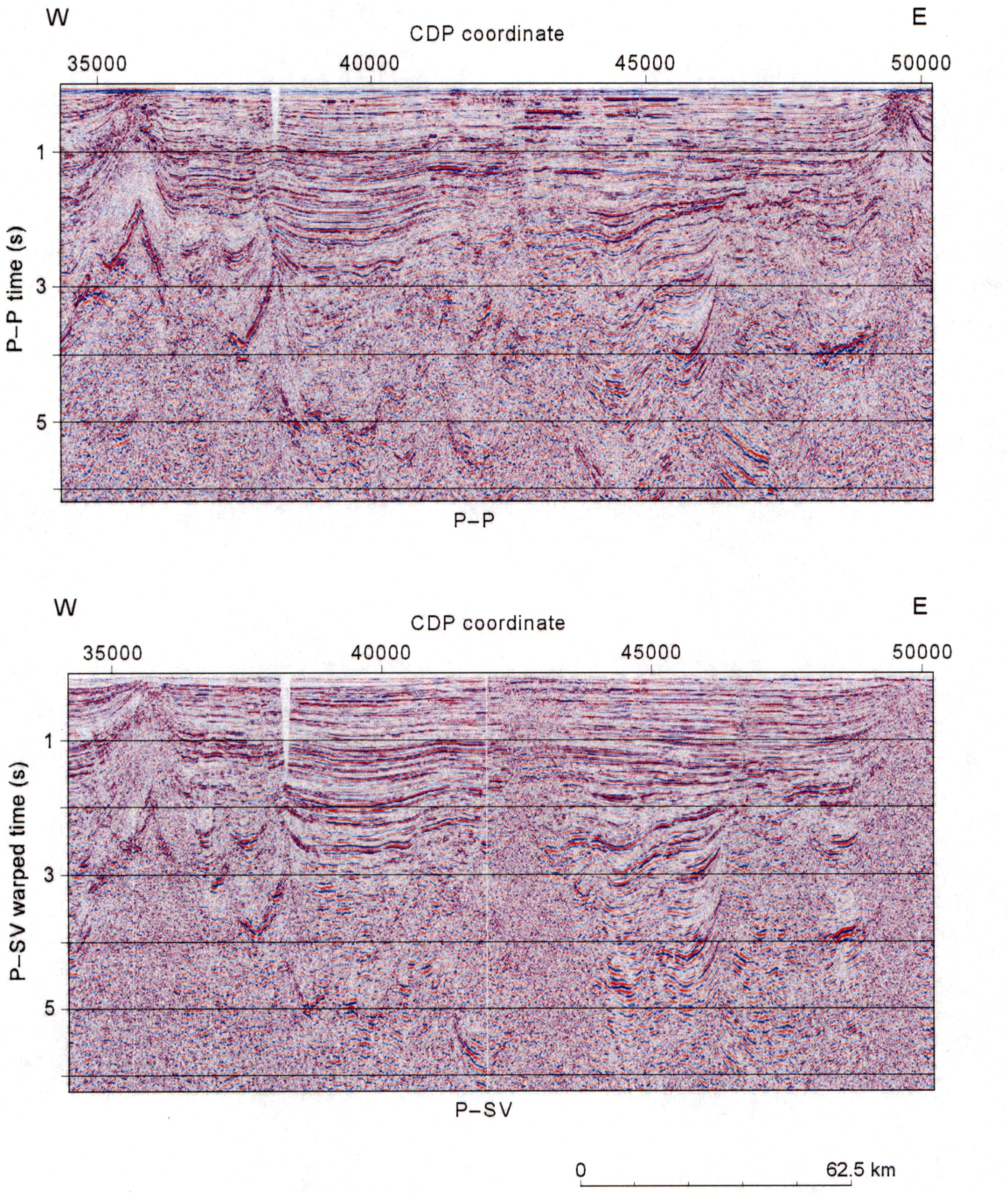

Figure 60. Uninterpreted P-P image (top) and P-SV image (bottom) along Example Line 6.

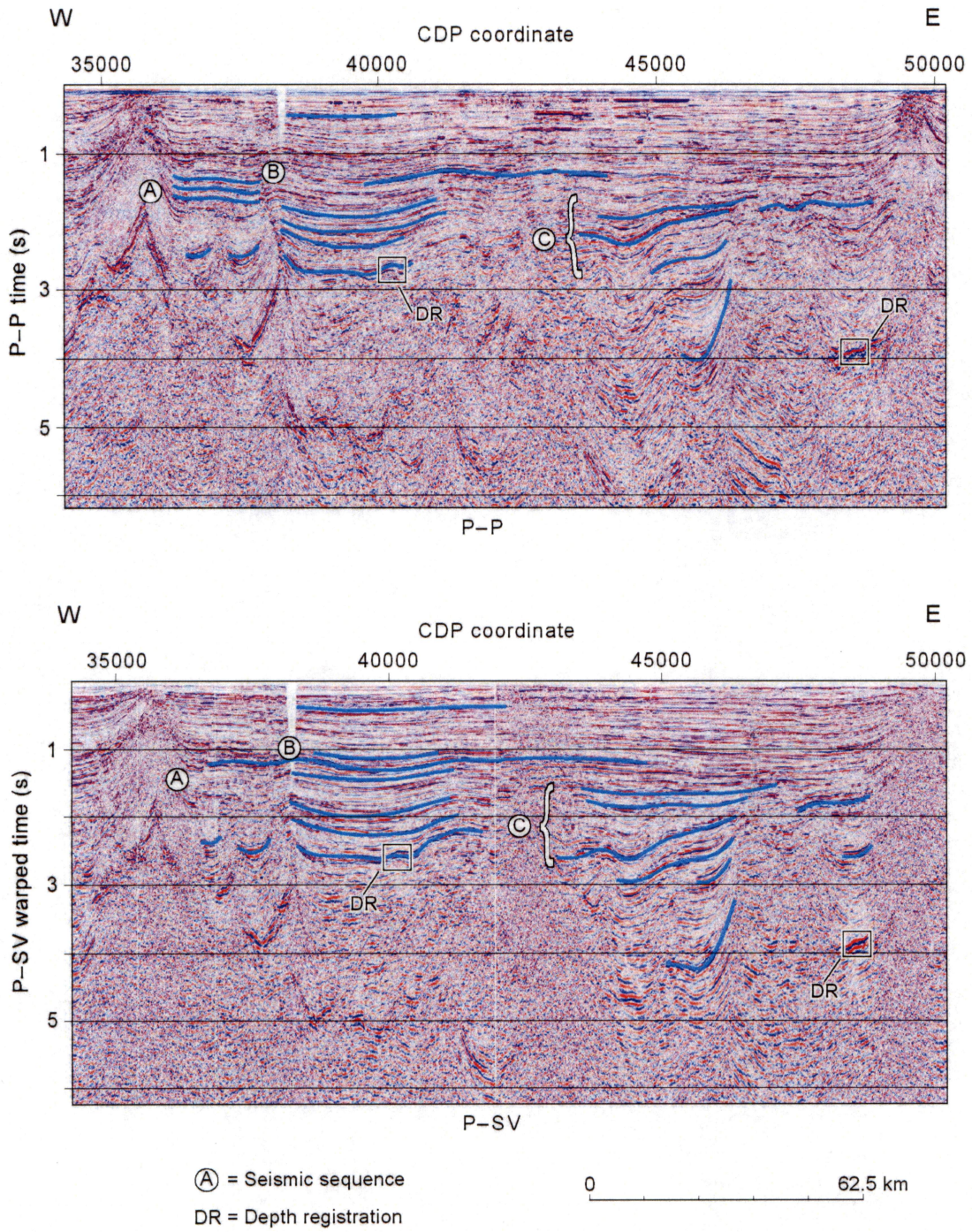

QAd5092(b)x

Figure 61. Interpreted P-SV sequences (bottom) along Example Line 6 and their equivalent interpreted P-P sequences (top). **DR** = depth-registration feature showing that time-warped P-SV geology is positioned ~100 ms earlier than P-P geology. Intervals **A** through **C** are depth equivalent and show that a P-SV sequence boundary often has no equivalent P-P sequence boundary, or that the depth-equivalent P-P event is much fainter than its companion P-SV boundary.

where ρ_{cl}.

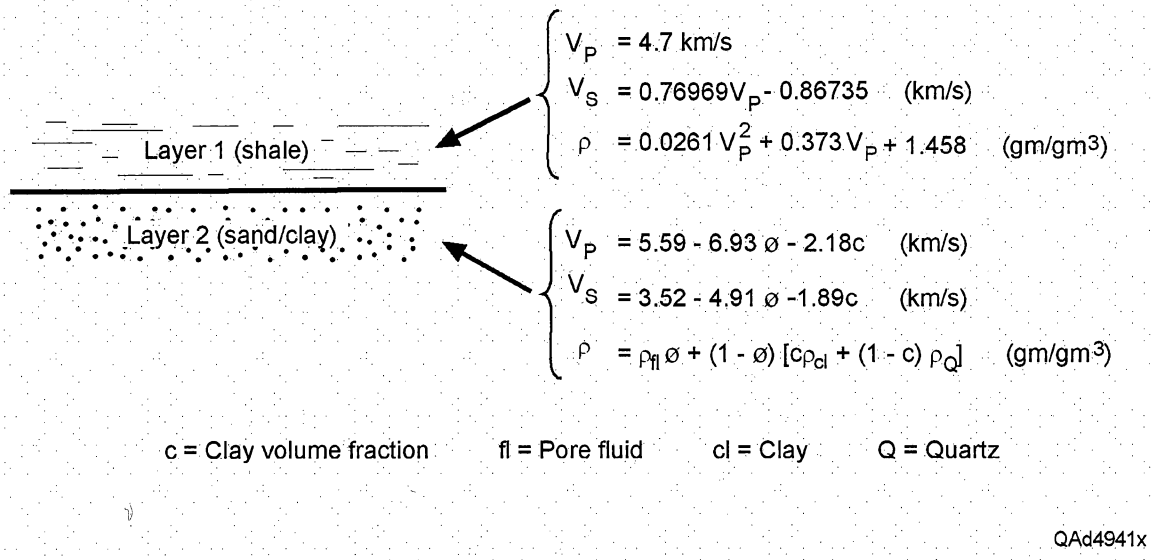

Figure 62. Earth model used to demonstrate effect of clay content on P-P and P-SV reflectivities. Equations used to specify properties of Layer 1 (shale) come from Castagna and others (1993). Those used to specify properties of Layer 2 are from Han and others (1986).

We kept properties of the upper reservoir-seal layer of this model constant, using values defined by equations in the figure, whereas clay content and pore fluid were varied in the lower reservoir layer. Effective pressure and porosity in the reservoir (Layer 2) were kept constant at 40 MPa and 20 percent, respectively. Resulting P-P and P-SV reflectivities for this two-layer interface are displayed in Figure 63.

These reflectivity curves provide an important message concerning P-P and P-SV images of siliciclastic rocks having variable clay content:

- For certain clay-content concentrations (c), the target layer is practically invisible to the P-P seismic mode but generates a strong P-SV reflection. For example, when c = 20 percent, P-P reflectivity is small and changes algebraic sign near an incidence angle of 20° for both a gas-filled sand and a brine-filled sand. These two reflectivity characteristics are classic examples of a reflection event that is minor, and probably invisible, in a final-processed P-P image. In contrast, P-SV reflectivity for each sand facies (gas or brine) when c = 20 percent is reasonably robust and has a constant algebraic sign at all incidence angles. This P-SV reflectivity behavior should create a significant P-SV reflection event.

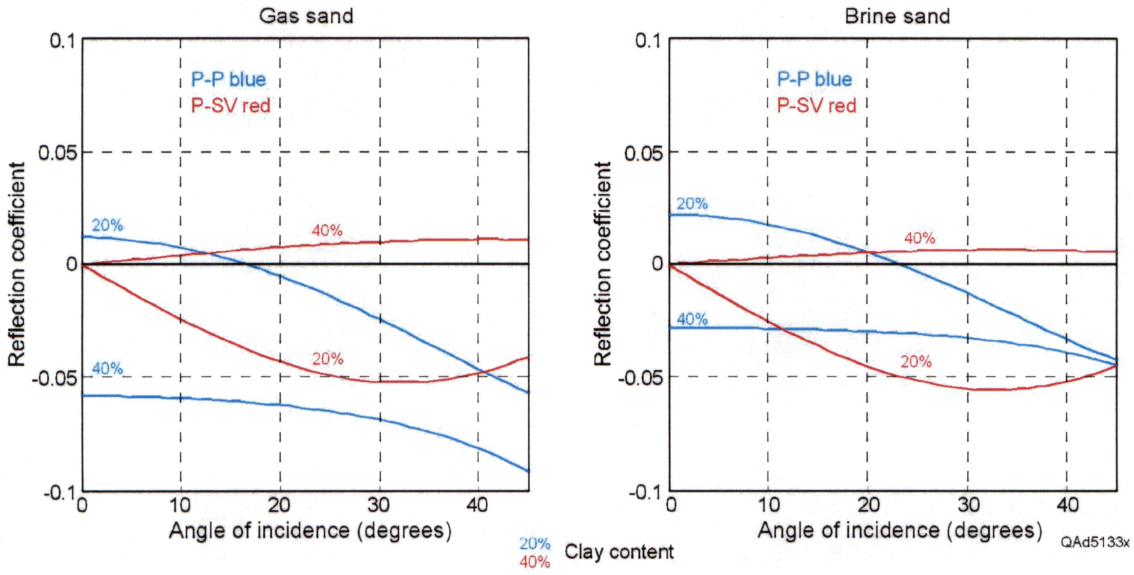

Figure 63. P-P and P-SV amplitude-vs-angle reflectivity behaviors for varying clay content in a target layer. Layer 2 of Figure 62 is assumed to be a deep unit with a porosity of 20 percent. (Left) Pore fluid is 100-percent gas. (Right) Pore fluid is 100-percent brine.

- At other clay-content concentrations, the target layer is a poor P-SV reflector but a robust P-P reflector. For example, when c = 40 percent, P-P reflectivity is 6 to 10 percent across the total angle range for a gas-filled sand (left) and 3 to 5 percent for a brine-filled sand (right). In contrast, P-SV reflectivity does not reach a 2 percent value for either sand-fluid facies until the incidence angle is 30° to 45°. This level of clay concentration will produce bold P-SV reflections and weak P-P reflections.

Each reflectivity curve changes only slightly when the reservoir is deeper and has a porosity of only 4 percent (Figure 64). Variations of clay content in siliciclastic facies explain why certain intervals in depth-registered P-P and P-SV data show significant differences between P-P and P-SV reflection character. Data displayed in Figures 31 through 37 and 51 through 56 are examples of such reflectivity behaviors.

Task not completed because project funding was eliminated for Year 3 of the project.

Figure 64. P-P and P-SV amplitude-vs-angle reflectivity behaviors for varying clay content in a target layer. Layer 2 of Figure 62 is assumed to be a deep unit with a porosity of 4 percent. (Left) Pore fluid is 100-percent gas. (Right) Pore fluid is 100-percent brine.

This rock-physics theory provides one explanation for the differences in deep-target P-P and P-SV reflectivities that were observed in our analysis of long-offset 4C OBC data (Figs. 31 through 37 and 50 through 61) and also establishes a logic that will help in identifying favorable and unfavorable reservoir facies for companies that elect to use elastic wavefield stratigraphy to evaluate deep gas targets.

Gas-Charged Sediments

One hydrocarbon exploration application that has caused multicomponent seismic data to be acquired across several offshore areas is the ability of the S-wave mode to image geology inside broad, thick intervals of gas-charged sediment where P-P seismic data show no usable reflections. The term ***P-wave wipeout zone*** is often used to describe this imaging problem. Numerous examples of P-wave and S-wave images across P-wave wipeout zones have been published, but the rock-physics cause of the P-P imaging problem has not been adequately documented. This report would not be a proper discussion of advantages of elastic wavefield stratigraphy over conventional seismic stratigraphy for deep gas-reservoir targets if we did not include comments on applications of elastic wavefield stratigraphy across intervals of thick, gas-charged sediments.

To date, published examples of differences between P-P and P-SV images of gas-charged sediment have illustrated situations in which sediment within the

wipeout zone is lithified and stratified. An example of such imaging from one of the 4C OBC surveys available for this study is shown as Figure 65.

Visual inspection of these images shows that the P-P mode provides poor, limited information about geological structure, depositional sequences, and sedimentary facies inside the image space dominated by gas-charged sediment (CDP coordinates 10,000 to 10,150). Conventional seismic stratigraphy (P-P mode only) would have little success in analyzing geological conditions within this poor-quality P-P image area. In contrast, the P-SV mode provides an image that is sufficient for structural mapping, as well as for analyzing seismic sequences and seismic facies. Both of these interpretation options are obvious advantages of elastic wavefield stratigraphy over conventional seismic stratigraphy in areas having gas-charged sediment.

Our evaluation of published attenuation theories for propagating P-P and P-SV modes has not shown a dramatic difference between P-P and P-SV attenuations in gas-charged sediments. Developing appropriate attenuation models will be ongoing research. For the present, we conclude that standard reflectivity analysis is sufficient to explain why P-P modes provide poor images in gas-charged sediment but P-SV modes do not.

A simple Earth model consisting of a shale layer atop a sand layer was used to evaluate P-P and P-SV reflectivity behaviors for types of siliciclastic rocks that occur in the GOM where P-wave wipeout zones are common. Two pore-fluid situations were modeled: (1) both layers had 100-percent brine saturation, and (2) both layers had a mixed pore fluid of 80-percent brine and 20-percent gas. The theory described by Castagna and others (1993) was used to develop V_P-to-V_S and V_P-to-ρ_b relationships for the 100 percent brine situation. Gassmann's (1951) theory was then used to alter pore fluid from 100-percent brine to a homogeneous 80/20 mix of brine and gas. Specific petrophysical properties used in the modeling are listed in the following table.

	Shale (100% brine)	Shale (20% gas)	Sand (100% brine)	Sand (20% gas)
V_P	3534 m/s	3188 m/s	3500 m/s	3370 m/s
V_S	1990 m/s	1994 m/s	1827 m/s	1847 m/s
ρ_b	2.45 gm/cm^3	2.44 gm/cm^3	2.207 gm/cm^3	2.16 gm/cm^3

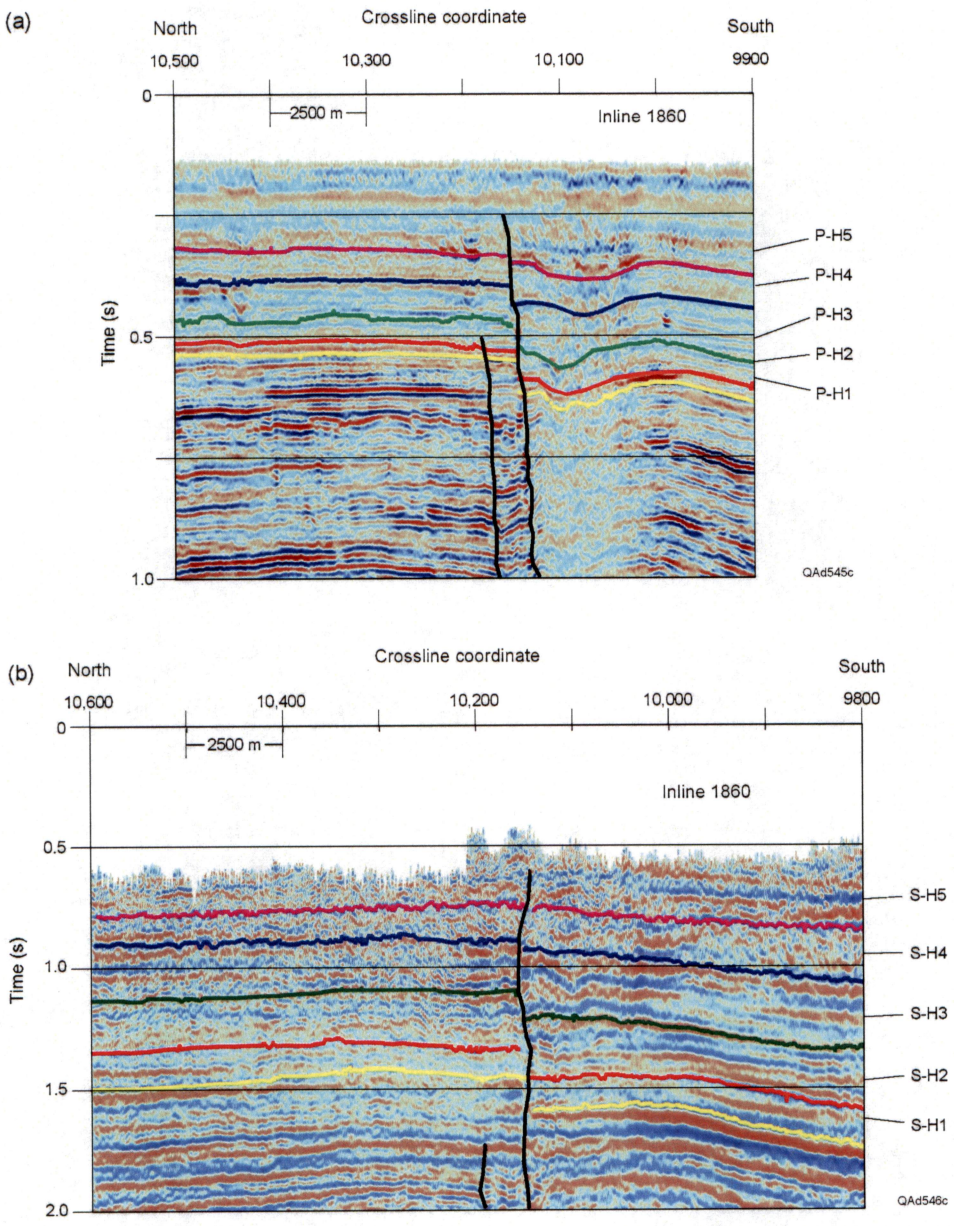

Figure 65. (a) P-P image and (b) P-SV image across gas-charged GOM sediments that are lithified and stratified. P-P horizons P-H1 through P-H5 are interpreted to be depth equivalent to P-SV horizons S-H1 through S-H5. The P-SV data image stratigraphy inside the P-wave wipeout zone extending from CDP coordinates 10,000 to 10,150.

P-P and P-SV reflectivity curves for these two pore-fluid conditions are shown in Figure 66. When pore fluid is 100-percent brine, P-P and P-SV reflectivities are approximately the same average magnitude (~5 percent) for incidence angles ranging from 0 to 25° (panel a). When pore fluid changes to 20-percent gas (panel b), P-SV reflectivity is unchanged, but P-P reflectivity has a smaller magnitude and undergoes a phase reversal that essentially eliminates P-P response across the first 25° of the incidence-angle range. P-SV imaging is thus not affected by the gas-charged sediment, but P-P imaging is seriously degraded. The effect would be similar to that exhibited by the data in Figure 65.

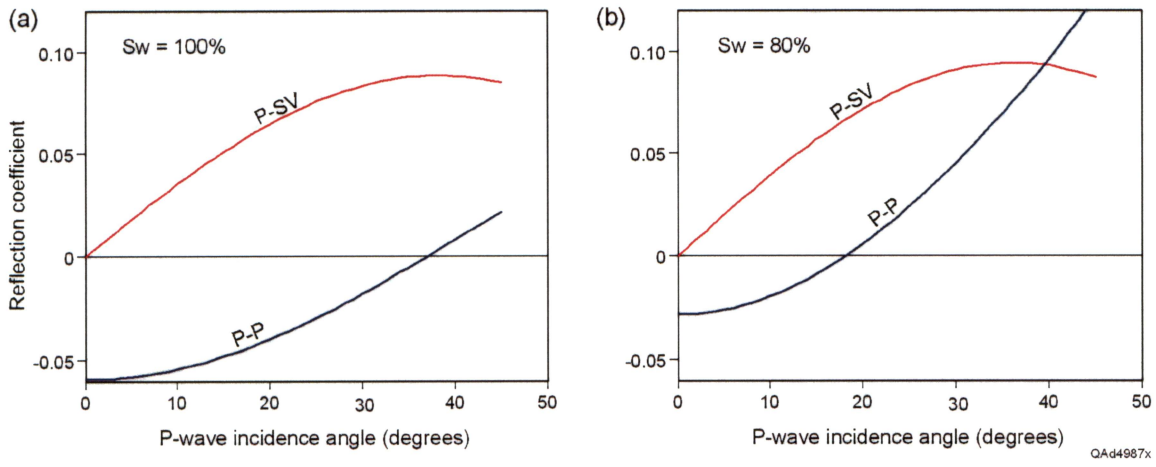

Figure 66. P-P and P-SV reflectivities for (a) brine-filled and (b) gas-charged sediments.

Salt-Sediment Interfaces

Salt-sediment boundaries are common imaging targets that exist at many depths across the northern shelf of the GOM, including the deep target range that is the focus of this research. Some of these boundaries are salt-sand interfaces; others are salt-shale interfaces. We analyzed the reflectivity behavior of P-P and P-SV wavefields for both types of interfaces to determine if one wave mode (P-P or P-SV) has an imaging advantage over the other for studying deep salt-related traps. This analysis was done using a simple 2-layer Earth model. In the first model, the bottom layer was salt (with properties V_P = 4550 m/s, V_S = 2630 m/s, and ρ = 2.16 gm/cm^3), and the top layer was sand (with properties Φ = 10%, V_P = 4679 m/s, V_S = 2840 m/s, and ρ = 2.476 gm/cm^3). In the second model, the upper layer was again salt with the properties defined above, and the lower layer was first a "soft" shale (with properties Φ = 20%, V_P = 3400 m/s, V_S = 1754 m/s, and ρ = 2.316 gm/cm^3) and then was a "hard" shale (with properties Φ = 5%, V_P = 4700 m/s, V_S = 2775 m/s, and ρ = 2.536 gm/cm^3). In our terminology, a "hard" shale is stiffer than salt; whereas, salt is stiffer than a "soft" shale.

Our modeled reflectivity behaviors are displayed as Figure 67. The P-P and P-SV reflectivities for a salt-sand interface (Fig. 67a) are almost identical to the reflectivities for the interface between salt and soft shale (Fig. 67b). There are two important principles for these types of salt-sediment interfaces:

1. P-P reflectivity is large and P-SV reflectivity is small for small angles of incidence, and
2. P-SV reflectivity is large and P-P reflectivity is small for large angles of incidence.

For most source-receiver offsets, this reflectivity physics means that in situations where the dip of a salt-sediment interface is small, the P-P mode is better for imaging the interface position than is the P-SV mode. In contrast, if the salt-sediment interface has a large dip angle, the P-SV mode should image the

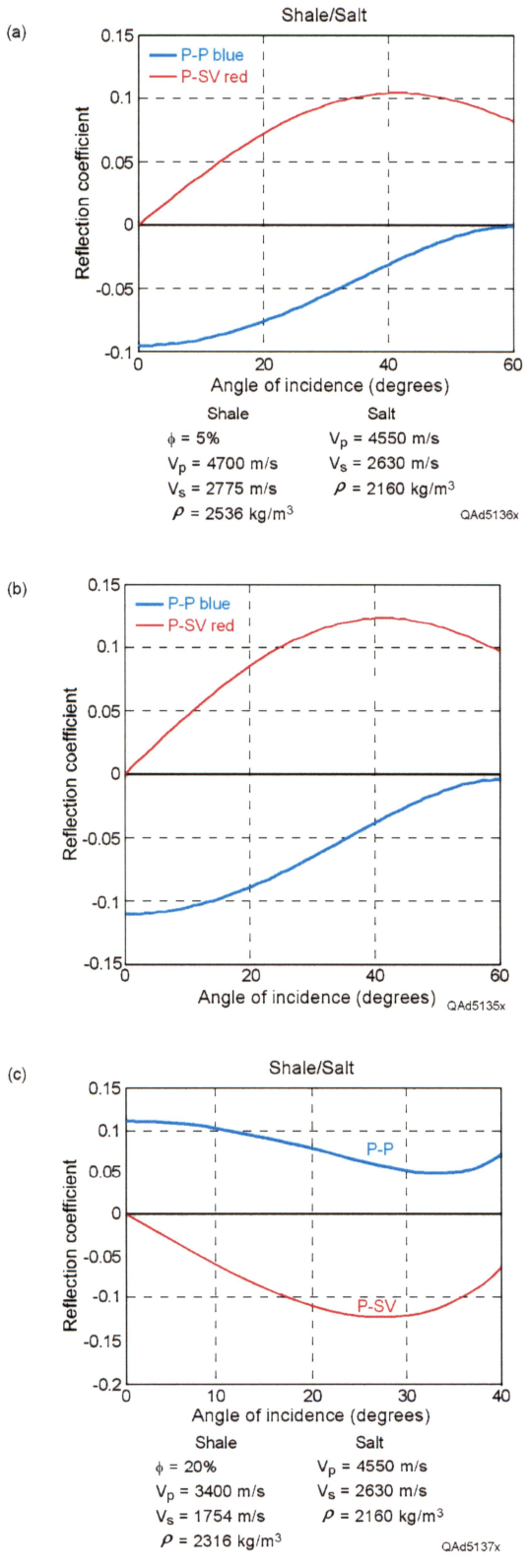

Figure 67. P-P and P-SV reflectivities for interfaces between (a) salt and sandstone, (b) salt and soft shale, and (c) salt and hard shale.

interface better than does the P-P mode. Examples of these reflectivity behaviors are demonstrated by the events near the base of sequence **D** identified on Figures 51 and 53. The base of sequence **D** in Figure 51 involves high-dip salt-sediment interfaces. These interfaces are bolder events in P-SV image space than they are in P-P image space. In Figure 53, the salt-sediment interfaces at the base of sequence **D** are low-dip boundaries. These interfaces are bolder reflections in P-P image space than they are in P-SV image space. When evaluating these interface dips, it is helpful to use the distance scale marked on each figure to judge the approach angle of raypaths arriving at the interface from source-to-receiver offsets of 10 km, the maximum offset used to acquire these 4C OBC data.

The reflectivity of an interface between salt and hard shale (Fig. 67c) is different from the reflectivities of salt-sand and soft shale-salt in that P-P reflectivity is robust at all incidence angles. For a hard shale to salt interface, the P-P mode will produce robust reflections not only at low-dip salt boundaries but also at high-dip boundaries.

Overpressured Intervals

Overpressured conditions are often encountered when drilling deep targets across the GOM. Overpressured intervals are characterized by an increase in pore pressure (which reduces the effective pressure acting on the rock matrix), increased porosity, reduced bulk density, and a reduction in wave propagation velocity. We considered it important to determine how these overpressure conditions affect P-P and P-SV reflectivity. Although our interpretation of the P-P and P-SV profiles across the Shelf-B and Shelf-C areas showed no obvious degradation of either P-P or P-SV image quality across reported overpressure domains, this rock physics analysis would still provide valuable answers to the question, "Is either wave mode, P-P or P-SV, a better choice for imaging deep geology embedded in an overpressure zone?".

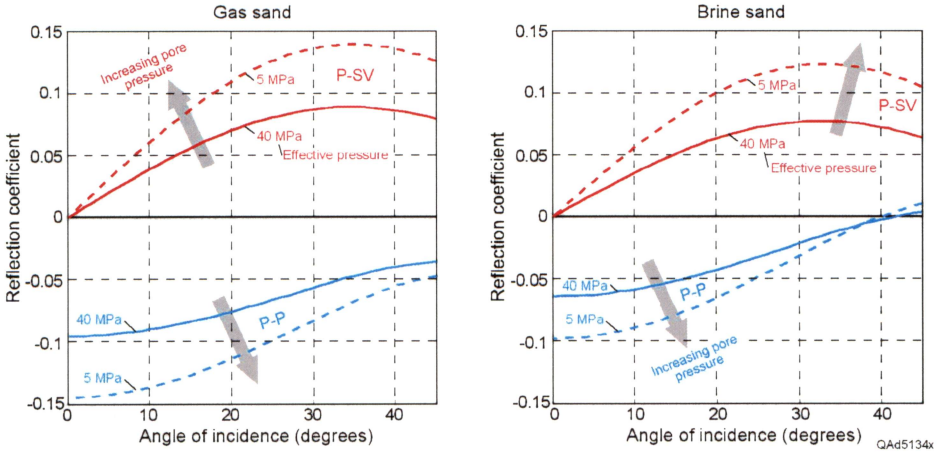

Figure 68. P-P and P-SV reflectivity behavior in overpressure regimes. The arrows indicate the direction of increasing overpressure (or decreasing effective pressure). The pore fluid in (a) is gas and in (b) is brine.

An example of typical P-P and P-SV reflectivity behavior that we calculated for deep sand-shale interfaces is exhibited as Figure 68. In these calculations, the effective pressure at the interface was reduced from 40 MPa (normal pressure) to 5 MPa (overpressure) to determine how overpressure affects P-P and P-SV reflection signal. The general behavior that we observed in these analyses is that P-P and P-SV reflectivity maintain their algebraic signs, both reflections increase as overpressure increases (as shown by the arrows in Figure 68), and the magnitudes of the increase in P-P reflectivity is approximately the same as the increase in the magnitude of the P-SV reflectivity. We conclude that neither the P-SV mode nor the P-P mode provide an imaging advantage over its companion modes in overpressure intervals. Either mode, P-P or P-SV, will produce images of overpressured geology that have equal quality.

Well Log Confirmation of Rock Physics Theory

Task not completed because project funding was eliminated for Year 3 of the project.

P-P and P-SV Image Registration Using VSP Data

Task not completed because project funding was eliminated for Year 3 of the project.

Common-Angle Migration of P-P and P-SV Data

Task not completed because project funding was eliminated for Year 3 of the project.

Conclusion

Ocean-bottom-cable (OBC) seismic technology allows long-offset seismic data to be acquired across congested production areas where long-offset towed-cable seismic technology is not feasible. Further, by using 4C sensors, 4-C OBC seismic technology provides both P-P and P-SV data, which allows elastic wavefield stratigraphy to be used to evaluate gas prospects. Towed-cable technology provides only P-P data and allows only conventional P-P seismic stratigraphy to be used in prospect evaluation.

This study focused on a large, 6,300 mi^2 (~16,000 km^2) area of the Louisiana shelf where 4-C OBC data were acquired and processed by WesternGeco with source-receiver offsets of 10 km. This large-offset geometry provided data that image deeper than any previous seismic reflection data in this congested production area. Analysis of these long-offset data shows that the P-P mode contains reflection signals from targets at depths of 60,000 ft (18 km), which is deeper than any reported seismic reflection effort across the northern shelf of the GOM. Equally important, the critical P-SV mode has reflection signal from depths of 42,000 ft (~13 km), which is much deeper imaging with converted-S data than what most geophysicists thought was possible.

Practical drilling targets across the Louisiana shelf are limited to depths of 30,000 ft (9 km) or less. Our research shows that both long-offset P-P and long-offset P-SV data provide good-quality, continuous reflections to these depths. The documentation that P-SV images are of a quality equal to that of P-P images at these deep depths is new, important information. Our study confirms that the fundamental requirement for good imaging of deep targets is acquiring long-offset seismic data. These research findings should encourage operators in the GOM basin to integrate long-offset 4-C OBC seismic technology into their prospect evaluations, particularly in areas where there are congested production facilities.

A question often posed by people who have limited experience in interpreting 4C seismic data is, “Why do P-P and P-SV images look so different across some stratigraphic intervals?”. Our research addressed this question by demonstrating that certain principles of rock physics, when applied to siliciclastic GOM rocks, result in P-P reflectivity at particular interfaces being significantly different from P-SV reflectivity at that same interface. We found three specific rock-interface conditions that are common across the GOM for which P-P reflectivity differs from P-SV reflectivity, these being interfaces involving: (1) variations in clay content, (2) gas-charged sediments, and (3) sediment-to-salt transitions. For each of these rock-interface targets, these rock physics principles are first illustrated by graphical displays of calculated P-P and P-SV reflectivity curves and are then applied to GOM well log data to confirm that the theoretically predicted differences in P-P and P-SV reflectivity do indeed occur at actual GOM rock interfaces.

References

Castagna, J. P., Batzle, M. L., and Kan, T. K., 1993, Rock-physics—the link between the rock properties and AVO response, *in* Castagna, J. P. and Backus, M. M., eds., Offset-dependent reflectivity theory and practice of AVO analysis: Tulsa, Society of Exploration Geophysicists.

Diegel, F. A., Karlo, J. F., Schuster, D. C., Shoup, R. C., and Trauvers, P. R., 1995, Cenozoic structural evolution and tectono-stratigraphic framework of the northern Gulf coast continental margin, *in* M. P. A. Jackson, D. G. Roberts, and S. Snelson, eds., Salt tectonics: a global perspective: AAPG Memoir 65, p. 109–151.

Exxon Production Research Company, 1985, Tectonic map of the world: available from American Association of Petroleum Geologists, Tulsa, OK.

Galloway, W. E., Bebout, D. G., Fisher, W. L., Dunlap, J. B., Jr., Cabrera-Castro, R., Lugo-Rivera, J. E., and Scott, T. M., 1991, Cenozoic, *in* A. Salvador, ed., The Gulf of Mexico Basin, Boulder, CO, Geological Society of America, The Geology of North America, v. J, p. 245–324.

Hardage, B. A., DeAngelo, M. V., Fomel, S., Fouad, K., Murray, P. E., Remington, R., and Sava, D., 2006, Elastic wavefield stratigraphy: an emerging seismic technology: Final report, DOE Contract DE-PS26-02NT15375.

Han, D. H., Nur, A., and Morgan, D., 1986, Effects of porosity and clay content on wave velocities in sandstones: Geophysics, v. 51, p. 2093-2107.

Peel, F. J., Travis, C. J., and Hossack, J. R., 1995, Genetic structural provinces and salt tectonics of the Cenozoic offshore U. S. Gulf of Mexico; a preliminary analysis, *in* M. P. A. Jackson, D. G. Roberts, and S. Snelson eds., Salt tectonics: a global perspective: AAPG Memoir 65, p. 153–175.

Sawyer, D. S., Buffler, R. T., and Pilger, R. H., Jr., 1991, The crust under the Gulf of Mexico basin, *in* A. Salvador, ed., The Gulf of Mexico Basin, Boulder, CO, Geological Society of America, The Geology of North America, v. J, p. 53–72.